

Exploring the Catalytic Activity of the [*BIG*⁺] Prion and Dynamics of tRNA T-loop
Modifications in *Saccharomyces cerevisiae*

by

Ethan Atticus Shaw

A dissertation accepted and approved in partial fulfillment of the
requirements for the degree of
Doctor of Philosophy
in Biology

Dissertation Committee:

Alice Barkan, Chair

David Garcia, Advisor

Eric Selker, Core Member

Julia Widom, Core Member

Michael Harms, Institutional Representative

University of Oregon

Spring 2024

© 2024 Ethan Atticus Shaw

DISSERTATION ABSTRACT

Ethan Atticus Shaw

Doctor of Philosophy in Biology

Title: Exploring the Catalytic Activity of the [*BIG*⁺] Prion and Dynamics of tRNA T-loop Modifications in *Saccharomyces cerevisiae*

RNA modifications affect stability, structure, and interactions with other molecules. They are important for the optimal functioning of RNA, and without them RNA can be degraded more easily and translation can become less efficient. The majority of known chemical modifications on RNA have been found on tRNAs. The modifications are so tightly packed together that many methods used to detect modifications on other RNAs are ineffective on tRNAs. In this work, I used a new and developing technology to detect RNA modifications - nanopore sequencing. Using direct RNA sequencing of tRNAs to detect modifications, I investigated 1) the catalytic activity of the yeast prion [*BIG*⁺] and 2) the incorporation of m⁵U₅₄, Ψ₅₅, and m¹A₅₈ in the T-loop of tRNAs.

[*BIG*⁺] causes yeast cells to proliferate more quickly with a shorter lifespan allowing them to thrive in nutritionally rich environments. These phenotypes could be caused by altered translation in these cells. Specifically, global translation is increased and certain genes are translated more quickly. However, the mechanism behind these changes is poorly understood. Here, I explore the catalytic activity of [*BIG*⁺]. [*BIG*⁺] arises from the protein Pus4, a pseudouridine synthase. I hypothesized that a change in the levels of pseudouridylation in [*BIG*⁺] cells could be driving the changes in translation. I observed that [*BIG*⁺] has retained its catalytic activity and a change in pseudouridylation is unlikely to explain why cells with [*BIG*⁺] proliferate more quickly.

Additionally, I co-developed one of the first direct RNA-sequencing methods to

comprehensively detect Ψ_{55} and m^1A_{58} in the T-loop of tRNAs by combining nanopore sequencing of yeast mutants with mass spectrometry. Using this technique, we were the first to validate the presence of a tRNA modification circuit, where Ψ_{55} promotes the formation of m^1A_{58} , in all yeast tRNA isoacceptors. Furthermore, we showed that m^1A_{58} is a dynamic modification that can change under stress. This method is a first step in being able to comprehensively detect and eventually quantify modifications in tRNAs. Being able to accurately detect these modifications will help us understand their complex roles.

This dissertation includes unpublished coauthored material.

CURRICULUM VITAE

NAME OF AUTHOR: Ethan Atticus Shaw

GRADUATE AND UNDERGRADUATE SCHOOLS ATTENDED:

University of Oregon, Eugene

California Polytechnic State University, San Luis Obispo

DEGREES AWARDED:

Doctor of Philosophy, Biology, 2024, University of Oregon

Master of Science, Biology, 2018, California Polytechnic State University, San Luis Obispo

Bachelor of Science, Biology, 2014, California Polytechnic State University, San Luis Obispo

AREAS OF SPECIAL INTEREST:

Molecular Biology

Genetics

PROFESSIONAL EXPERIENCE:

Graduate Teaching Assistant, University of Oregon, Sep. 2018-Jun. 2019

Graduate Teaching Assistant, California Polytechnic State University, San Luis Obispo, Sep 2016-Jun 2018

Research Assistant, Santa Cruz Biotechnology, Paso Robles, CA, May 2015-Jul 2016

Undergraduate Researcher, Hillers Lab, Department of Biology, California Polytechnic State University, San Luis Obispo, Sep. 2012-Dec. 2014

Undergraduate Researcher, Rafael Jimenez-Flores Lab, Department of Dairy Science, California Polytechnic State University, San Luis Obispo, Apr. 2012-Sep. 2012

GRANTS, AWARDS, AND HONORS:

Raymond-Stevens Fellowship, University of Oregon, 2024

Molecular Biology and Biophysics Program Trainee, National Institute of Health, 2019-2021

Stanley and Lucille Adamson Award, University of Oregon, 2019

PUBLICATIONS:

Garcia, D. M., Campbell, E. A., Jakobson, C. M., Tsuchiya, M., Shaw, E. A., DiNardo, A. L., Kaeberlein, M., & Jarosz, D. F. (2021). A prion accelerates proliferation at the expense of lifespan. *eLife*, 10.

<https://doi.org/10.7554/eLife.60917>

ACKNOWLEDGMENTS

I would like to thank Dr. David Garcia for being an amazing mentor. His mentorship and unwavering support allowed me to become the scientist that I am today. I would like to thank my dissertation advisory committee members: Dr. Alice Barkan, Dr. Mike Harms, Dr. Julia Widom, Dr. Eric Selker, and Dr. Jeff McKnight. They were exceptionally helpful in planning future directions and keeping me on track. I would like to express sincere appreciation to Dr. Ken Hillers for sparking my interest in genetics and molecular biology. I wouldn't have entered a Ph.D. program without his mentorship.

I would like to show genuine appreciation for all of the Garcia Lab members. They have all contributed to helping my work progress in lab meetings and random conversations. I would particularly like to thank Julia Reinsch who sat next to me and was always open to discussing tRNA biology and nanopore sequencing. She also helped me produce heatmaps for my dissertation. I also owe thanks to my collaborators Dr. Miten Jain, Niki Thomas, Dr. Robin AbuShumays, and Dr. Mark Akeson who helped me learn all the intricate details about direct RNA sequencing and tRNA library preparation.

I would like to thank all of my Ph.D. cohort members for always being there for me during the tough times of graduate school. I would especially like to acknowledge Dr. Jordan Munroe, Dr. Elizabeth Vargas, Dr. Michael Shavlik, Dr. Julia Ngo, and (soon to be Dr.) Zac Bush for being a welcome distraction away from lab work. I am also grateful for the relationship with my fiancée (soon to be Dr.) Kona Orlandi. She has helped me become a better scientist and person.

Finally, I would like to express gratitude to my family who have always been there for me. I would like to thank my parents, Mark and Catherine Shaw, who helped me

become the person I am today.

This work was supported by the National Institutes of Health MIRA grant R35 GM143125 to Dr. David Garcia and the National Institutes of Health Training Grant T32GM00775942 to me.

TABLE OF CONTENTS

Chapter	Page
I. INTRODUCTION	16
RNA Modification	16
Pus4.....	17
Pseudouridine.....	19
tRNAs	20
Prions	22
Bridge.....	25
II. EXPLORING THE ROLE OF PSEUDOURIDYLATION IN THE S. CEREVISIAE PRION [<i>BIG</i> ⁺]	26
Introduction.....	26
Results.....	28
Pseudouridylation is Unchanged on the mRNA <i>TEF1</i> in [<i>BIG</i> ⁺] Cells.....	28
Direct tRNA Sequencing Miscall Analysis Allowed for Semi-quantitative Changes in the Levels of Ψ_{55} to be Detected Across tRNAs	29
No Detectable Difference in Ψ_{55} in [<i>BIG</i> ⁺] Cells	33
A Catalytic Mutant, Pus4 R286K, has Similar Levels of Pseudouridylation as a <i>pus4</i> Δ Strain.....	34
The [<i>BIG</i> ⁺] Prion can be Initiated with Pus4 R286K.....	37
Discussion.....	39
Materials and Methods.....	41
Yeast Strains	41
Yeast Growth Conditions.....	41

Yeast Plasmid Transformation.....	42
Total RNA Isolation.....	43
CLAP	44
tRNA Isolation	44
Nanopore Sequencing of tRNA	44
IVT tRNA Construction and Sequencing	44
Bioinformatic Pipeline for Heatmaps	45
Modifying Pus4 Expression	45
Protein Preparation.....	46
Western Blot	47
[<i>BIG</i> ⁺] Induction	47
Firefly Luciferase Assay	48
Bridge.....	49
III. COMBINING NANOPORE DIRECT RNA SEQUENCING WITH GENETICS AND MASS SPECTROMETRY FOR ANALYSIS OF T-LOOP BASE MODIFICATIONS ACROSS 42 YEAST tRNA ISOACCEPTORS	50
Introduction.....	50
Results.....	52
Direct Sequencing of Yeast tRNAs	53
DRS Detects Conserved Pseudouridine Modifications in the T-loop of Yeast tRNAs	56
DRS Detects Conserved 1-Methyladenosine Modifications in the T-loop of Yeast tRNAs	60
Agreement Between m ¹ A ₅₈ Annotations by DRS and Other Methods.....	64
5-Methyluridine Does not Yield Robust Base Miscalls in the T-loop.....	65

Ψ ₅₅ Promotes m ¹ A ₅₈ Installation in Certain tRNAs	66
Nanopore DRS Reveals Increased m ¹ A ₅₈ Frequency on Some tRNAs Upon Nutrient Depletion	68
Mass Spectrometry Measurements Confirm and Extend Evidence of Interrelated Changes to tRNA Modifications in Mutant Strains	70
Nanopore-based Predictions of m ¹ A ₅₈ Sites are Confirmed by LC-MS/MS-based Direct tRNA Sequencing.....	74
Development of a Model to Predict T-loop Modifications in tRNA	75
Extending Adapter Length for tRNA Ionic Current Analysis	77
Discussion.....	79
Materials and Methods.....	82
Yeast Strains	82
Yeast Growth Conditions.....	84
tRNA Purification	85
Splint Adapter Preparation.....	86
tRNA Sequencing	86
Ligation with Longer Splints	87
IVT Construction and Nanopore Sequencing	88
Bioinformatic Methods	89
Global Ribonucleoside Modification Profiling by LC-MS/MS.....	91
LC-MS/MS Bottom-up RNA-sequencing	91
Western Blot	93
Bridge.....	94
IV. CONCLUDING SUMMARY	95
APPENDICES	99

A. SUPPLEMENTARY FIGURES FOR CHAPTER III.....	99
B. SUPPLEMENTARY TABLES FOR CHAPTER III	104
REFERENCES	110

SUPPLEMENTAL FILES

Excel Sheet with Supplemental Tables 3.2, 3.5, 3.7, 3.8, 3.10, 3.12

Excel Sheet with Supplemental Table 3.3

LIST OF FIGURES

Figure	Page
1. Figure 1.1 tRNA secondary structure shown with the Pus4-dependent Modification- Ψ_{55}	18
2. Figure 1.2 The isomerization of uridine to pseudouridine.....	19
3. Figure 1.3 All known modifications found across cytoplasmic tRNAs in <i>S. cerevisiae</i>	22
4. Figure 1.4 Yeast prion propagation	24
5. Figure 2.1 Measuring Ψ_{239} on <i>TEF1/2</i> in [<i>BIG</i> ⁺] cells.....	29
6. Figure 2.2 Titrating Pus4 expression results in changes in the levels of Ψ_{55} detected by nanopore sequencing	32
7. Figure 2.3 Levels of Ψ_{55} remain unchanged in [<i>BIG</i> ⁺] cells.....	34
8. Figure 2.4 Pseudouridylation by Pus4 is reduced in the Pus4 R286K mutant across all tRNAs and on the <i>TEF1/2</i> mRNA	36
9. Figure 2.5 Catalytic activity of Pus4 is not required to induce [<i>BIG</i> ⁺].....	38
10. Figure 3.1 Overview of tRNA library preparation, sequencing, and alignment strategy	54
11. Figure 3.2 Heatmaps representing comprehensive alignments of 42 <i>S. cerevisiae</i> isoacceptors exhibit miscalls coincident with modified positions in the T-loop...	58
12. Figure 3.3 Reference match probabilities identify changes corresponding to modifications in the T-loop across 42 isoacceptor tRNAs	63
13. Figure 3.4 Nanopore reveals increased m ¹ A ₅₈ frequency on some tRNAs upon nutrient depletion	69
14. Figure 3.5 LC-MS/MS confirms DRS-based modification predictions	73
15. Figure 3.6 Longer adapters enable ionic current analysis using Nanopolish	79
16. Supplementary Figure 3.1 Heatmap representing IVT tRNA sequences of 42 <i>S. cerevisiae</i> isoacceptors.....	99

17. Supplementary Figure 3.2 Pus4 catalytic mutant	100
18. Supplementary Figure 3.3 Reference match probability maps for <i>trm61Δ</i> match results obtained for <i>trm6Δ</i>	101
19. Supplementary Figure 3.4. Two different mass spectrometry techniques allow for the bulk quantification of each modification in a pool of total tRNA or the sequence specific location of RNA modifications.....	102
20. Supplementary Figure 3.5. m ⁵ U ₅₄ , <i>pus4Δ</i> , m ¹ A ₅₈ , and T-loop modification associated miscall profile classification accuracies	103

LIST OF TABLES

Table	Page
1. Supplementary Table 3.1 Yeast strains used in this study	104
2. Supplementary Table 3.2 The RNA and DNA oligonucleotides.....	105
3. Supplementary Table 3.3 Global and isoacceptor-specific profiles	105
4. Supplementary Table 3.4 Sequence and alignment statistics for tRNA purified from <i>S. cerevisiae</i>	106
5. Supplementary Table 3.5 Custom BY4741 strain specific 42 yeast tRNA isoacceptor reference sequences	106
6. Supplementary Table 3.6 Isoacceptor aligned reads ranges	107
7. Supplementary Table 3.7 Raw aligned reads for each replicate	107
8. Supplementary Table 3.8 The T-loop sequences from 42 <i>S. cerevisiae</i> isoacceptors.....	107
9. Supplementary Table 3.9 Predictions for the presence or absence of m ¹ A.....	108
10. Supplementary Table 3.10 The posterior probabilities.....	109
11. Supplementary Table 3.11 Classes of tRNAs as defined by the influence of Ψ_{55} on the catalysis of m ¹ A ₅₈	109
12. Supplementary Table 3.12 Mass spectrometry ribonucleoside modification profiling abundances.....	109

CHAPTER I

INTRODUCTION

This dissertation contains co-authored material. I wrote the introduction and conclusion- chapters I and IV. I was the primary contributor for the data collection, data analysis, and writing for chapter II. Chapter II has one figure, Figure 2.1, that has been published with co-authors. The entirety of chapter III is from a manuscript that is currently in revision and is co-authored by me.

RNA modifications

RNA consists of four canonical bases: adenine (A), uracil (U), guanine (G), and cytosine (C). These bases can pair with each other, A to U and G to C, through hydrogen bonding with mutual complementary recognition. This canonical pairing of bases creates fundamental interactions that allow an RNA to fold into its proper secondary structure. However, these bases can also be post-transcriptionally altered by chemical modifications, dramatically affecting the RNA structure. Over 150 RNA modifications have been identified across coding and noncoding RNAs, including mRNAs, tRNAs, rRNAs, snoRNAs, and snRNAs (Cappannini et al., 2024). These modifications facilitate many different roles but are most commonly known for increasing the stabilization of functional RNA structures (Helm, 2006).

RNA modifying enzymes are responsible for catalyzing these modifications. Disruptions to these enzymes or to their RNA modification sites are associated with human health problems, including neurological disorders, metabolic disorders, and cancers (Delaunay et al., 2024). RNA modifications are found in all domains of life, and the same modification can often be found in an identical position on an RNA from yeast

and the orthologous RNA from another organism, like humans, suggesting a conserved function (Cappannini et al., 2024). This makes *Saccharomyces cerevisiae*, or budding yeast, a powerful model organism to better understand RNA modifying enzymes and their accompanying modifications. Additionally, *S. cerevisiae* has 6,000 genes across ~12,000kb of genomic DNA that is subdivided into 16 chromosomes (Duina et al., 2014; Engel et al., 2014). Nearly 1/3 of all protein-encoding genes in yeast contain an ortholog among mammalian protein sequences, (Botstein et al., 1997) and *S. cerevisiae* are genetically tractable cells that divide every 90 minutes making them ideal for experiments within molecular biology.

Pus4

Pus4 is one of nine stand-alone Pus (Pseudouridine synthase) enzymes in *Saccharomyces cerevisiae* that catalyze the isomerization of uridine to pseudouridine by recognition of particular sequences and/or secondary structure (Rintala-Dempsey & Kothe, 2017). The only other pseudouridine synthase in yeast, Cbf5, relies on guide-RNAs for pseudouridylation of a target sequence (Meier, 2005). The nine stand-alone Pus enzymes can target many different types of coding and noncoding RNA molecules.

Specifically, Pus4 has been shown to modify mRNA, tRNA, and snoRNA (Carlile et al., 2014). It is notably responsible for producing pseudouridine-55 (Ψ_{55}), a highly conserved modification present across tRNAs throughout life (**Figure 1.1**). In *S. cerevisiae*, Pus4 is solely responsible for Ψ_{55} across all cytoplasmic and mitochondrial tRNAs except for the initiator methionine which doesn't contain a Ψ_{55} . However, the deletion of *PUS4* does not seem to affect fitness when yeast are grown in optimal

conditions which makes the purpose of the conserved Ψ_{55} modification unclear (Becker et al., 1997).

Pus4 is part of the TruB family of pseudouridine synthases and is conserved throughout life from bacteria to humans. It is 45.3 kDa and contains a TruB catalytic domain where a conserved catalytic aspartate is necessary for pseudouridylation (Rintala-Dempsey & Kothe, 2017). In addition to its catalytic activity, it is thought that Pus4 may

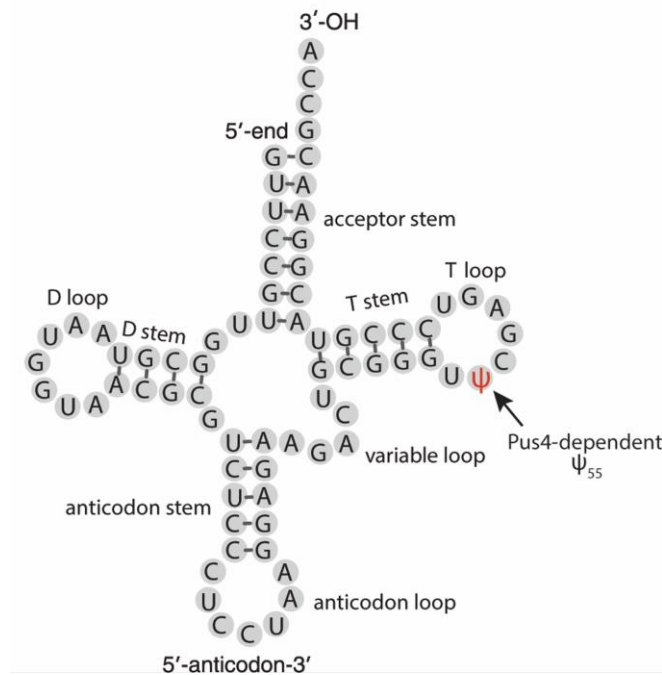


Figure 1.1. tRNA secondary structure shown with the Pus4-dependent modification- Ψ_{55} . Almost all tRNAs contain a secondary structure composed of 3 hairpin loops: the D-loop, the anticodon loop, and the T-loop. They also contain a terminal helical stem called the acceptor stem. tRNA Arginine^{CCU} from *S. cerevisiae* is being used as an example to show the typical tRNA secondary structure and where Pus4 modifies tRNAs, the second position in the T-loop. Modified from (C. Li et al., 2016).

have an additional role. The bacterial homolog of Pus4, TruB, acts as a tRNA chaperone in addition to being a pseudouridine synthase (Keffer-Wilkes et al., 2016). TruB binds and unfolds tRNAs allowing misfolded tRNAs a second chance at folding. In the Garcia Lab, we have observed different growth rates from a catalytically inactive Pus4 mutant

and a Pus4 deletion mutant under different stress conditions. This suggests that Pus4 can affect a yeast cell's ability to proliferate in some way other than through pseudouridylating RNA.

Pseudouridine

Pseudouridine (Ψ) is a glycoside isomer of Uridine (U) (X. Li et al., 2016). It is formed when a pseudouridine synthase breaks the N-C glycosidic bond between the sugar and base, the base is flipped 180°, and a new C-C bond is formed (**Figure 1.2**). The base

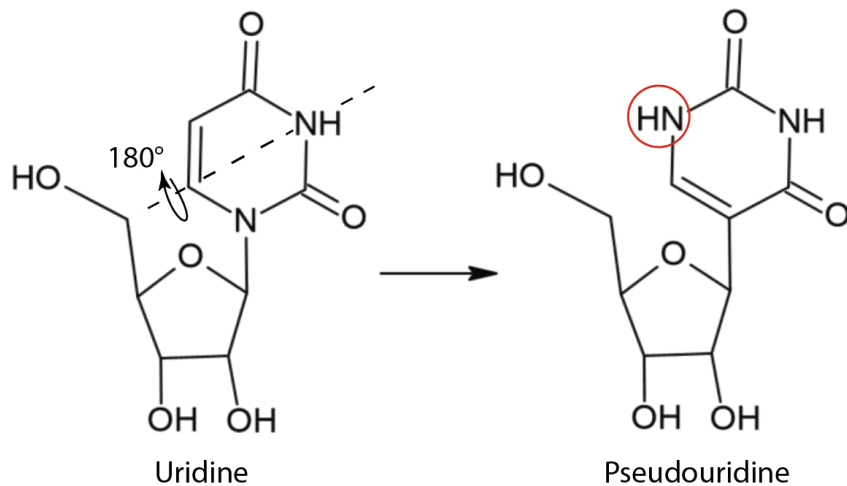


Figure 1.2. The isomerization of uridine to pseudouridine. A pseudouridine synthase can break the N-C glycosidic bond between the sugar and the base in uridine. This allows for the base to flip 180° and reattach to the sugar with a new C-C bond. The nitrogen group circled in red on pseudouridine shows the additional hydrogen bond donor that is formed after the base is flipped.

in pseudouridine contains an additional hydrogen bond donor, which can form a new stable hydrogen bond (Griffey et al., 1985). Additionally, pseudouridine formation can promote base stacking in RNA (Davis, 1995).

Pseudouridine was the first RNA modification discovered over 70 years ago, and it is also the most abundant (Cohn & Volkin, 1951). Pseudouridine has been found in many different types of RNA including rRNA, tRNA, and mRNA (Penzo et al., 2017). In

tRNAs, the presence of pseudouridine can stabilize tertiary structure and facilitate proper folding (Cabello-Villegas & Nikonowicz, 2005; Denmon et al., 2011; Vendeix et al., 2012). This is the case for many pseudouridines positioned at different locations along the tRNA sequence including at Pus4-dependent Ψ_{55} (Nobles et al., 2002). In the anticodon of tRNAs, the presence of pseudouridine can change the efficiency of a tRNA's ability to translate specific codons (Tomita et al., 1999). Pseudouridine can also affect the deposition of other modifications across a tRNA molecule. It can be involved in a modification circuit where its presence directly promotes the formation of other modifications, such as m^1A_{58} (Barraud et al., 2019).

In mRNAs, pseudouridine has been found in the coding region, the 5'-UTR, and the 3'-UTR (Carlile et al., 2014). When present in the coding region pseudouridine can slow down translation elongation, and amino acids from non-cognate tRNAs are incorporated more frequently in Ψ -containing codons (Eyler et al., 2019). It was also found that replacing uridine with pseudouridine across the entire transcript can double the amount of protein produced (Karikó et al., 2008). Additionally, when pseudouridine was added into a stop codon to replace uridine, it converted a nonsense codon to a sense codon (Karijolich & Yu, 2011).

tRNAs

The Central Dogma of molecular biology states that DNA gives rise to RNA, and RNA gives rise to protein (Crick, 1970). Translation, a principal component of the Central Dogma, is the process by which RNA is translated to protein. Specifically, during translation the genetic code in mRNA is deciphered sequentially into amino acids that

make up an encoded protein. The molecules responsible for linking the codons in mRNA with their proper amino acids are called tRNAs, or transfer RNAs.

The determination of the first tRNA sequence was done by Robert Holley in 1965 for tRNA^{AGC} from *S. cerevisiae* (Robert Holley, 1965). In eukaryotes, tRNAs are typically between 76 and 90 nucleotides long (Sharp et al., 1985). All tRNAs form a “cloverleaf” secondary structure composed of 3 hairpin loops and a terminal helical stem (**Figure 1.1**, Goodenbour & Pan, 2006). Two of the hairpin loops, the D-loop and the T-loop, fold onto each other to form a kissing interaction through complementary base pairing (Brunel et al., 2002). The resulting L-shaped tertiary structure allows tRNAs to function properly in the ribosome during translation.

tRNAs are the most densely modified RNA species (Phizicky & Alfonzo, 2010). In a study using over 500 tRNA sequences from archaea, eubacteria, fungi, animals, plants, chloroplasts, mitochondria, and viruses, 11.9% of nucleotides were found to be modified (Sprinzl & Vassilenko, 2005). In *S. cerevisiae* specifically, cytoplasmic tRNAs can contain 25 different modifications at 36 possible positions (**Figure 1.3**, Phizicky & Hopper, 2010). Modifications found in the anticodon region can expand or restrict the possible options of codons that a tRNA can pair with (T. Suzuki, 2021). Additionally, these modifications can be involved in reading frame maintenance (T. Suzuki, 2021). Outside of the anticodon loop, modifications have been shown to stabilize the higher-order structure of tRNAs and ensure accurate and efficient aminoacylation (T. Suzuki, 2021).

daughter cell has an equal chance of inheriting the prion from the mother cell.

Additionally, yeast prions require chaperone proteins for propagation (**Figure 1.4**, Liebman & Chernoff, 2012). Chaperone proteins in yeast, including Hsp104, Hsp70, and Hsp40, help to disaggregate and refold stress-damaged proteins (Glover & Lindquist, 1998). Yeast prions can be depleted by either the overexpression or deletion of one of these chaperone proteins (Liebman & Chernoff, 2012). There have been over a dozen yeast prions discovered, with many more potential candidates identified in several screens (Alberti et al., 2009; Chakrabortee et al., 2016; Dennis & Garcia, 2022; Liebman & Chernoff, 2012).

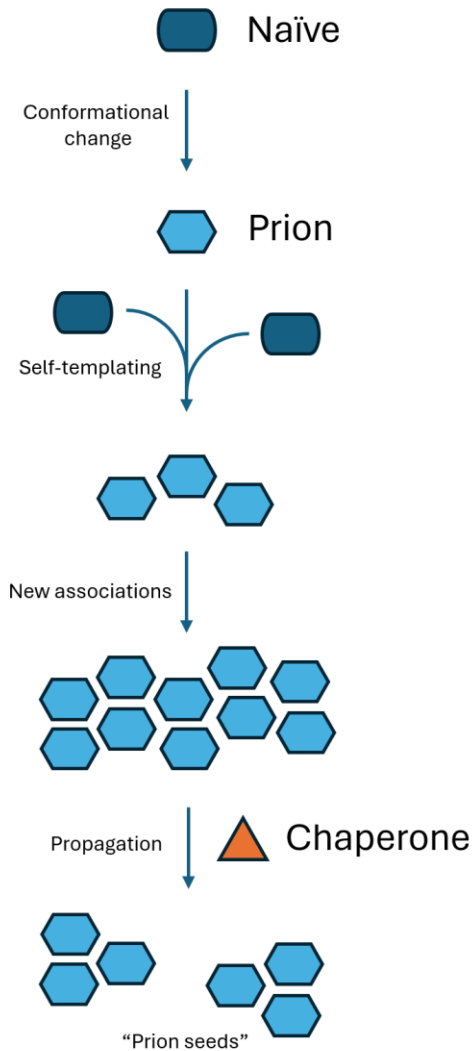


Figure 1.4. Yeast prion propagation. Proteins in their standard, endogenous form are known as naïve proteins. For a yeast prion to form, a naïve protein undergoes a conformational change to form a prion. The prion can self-template its conformation onto the naïve version making more copies of itself. Prions can form new associations with themselves or other proteins often forming an assembly or aggregation. These aggregates in the cytoplasm need chaperone proteins to separate them into new “prion seeds” that are passed on to future generations.

The growing number of prions identified indicates that they may have an important biological role. Studying prions in yeast has not only highlighted their ancient existence, but also revised our understanding of their possible functions. Prions in mammals arise from the same protein, PrP, which forms an amyloid and can cause

various fatal diseases (Caughey & Chesebro, 2001). Conversely, prions in yeast come from numerous proteins, and they do not all form amyloids (Dennis & Garcia, 2022). Yeast prions have provided a mechanism for inheritance that relies on protein conformation rather than nucleotide sequence, and they can actually confer beneficial traits (Du et al., 2008; Jarosz et al., 2014; G. Suzuki et al., 2012; True & Lindquist, 2000).

In a screen searching for yeast prion proteins across the *S. cerevisiae* proteome, Pus4 came out as a positive hit (Chakrabortee et al., 2016). It was later confirmed that Pus4 can form the prion known as [BIG⁺] (Garcia et al., 2021). In this work, I was interested in investigating this newly discovered yeast prion protein, which allows cells to grow bigger, proliferate faster, and enhance their translation machinery, but at the cost of a decreased lifespan (Garcia et al., 2021).

Bridge

I described how Pus4 is a highly conserved pseudouridine synthase that can target several RNAs including tRNAs at position 55 in the T-loop. Pus4 can also change conformation into a prion protein known as [BIG⁺]. In chapter II, I investigate if the change in conformation from Pus4 to [BIG⁺] changes its catalytic activity. I looked to see if the levels of pseudouridylation change on Pus4 targets throughout yeast cells. Additionally, I investigate if catalytic activity is necessary for the initiation of the [BIG⁺] state.

CHAPTER II

EXPLORING THE ROLE OF PSEUDOURIDYLATION IN THE *S. CEREVISIAE* PRION

[*BIG*⁺]

I was the primary contributor for the data collection, data analysis, and writing for this chapter. The data for Figure 2.1 was collected by me, and it is published in: Garcia, D. M., Campbell, E. A., Jakobson, C. M., Tsuchiya, M., Shaw, E. A., DiNardo, A. L., Kaeberlein, M., & Jarosz, D. F. (2021). A prion accelerates proliferation at the expense of lifespan. *eLife*, 10. <https://doi.org/10.7554/eLife.60917>.

Introduction

The yeast prion known as [*BIG*⁺] is an alternatively folded version of the protein Pus4 (Garcia et al., 2021). The prion is named [*BIG*⁺] for better in growth, as cells with the prion proliferate more quickly and grow larger in saturated conditions. It was first discovered after transiently overexpressing Pus4 (Chakrabortee et al., 2016). Transient overexpression of a protein has been established as a method capable of inducing prion formation (Derkatch et al., 1996; Liebman & Chernoff, 2012; Masison & Wickner, 1995). Additionally, prions self-template from the naïve (original, endogenous) protein to propagate. When *PUS4* was deleted from a [*BIG*⁺] cell, the large cell phenotype was lost (Garcia et al., 2021). Yeast prions also rely on chaperone proteins to propagate, and when Hsp70 was transiently inhibited the cells returned to normal size (Garcia et al., 2021). The [*BIG*⁺] cell size phenotype was also inherited in a non-mendelian fashion, and the localization of Pus4 changed in [*BIG*⁺] cells. These data are consistent with a prion-based mechanism (Garcia et al., 2021).

[*BIG*⁺] is written in brackets denoting cytoplasmic inheritance and capital letters indicating its dominant phenotype. Yeast have an increased proliferation rate with

[*BIG*⁺], and they can outcompete their naïve counterparts (Garcia et al., 2021). However, this comes at a cost. These cells have decreased chronological and replicative lifespans (Garcia et al., 2021). These phenotypes can be beneficial to cells in fluctuating environments, particularly those where nutrients are plentiful since cell division is an energetically costly process.

The mechanism driving cells to proliferate more quickly and grow larger is not well understood. RNA-seq showed that there are little changes in mRNA levels between naïve and [*BIG*⁺] cells (Garcia et al., 2021). Additionally, bulk tRNA levels between [*BIG*⁺] cells and naïve cells measured with a nucleic acid fragment analyzer remain unchanged (Garcia et al., 2021). However, there are some changes in [*BIG*⁺] cells at the protein level. It is known through an [³⁵S]-methionine pulse labeling experiment, that [*BIG*⁺] cells have an increased rate of translation (Garcia et al., 2021). Additionally, there are more polysomes present in [*BIG*⁺] cells indicating altered translation levels (Garcia et al., 2021). Translation has also been linked to cell size, proliferation, and lifespan in the past (Kaeberlein, 2010; Tanenbaum et al., 2015; “The Regulation of Cell Size,” 2013). It seems likely that the key to understanding [*BIG*⁺] will be uncovering what drives the global translational changes. Recent data from the Garcia Lab has shown that ribosomes stall less frequently on an mRNA reporter in [*BIG*⁺] cells than naïve cells. This is one possible explanation for increased translation.

It is also possible that when Pus4 changes conformation to [*BIG*⁺], its catalytic site becomes more or less accessible. This could change the amount of pseudouridylation at Pus4 target sites, which could then alter global translation. Other prions have been shown to change the activity of their naïve protein counterpart either in a loss-of-function

or gain-of-function manner (Chakravarty et al., 2020; Liebman & Chernoff, 2012). In this work, I investigated the hypothesis that the [*BIG*⁺] prion altered Pus4 pseudouridylation levels in RNAs, resulting in the observed [*BIG*⁺] growth phenotypes.

Results

Pseudouridylation is unchanged on the mRNA *TEF1* in [*BIG*⁺] cells

To explore whether the change in conformation of Pus4 to [*BIG*⁺] would alter its ability to pseudouridylate, I wanted to measure the levels of pseudouridylation across Pus4 targets in yeast. Earlier work showed that pseudouridylation levels were maintained on a tRNA, Ala(AGC), in [*BIG*⁺] cells (Garcia et al., 2021). I was curious if pseudouridylation levels were changed on the *TEF1* mRNA. This mRNA encodes a translation elongation factor involved in guiding amino-acylated tRNAs to the ribosomes during translation.

Pus4 was known to pseudouridylate position 239 on *TEF1* (Lovejoy et al., 2014). To test if there was a change in pseudouridylation at this position, I used an RT-PCR based method that can quantify the ratio of Ψ/U at single nucleotide resolution. The method, CMC-RT and ligation assisted PCR analysis of pseudouridine modification (CLAP), relies on a bulky chemical group forming an adduct with the pseudouridine base that terminates reverse transcription (Zhang et al., 2019), **Figure 2.1A**). I found similar levels of Ψ₂₃₉ on *TEF1* when comparing [*BIG*⁺] and naïve strains (**Figure 2.1B**). Additionally, Ψ₂₃₉ on *TEF1* was depleted to only background levels in our *pus4*Δ strain due to spontaneous cleavage near the target site or Pus4-independent pseudouridylation (**Figure 2.1B**).

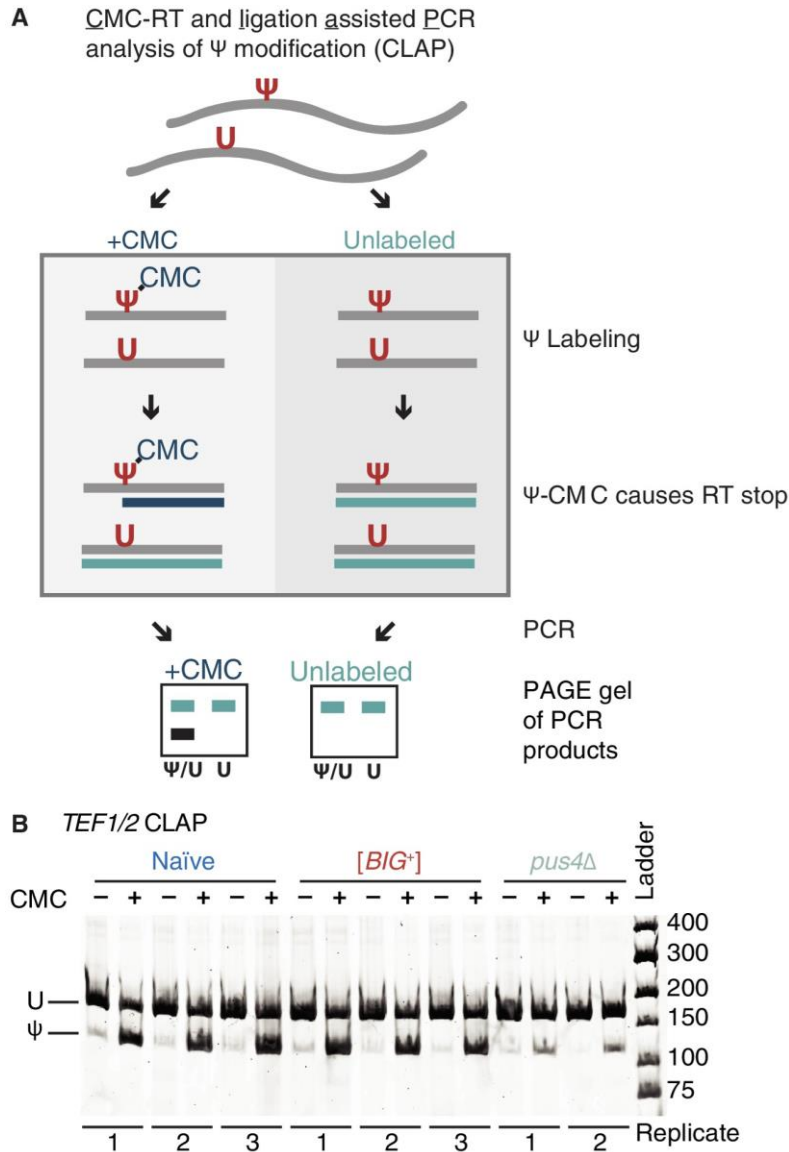


Figure 2.1. Measuring Ψ_{239} on *TEF1/2* in $[BIG^+]$ cells (Garcia et al., 2021).
A. Flowchart for CMC-RT and ligation-assisted PCR analysis of Ψ modification (CLAP).
B. Native PAGE showing the CLAP result for *TEF1/TEF2* mRNA from multiple replicates of naïve (3), $[BIG^+]$ (3), or *pus4Δ* (2). Shorter bands indicating pseudouridylation that appear in CMC-unlabeled or *pus4Δ* samples may reflect either background signal from spontaneous cleavage near the target site or Pus4p-independent modification of this site.

Direct tRNA sequencing miscall analysis allowed for semi-quantitative changes in the levels of Ψ_{55} to be detected across tRNAs

Although the levels of Ψ_{239} remained unchanged on *TEF1* between $[BIG^+]$ and naïve cells, Pus4 pseudouridylates U_{55} on every tRNA in *S. cerevisiae* except for the

initiator methionine tRNA (**Figure 1.1**, (Simsek & RajBhandary, 1972). I wanted to determine if the levels of Ψ_{55} changed on any tRNAs in [*BIG*⁺] cells. In the past, modifications were identified on tRNAs using costly and time-consuming biophysical methods (RajBhandary & Köhrer, 2006; Yoluç et al., 2021). To look at more tRNAs per experiment, next generation sequencing methods were being produced to study modifications. These relied on reverse transcription terminating at the site of a modification or a reverse transcriptase adding a non-canonical base at a modification site (Behrens et al., 2021; Derkatch et al., 1996; Liebman & Chernoff, 2012; Masison & Wickner, 1995). This would leave traces of modifications left behind that could be identified when sequencing the reverse-transcribed DNA. However, tRNAs have many modifications that can inhibit reverse transcription making these techniques less practical. Additionally, many of these methods could only detect one modification at a time.

A newer method that could detect modifications across all cytoplasmic tRNAs in *S. cerevisiae* at once was direct RNA sequencing of tRNAs using nanopore sequencing. This method does not rely on sequencing reverse-transcribed DNA, but rather it directly sequences RNA molecules with their modifications still intact. The detection of pseudouridine through nanopore sequencing is performed by a miscall analysis where the presence of pseudouridine causes the sequencing basecaller to call a nucleotide other than uridine, usually a cytosine. It has been shown that there is an increase in miscalls at a particular position when the ratio of Ψ to U increases in mRNA (Begik et al., 2021a; Huang et al., 2021; Tavakoli et al., 2023). However, it was unknown if pseudouridine could be detected on tRNAs in a semi-quantitative way due to the high density of modifications and the shorter length of tRNA molecules.

I wanted to test if it was possible to observe changes in the amount of pseudouridine on tRNA at position 55. To do this, I transformed a plasmid with a galactose-inducible *PUS4* into a *pus4* Δ yeast strain so that the only source of Pus4 was coming from the plasmid. I grew this strain in varying amounts of galactose to “titrate” the amount of Pus4 expressed, which I hypothesized would change the ratio of Ψ_{55} to U₅₅. A western blot analysis showed that with different concentrations of galactose, the amount of Pus4 present in the cells changed (**Figure 2.2A**). To make the western blot more quantitative a loading control will be necessary in a repeated experiment. Alternatively, qRT-PCR could be used to assess the amount of *PUS4* mRNA between each of the strains.

I produced heatmaps using the miscall analysis showing the reference match probabilities for each position along the T-loops across every cytoplasmic *S. cerevisiae* tRNA isoacceptor. A high reference match probability shown in blue means that the base called at that particular position matched the reference base more often, while a low reference match probability shown in yellow means that the base called at that particular position did not match the reference base often. The heatmaps showed that reference match probability at position 55 changed depending on how much Pus4 was present in vivo (**Figure 2.3B**). As the amount of Pus4 decreased, the reference match probability increased at position 55 as expected because there was less Ψ_{55} , and thus more of these positions were base called as uridines (**Figure 2.3B**). I concluded that this type of analysis could in fact show relative differences in the amount of Ψ_{55} present across tRNAs.

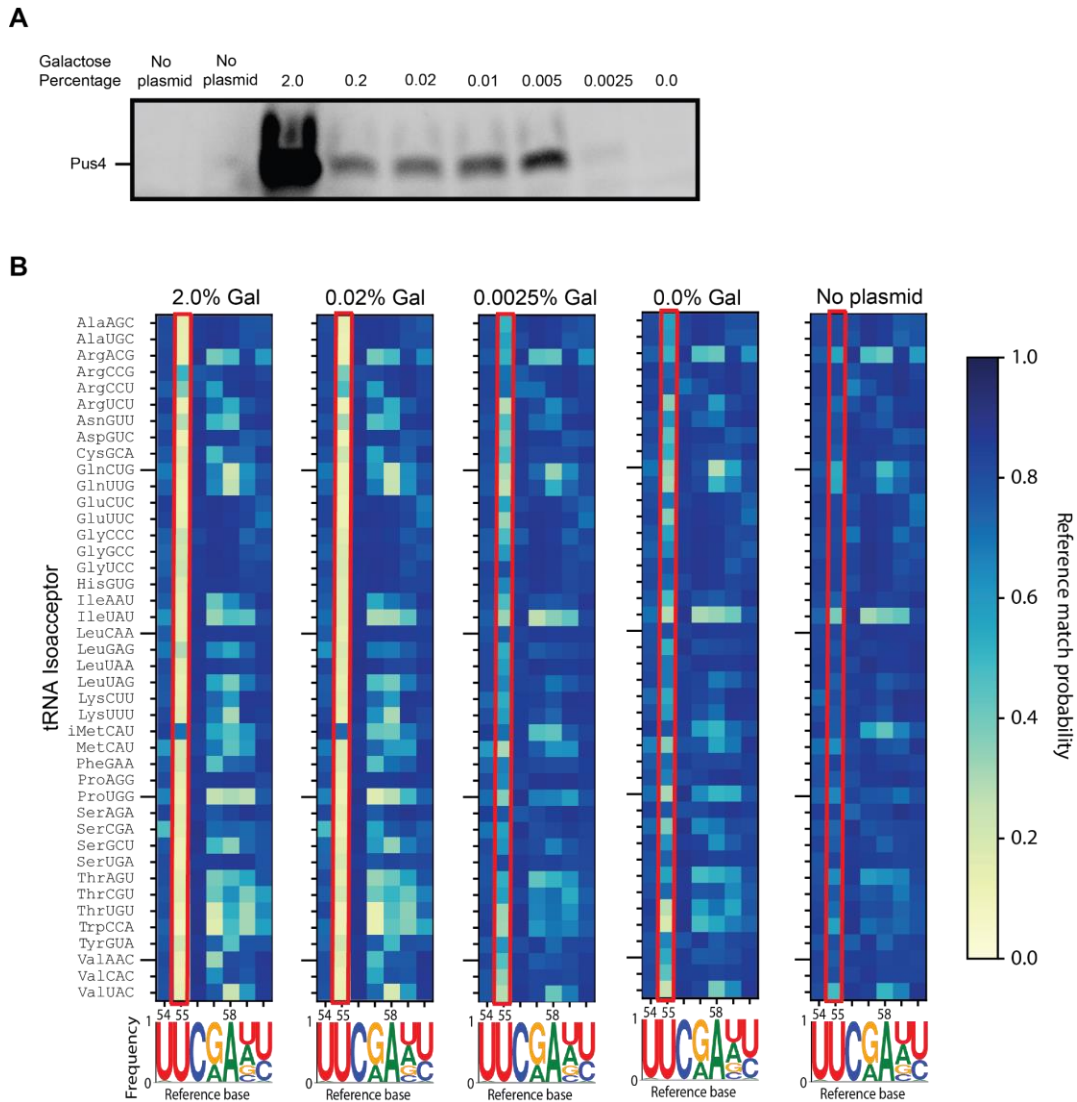


Figure 2.2. Titrating Pus4 expression results in changes in the levels of Ψ_{55} detected by nanopore sequencing. A) A western blot showing what percent of galactose made up the sugar component in the SD-URA medium, maintaining a total of 2% sugar in each culture that was made up of galactose, raffinose, or both. Two control lanes are shown in which yeast was grown without a plasmid containing a galactose inducible Pus4 gene. The varying intensity of the bands correspond to the amount of Pus4 that was present in the total protein isolation from different yeast cultures. B) Heat maps showing a range of reference match probabilities across the T-loop of all cytoplasmic *S. cerevisiae* isoacceptors for cultures grown with varying amounts of galactose. The position of interest, U₅₅/ Ψ_{55} , is boxed in red on each heatmap. A high reference match probability (blue) shows the expected base was often called by the basecaller matching the reference sequence, and a low reference match probability (yellow) shows that a call was often made that did not match the reference sequence. The x-axis shows the position along the T-loop of a tRNA, and the sequence logo below represents how often a nucleotide is present in the reference at each position, where the height of the letter corresponds to how often it is present.

No detectable difference in Ψ_{55} in $[BIG^+]$ cells

I wanted to use this miscall analysis to observe if there were changes in Ψ_{55} levels across tRNAs in $[BIG^+]$ cells. If $[BIG^+]$ changes the ability of Pus4 to pseudouridylate tRNAs, tRNAs could destabilize causing broad translational changes. When comparing naïve and $[BIG^+]$ tRNAs, no observable differences were detected in reference match probability (**Figure 2.3A**). A control strain with the *PUS4* gene deleted showed an expected decrease in reference match probability at position 55. (**Figure 2.3A**). To see small changes between heatmaps more easily, a subtractive heatmap was made where the difference in reference match probability between naïve and $[BIG^+]$ could be observed (**Figure 2.3B**). There were no distinguishable differences in the levels of Ψ_{55} in $[BIG^+]$ cells (**Figure 2.3B**) These data confirm that $[BIG^+]$ does not form an amyloid because all yeast prions that form amyloids have loss-of-function phenotypes (Liebman & Chernoff, 2012). Additionally, since the amount of pseudouridine stays relatively consistent, it is likely that $[BIG^+]$ increases global translation through an alternative function excluding pseudouridylation. Although, the presence of ectopic pseudouridylation has not been ruled out.

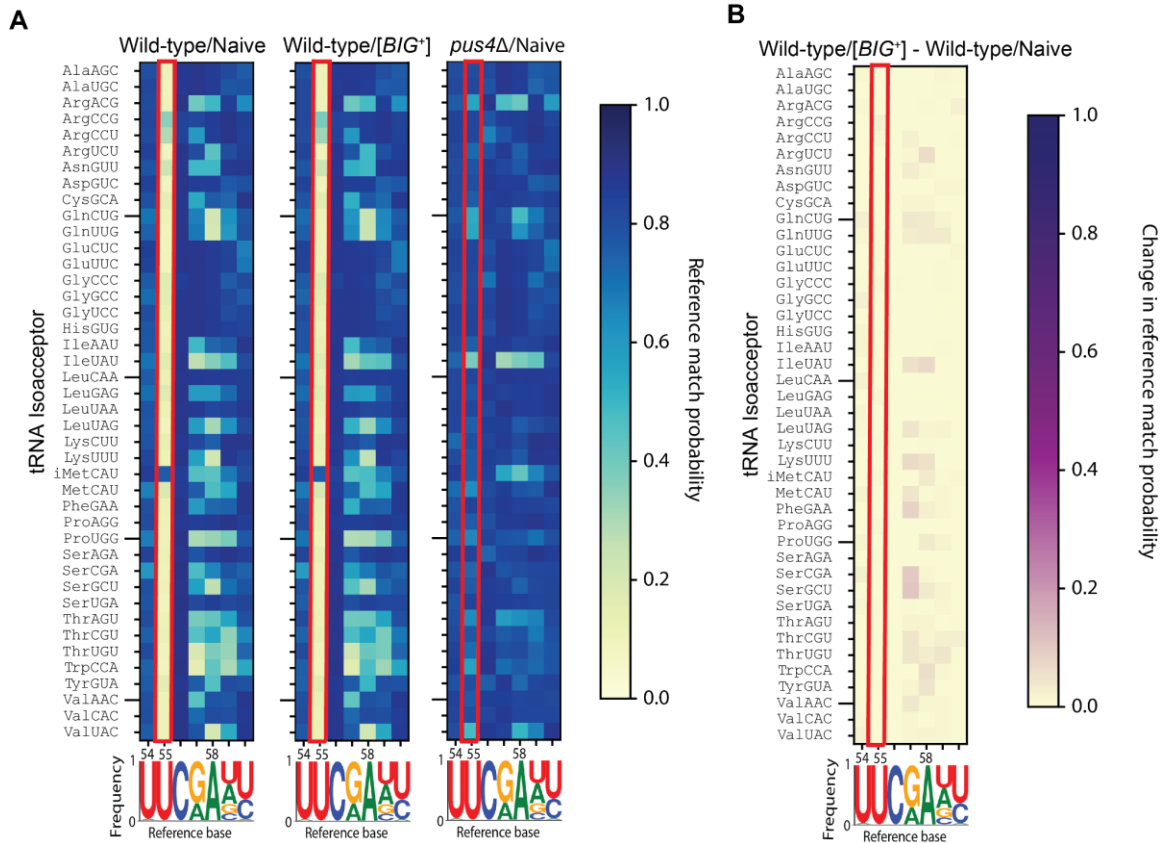


Figure 2.3. Levels of Ψ55 remain unchanged in [BIG⁺] cells. A) Heat maps showing a range of reference match probabilities across the T-loop of all cytoplasmic *S. cerevisiae* isoacceptors comparing naïve and [BIG⁺] cells. The position of interest, U/Ψ55, is boxed in red on each heatmap. A high reference match probability (blue) shows the expected base was often called by the basecaller matching the reference sequence, and a low reference match probability (yellow) shows that a call was often made that did not match the reference sequence. The x-axis shows the position along the T-loop of a tRNA, and the sequence logo below represents how often a nucleotide is present in the reference at each position across all tRNAs where the height of the letter corresponds to how often it is present. A control heatmap, *pus4*Δ, shows when there is no pseudouridylation by Pus4 occurring at position 55. B) A subtractive heatmap showing the difference in reference match probability between [BIG⁺] and naïve cells. A high difference in reference match probability between [BIG⁺] and naïve cells is shown in purple and a low difference in reference match probability is shown in yellow.

A catalytic mutant, Pus4 R286K, has similar levels of pseudouridylation as a *pus4*Δ strain

Since there were no major changes in pseudouridylation levels in [BIG⁺] cells across many different Pus4 targets, I wondered if pseudouridylation was dispensable for

the form and function of the $[BIG^+]$ prion. One way to assess if Pus4 catalytic activity was important for $[BIG^+]$, was to make a catalytically inactive Pus4. All the other functions of Pus4, except for pseudouridylation, would remain intact. A catalytic mutant had been made previously for Pus4's bacterial homolog, TruB (Friedt et al., 2014). A Pus4 catalytic mutant was made in the Garcia Lab using homology to TruB by changing arginine to lysine at position 286 (Pus4 R286K). To test if catalytic activity was reduced across tRNAs, I used direct tRNA sequencing and created heatmaps of reference match probabilities to compare tRNAs from a wild-type strain, a Pus4 R286K strain, and a *pus4* Δ strain (**Figure 2.4A**). The tRNAs from the Pus4 R286K and the *pus4* Δ strain showed an expected higher reference match probability at position 55 than from wild-type (**Figure 2.4A**). To see if any catalytic activity remained in the Pus4 R286K protein a subtractive heatmap was made showing the difference between the reference match probabilities of tRNAs from Pus4 R286K and *pus4* Δ (**Figure 2.4B**). The heatmap showed that pseudouridylation at position 55 was depleted to *pus4* Δ levels. (**Figure 2.4B**).

I also wanted to see if the Pus4 R286K mutant could pseudouridylate mRNAs. CLAP was performed on *TEF1* in the mutant strain to see if the ratio of Ψ_{239} to U₂₃₉ was decreased. As expected, there was a decrease in the amount of Ψ_{239} on *TEF1* in the Pus4 R286K mutant (**Figure 2.4C**). The amount of Ψ_{239} was reduced to background levels similar in intensity to *pus4* Δ from **Figure 2.1B**.

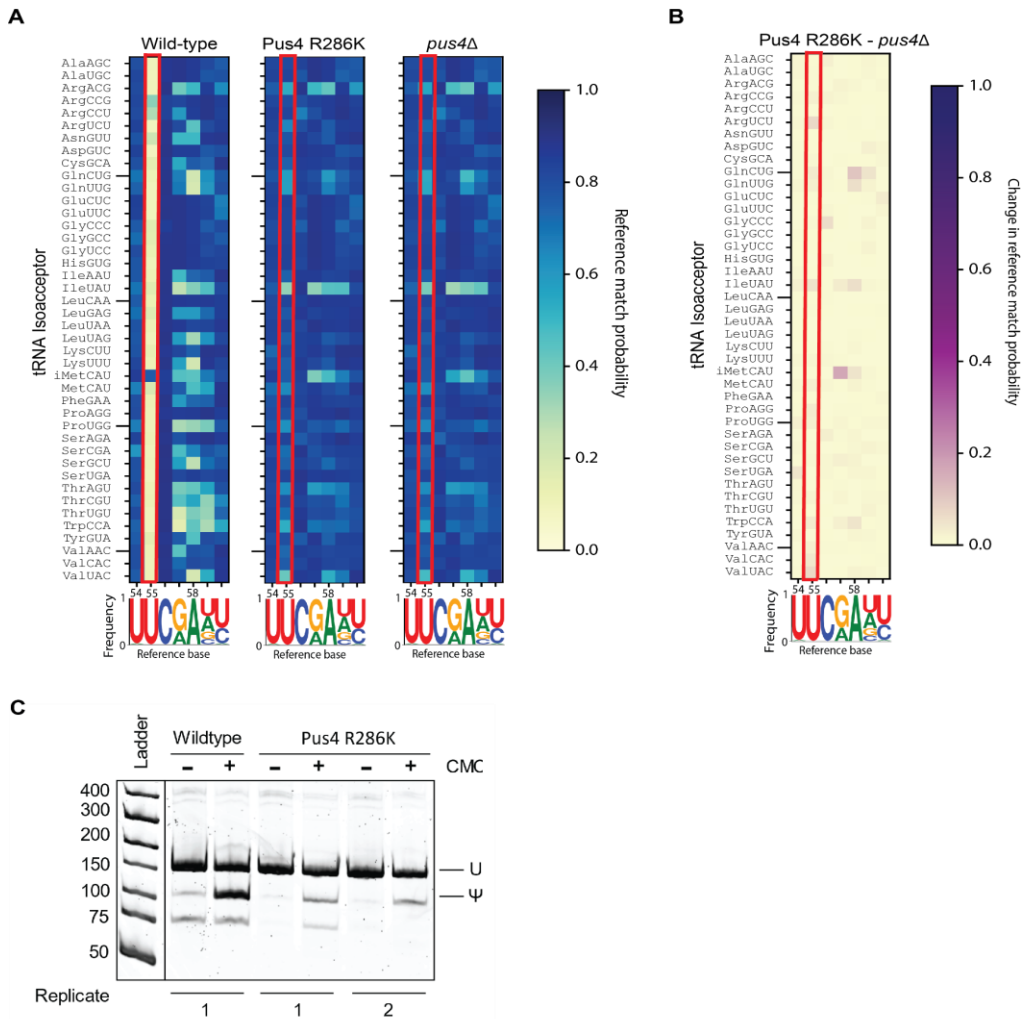


Figure 2.4. Pseudouridylation by Pus4 is reduced in the Pus4 R286K mutant across all tRNAs and on the *TEF1/2* mRNA. A) Heat maps showing a range of reference match probabilities across the T-loop of all cytoplasmic *S. cerevisiae* isoacceptors comparing wild-type, Pus4 R286K, and *pus4Δ* strains of yeast. The position of interest, U/Ψ55, is boxed in red on each heatmap. A high reference match probability (blue) shows the expected base was often called by the basecaller matching the reference sequence, and a low reference match probability (yellow) shows that a call was often made that did not match the reference sequence. The x-axis shows the position along the T-loop of a tRNA, and the sequence logo below represents how often a nucleotide is present in the reference at each position where the height of the letter corresponds to how often it is present. B) A subtractive heatmap showing the difference in reference match probability between Pus4 R286K and *pus4Δ* cells. A high difference in reference match probability between R286K and *pus4Δ* cells is shown in purple and a low difference in reference match probability is shown in yellow. C) Native PAGE showing the CLAP result for *TEF1/TEF2* mRNA from two replicates from Pus4 R286K yeast and wild-type yeast. Shorter bands indicating pseudouridylation that appear in CMC-unlabeled or *pus4Δ* samples may reflect either background signal from spontaneous cleavage near target site or Pus4p-independent modification of this site.

The [BIG⁺] prion can be initiated with Pus4 R286K

The presence of [BIG⁺] can affect the translation efficiency of certain mRNAs (Garcia et al., 2021). Previously, to assess the impact [BIG⁺] had on the translation of mRNAs composed of different codons, a luciferase assay was performed. Two different versions of a firefly luciferase gene were used: one that contained the normal suite of firefly mRNA codons, and a second that contained the least common codons throughout the *S. cerevisiae* genome for each amino acid. There was no significant increase in luminescence between [BIG⁺] cells and naïve cells when the luciferase gene with the standard codons was used (Garcia et al., 2021). However, [BIG⁺] cells produced about 50% more luciferase when the gene was composed of rare codons (Garcia et al., 2021).

To test if catalytic activity is necessary for the initiation of [BIG⁺], I attempted to induce [BIG⁺] formation by transiently overexpressing wild-type Pus4 or Pus4 R286K off a plasmid in wild-type yeast cells. Transient overexpression of a protein is a technique that is commonly used to induce the formation of yeast prions, and it has been used on Pus4 in the past (Chakrabortee et al., 2016; Derkatch et al., 1996; Liebman & Chernoff, 2012; Masison & Wickner, 1995). In this assay, cells experienced transient overexpression of Pus4 followed by growth in optimal conditions for ~50 generations for recovery. After, a luciferase assay was used as a way to see if the formation of [BIG⁺] had been successfully induced.

The luciferase assay was performed on cells that had either experienced prior overexpression of wild-type Pus4 or Pus4 R286K from a plasmid. As a control, a wild-type strain still received the same plasmid but the overexpression of Pus4 was not induced. A plasmid containing luciferase composed of rare codons or normal codons was

subsequently transformed into the yeast strains of interest. There was a slight increase of luminescence in strains of yeast that had experienced either wild-type Pus4 or Pus4 R286K overexpression from the plasmid with the normal suite of luciferase codons, but it was not statistically significant (**Figure 2.5**). However, when using the rare codons there was a significant increase in luminescence from both strains. (**Figure 2.5**). Importantly, this [*BIG*⁺] phenotype was induced when wild-type Pus4 or Pus4 R286K was transiently overexpressed. Pus4's catalytic activity was dispensable for the initiation of [*BIG*⁺].

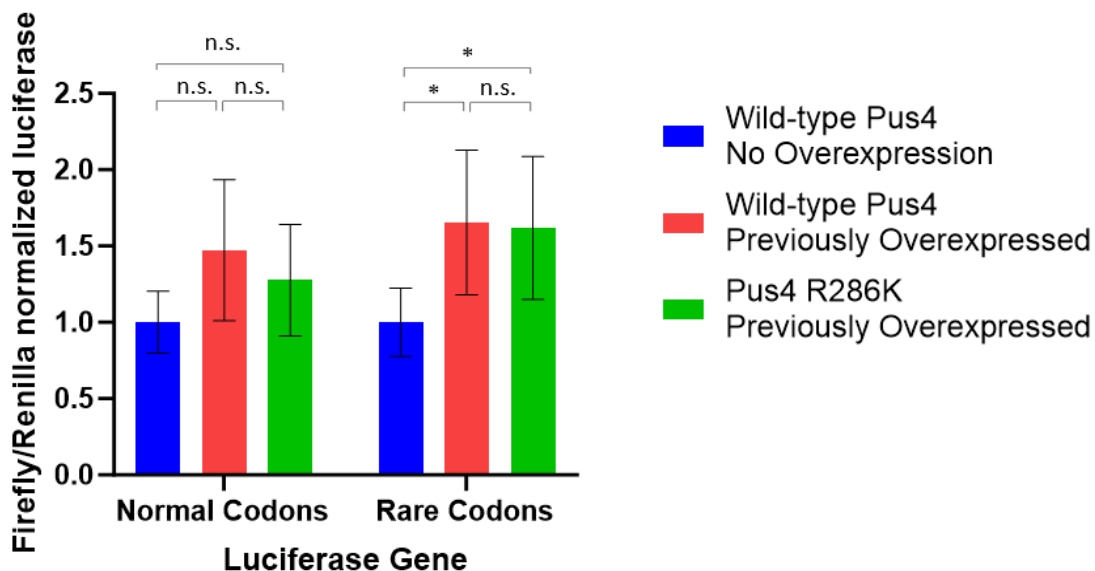


Figure 2.5. Catalytic activity of Pus4 is not required to induce [*BIG*⁺]. Luciferase assays were performed on yeast that had previously experienced an overexpression of wild-type Pus4 (red) or Pus4 R286K (green). These were normalized to the control data from yeast that did not undergo any overexpression (blue). The y-axis is showing luminescence from luciferase that is normalized to luminescence from renilla and to cell density (OD₆₀₀). The x-axis shows the type of codons that made up the luciferase gene. Luciferase with normal codons was made from the sequence originally found in the firefly genome, and the luciferase with rare codons was made up of the rarest codon in *S. cerevisiae* for each amino acid. The error bars represent standard deviation of 4 replicates from yeast that did not previously undergo an overexpression, and 16 replicates from both overexpressed wild-type Pus4 and Pus4 R286K. The significance was measured from an unpaired t-test and an * corresponds to a p-value<0.05.

Discussion

Yeast proteins that form prions self-template their new conformation onto their naïve protein counterparts (Kushnirov & Ter-Avanesyan, 1998; Wickner, 2016). In many examples, this leads to amyloid aggregates where the protein is sequestered away and unable to perform its normal biological function in the cell. However, [*BIG*⁺] does not seem to form amyloids (Garcia et al., 2021). This makes determining the mechanism driving the translation phenotypes observed in [*BIG*⁺] cells more challenging, as it's not from a simple loss-of-function of Pus4. It has been shown that another yeast prion, [*SMAUG*⁺], actually causes a gain-of-function phenotype, in which [*SMAUG*⁺] hyperactivates its function in degrading its RNA targets (Chakravarty et al., 2020). I hypothesized that a change in the pseudouridylation activity of Pus4 in [*BIG*⁺] cells could explain the altered translation observed.

I first tested pseudouridylation levels at position 239 on the mRNA *TEF1*, a target of Pus4. Tef1 is a translation elongation factor that binds to and delivers aminoacylated tRNAs to the ribosome. It has been shown that the presence of pseudouridine on mRNA can affect its capacity to be translated. If a change in pseudouridylation on *TEF1* could affect the amount of Tef1 protein produced, this could affect global translation. However, I saw that there was no significant change in the amount of Ψ_{239} on *TEF1* in prion cells.

Pus4 modifies position 55 on every tRNA except for the initiator methionine. This modification is conserved throughout life making it plausible that this modification is important for the form and function of tRNAs. A possible change in the structural stability of some tRNAs caused by a change in the amount of Ψ_{55} could have broad effects on translation efficiency. I was able to measure the levels of Ψ_{55} on every

cytoplasmic tRNA in *S. cerevisiae* and found that there were no significant differences in the amount Ψ_{55} between naïve and $[BIG^+]$ cells. It seems as if the conformational change from Pus4 to $[BIG^+]$ does not affect its catalytic activity. Additionally, when Pus4 catalytic activity was impaired, it still had the capability of forming the $[BIG^+]$ prion.

Catalytic activity appears to be dispensable for the initial formation of $[BIG^+]$. However, it is still unknown if catalytic activity is important for the continued propagation of $[BIG^+]$. In this study, a large number of catalytically inactive Pus4 molecules induced $[BIG^+]$ formation. After the transient overexpression, only wild-type, endogenous Pus4 remained to continue the production and propagation of the prion. In the future, it will be important to determine if catalytic activity is required for the propagation of $[BIG^+]$ and not just the initiation of the $[BIG^+]$ state. This experiment can be performed by knocking out the catalytic activity of endogenous Pus4 in a $[BIG^+]$ strain of yeast and then performing a luciferase assay to check for the presence of $[BIG^+]$.

It seems probable that pseudouridylation does not play a role in the formation of $[BIG^+]$ or the translational changes observed in $[BIG^+]$ cells. In the future I would like to determine how $[BIG^+]$ cells have an increased proliferation rate and enhanced translation. It is possible Pus4 has another function besides pseudouridylation that is altered in $[BIG^+]$. It has been shown that TruB, the bacterial version of Pus4, also acts as a tRNA chaperone along with being a pseudouridine synthase (Keffer-Wilkes et al., 2016). The change in conformation of Pus4 to $[BIG^+]$ could modify its chaperone capabilities while still maintaining catalytic activity. This can be tested by making a Pus4 mutant that lacks its ability to function as a tRNA chaperone without inhibiting its catalytic activity. I could then make this mutation in a $[BIG^+]$ strain to see if the $[BIG^+]$ cells revert to naïve.

Materials and Methods

Yeast strains

Strain	Phenotype	Genotype	Source
YDG1	Wild-type	MATa, <i>his3</i> Δ 1, <i>leu2</i> Δ 0, <i>met15</i> Δ 0, <i>ura3</i> Δ 0	This study
YDG127	Lacks Ψ_{55}	MATa, <i>PUS4</i> ::KanMX, <i>his3</i> Δ 1, <i>leu2</i> Δ 0, <i>met15</i> Δ 0, <i>ura3</i> Δ 0	Yeast Knockout Library (Giaever et al., 2002)
YDG162	[<i>BIG</i> ⁺]	MATa, <i>his3</i> Δ 1, <i>leu2</i> Δ 0, <i>met15</i> Δ 0, <i>ura3</i> Δ 0, [<i>BIG</i> ⁺]	Yeast Knockout Library (Giaever et al., 2002)
YDG630	Catalytically dead PUS4. Lacks Ψ_{55}	MATa, <i>PUS4</i> -R286K, <i>his3</i> Δ 1, <i>leu2</i> Δ 0, <i>met15</i> Δ 0, <i>ura3</i> Δ 0	This study

Yeast growth conditions

Yeast strains were struck out from the -80°C freezer onto YPD plates and grown for 2 days at 30°C. Three colonies were used to inoculate three culture tubes containing 3mL of YPD media. The tubes were grown overnight on a roller drum wheel at 30°C. The next morning the cultures were diluted in 5mL YPD media to an OD₆₀₀ of 0.1. The cultures were grown for ~6 hours at 30°C on a roller drum wheel to an OD₆₀₀ of ~0.8. The yeast was centrifuged in 15mL conical tubes at 3,000g and 4°C for 2 minutes. The

supernatant was removed, and the yeast was resuspended in 1mL of cold PBS and transferred to microcentrifuge tubes. The tubes were then centrifuged at 9500RPM for 1 minute at 4°C. The supernatant was poured out, and the microcentrifuge tubes were immediately placed into liquid nitrogen to flash freeze yeast in log phase.

Yeast plasmid transformation

Plasmids were transformed into yeast for overexpressing Pus4 to induce [*BIG*⁺], producing variable amounts of Pus4 to measure pseudouridylation, or measuring luciferase luminescence. Yeast was struck out from the -80°C freezer onto YPD plates and incubated at 30°C for 2 days. A colony was transferred into 4mL of YPD for an overnight growth in the 30°C incubator rotating on the wheel. The next day the culture was diluted to an OD₆₀₀ of 0.1 in 5mL of fresh YPD and left on the wheel at 30°C. About 5 hours later when the yeast had grown to mid log-phase, the cells were spun down at 3,000g. The media was decanted and the pellet was resuspended in 5mL of sterile TE. The cells were pelleted again at 3,000g for 3 minutes. The supernatant was decanted, and the pellet was resuspended in 5mL of LiOAc mix (50mL 1M LiOAc, 50mL 10x TE, and 400mL sterile water). The cells were spun down again at 3,000g for 3 minutes. The supernatant was decanted, and the pellet was resuspended in 0.5mL of LiOAc mix. In an eppendorf tube 1µg of plasmid in 10µL was added along with 10µL of 10mg/mL salmon sperm and 100µL of the yeast mixture. A control was also used with 10µL of water with no plasmid. After combining, 700µL of PEG mix (100mL of 40g PEG, 10mL 10x TE, 10mL 1M LiOAc, and sterile water) was added to the tube. The solution was pipetted up and down to mix. The tubes were incubated for 30 minutes at room temperature then 48µL of DMSO was added. The solution was mixed by pipetting up and down then

incubated for 15 minutes at 42°C. The yeast was spun down for 1 minute at 5,000RPM in the centrifuge, and the supernatant was pipetted off of the pellet. To wash the remaining PEG off of the yeast an additional 1mL of YPD was used to resuspend the pellet. The yeast was spun down one last time for 1 minute at 5,000RPM. The supernatant was pipetted off of the pellet, and the pellet was resuspended in 200µL of water. The yeast was then spread onto SD-URA plates with sterile glass beads to select for yeast that had taken up the plasmid.

Total RNA isolation

The yeast pellets, generated from cultures described above, were removed from the -80°C freezer and thawed on ice. The pellets were resuspended with 400µL of TES buffer made with a final concentration of 10mM Tris pH 7.5, 10mM EDTA, and 0.5% SDS. To lyse open the yeast cells, 400µL of acidic phenol was added, and the tubes were incubated for an hour at 65°C with 10 seconds of vortexing every 15 minutes. The lysates were placed on ice for 5 minutes and centrifuged at 13,000RPM for 10 minutes at 4°C. The top aqueous layer was transferred to a fresh tube followed by the addition of 400µL of chloroform. The solution was vortexed for 10 seconds and centrifuged once again at 13,000RPM for 10 minutes at 4°C. These steps were repeated one more time- the aqueous layer was removed, chloroform was added, and the tubes were vortexed and centrifuged. The aqueous layer was removed one last time into a clean microcentrifuge tube and 1/10 volume of 3M NaAc pH5.5 and 2.5 volumes of cold 100% EtOH were added. The tubes were incubated at -80°C for an hour and centrifuged at 13,000RPM for 10 minutes at 4°C. The supernatant was removed and 500µL of cold 70% EtOH was added. The tubes were centrifuged again at 13,000RPM for 10 minutes at 4°C, and the

pellet was resuspended in 25 μ L of water. Total RNA was then used for CLAP or for tRNA purification.

CLAP

CLAP was performed on total RNA isolated from wild-type/naïve cells, wild-type/[*BIG*⁺] cells, *pus4* Δ /naïve and Pus4 R286K/naïve cells. See (Garcia et al., 2021) for detailed protocol.

tRNA isolation

An 8% acrylamide gel was made using National Diagnostics SequaGel 19:1 Denaturing Gel System. The gel was pre-run at 45mA for 30 minutes. Total RNA was diluted to 10 μ L at 10 μ g/ μ L, and 10 μ L of 2x RNA Loading Dye (NEB) was mixed with the RNA. The RNA was incubated at 70°C for 8 minutes and loaded into the gel. The gel was run at 60mA for one hour in 1X TBE pH 8.3. It was removed from the gel apparatus and stained with SYBR Gold (invitrogen) for visualization on an Amersham Typhoon (Cytiva). tRNA was isolated by cutting the gel to select RNA from 60-85 nt in length. The gel fragments were placed into a microcentrifuge tube with 450 μ L of 0.3M NaCl and incubated on a tube inverter overnight at 4°C. The next day the liquid was transferred to a fresh microcentrifuge tube and 1.05mL of 100% EtOH was added. The tubes were incubated at -80°C for an hour and then centrifuged at 13,000RPM for 30 minutes at 4°C. The supernatant was removed, and the pellet was allowed to air dry for 10 minutes. The pellet was resuspended in 20 μ L of water, and the tRNA was stored at -80°C.

Nanopore sequencing of tRNA

See nanopore sequencing of tRNA in materials and methods of chapter III

IVT tRNA construction and sequencing

See IVT tRNA construction and sequencing in materials and methods of chapter III

Bioinformatic pipeline for heatmaps

Ionic current files were basecalled with Guppy v3.0.3 and aligned with BWA-MEM (parameters “-W 13 -k 6 -x ont2d”) to a custom BY4741 strain specific yeast isoacceptor reference generated using tRNAscan-SE (Chan et al., 2021; H. Li, 2013; Wick et al., 2019; Winston et al., 1995). Each isoacceptor reference also included the corresponding adaptor sequences (**Supplementary Table 12**). The FASTQ files were concatenated and processed to convert all “U” nucleotide calls to “T” (following analysis software will not work without this step). Alignments were then filtered to a mapping quality score of greater than one (Q1) using samtools (H. Li et al., 2009). Alignment and error hidden markov models (EM) for each experimental condition were produced with marginAlign and used to calculate posterior probabilities with the subprogram marginCaller (parameter “--threshold 0”) (Jain et al., 2015). The IVT alignment model was used for the “error model” in all experiments. This model incorporates mismatch, insertion and deletion information. The resulting posterior probabilities were visualized in heatmaps with matplotlib (Hunter, 2007).

Modifying Pus4 expression

SD-URA media was made with no sugar, so that varying concentrations of galactose and raffinose could easily be made. After sugar was added, the media always contained a total of 2% sugar composed of galactose, raffinose, or both. Media was made with 2% galactose, 0.2% galactose, 0.01% galactose, 0.005% galactose, 0.0025% galactose and 0% galactose.

A plasmid with Gal-inducible Pus4 (PDG112) was transformed into YDG127 (*pus4*Δ) following a standard yeast transformation protocol. This yeast was struck out onto SD-URA plates or YPD plates for a no plasmid control and incubated at 30°C for 2 days. Culture tubes with 5mL of YPD were inoculated with yeast colonies for an overnight incubation at 30°C. The next day the cultures were diluted into new tubes containing varying amounts of galactose to alter Pus4 expression. Once the cultures reached mid log-phase they were flash frozen, leaving enough yeast for a protein prep and for a total RNA isolation.

Protein preparation

Yeast pellets were removed from the -80°C freezer and placed on ice for a few minutes to thaw. The pellets were resuspended in 100uLs 20% TCA and transferred to a bead beater tube (Sarstedt 2 mL-screw top tube). About 100μL of sterile glass beads were added to each tube. The tubes were placed in the bead beater being very careful that the lids are screwed on tightly, and the tubes were shaken for 4 minutes. The tubes were briefly spun down in the centrifuge. The supernatant was transferred to a fresh microfuge tube. The beads were rinsed with 100uLs of 5% TCA, vortexed briefly, and briefly spun down in the centrifuge. The supernatant to the combined supernatant tube, and the bead washing was repeated again. The combined supernatant was spun down in the centrifuge for 10 min at 3000xg and 4°C. While the supernatant was in the centrifuge, 50uLs BME was added to 950uLs of SDS-PAGE loading buffer. After the spin, the supernatant was discarded by thoroughly pipetting off all liquid. The pellet was resuspended in 200μL of SDS-PAGE loading buffer. After the solution turns yellow, 75uLs of 1.5M Tris pH 8.8 was added and the solution turned blue again. The solution was then boiled at 95C for 3

minutes. The samples were spun down for 10 minutes at 3000xg and 4°C. The supernatant was transferred to a fresh tube, and the samples were stored at -20°C.

Western blot

First SDS-PAGE was performed to separate out total protein from the yeast protein prep. A stain-free 10 well 50µL gel was run with 1X SDS running buffer. Protein was transferred to a nitrocellulose membrane, blocked in a 5% milk solution in 1X PBS-T and probed for Pus4 using a 1:500 dilution of Invitrogen rabbit polyclonal anti-HA antibody as a primary antibody, and a 1:1000 dilution of Sigma goat anti-rabbit HRP conjugated antibody as the secondary antibody. The antibodies were diluted in 5% milk solutions in 1X PBS-T and each incubation in antibody was followed by three washes in 1X PBS-T. The blot was imaged on an Amersham Typhoon using Bio-Rad Clarity Western ECL Substrate.

[BIG⁺] induction

Yeast that contained either a plasmid with a Gal-inducible wild-type Pus4 or a Gal-inducible R286K Pus4 were struck out from the -80°C freezer onto SD-URA plates and grown for 2 days at 30°C. Three colonies were used to inoculate three culture tubes containing 3mL of YPD media. Colonies were transferred into 200µL of SD-URA w/ Raffinose in a 96 well plate. The plate was incubated at 30°C for 2 days. The plate was removed from the incubator and diluted 1:1,000 into a fresh plate with 200µL of SD-URA w/ Galactose or a control plate with 200µL of SD-URA w/ Raffinose for no overexpression. The plate was incubated for 2 days at 30°C. Yeast was then struck out onto 5-FOA plates in order to select for yeast that had dropped their plasmid. Colonies were then transferred to YP-Glycerol plates and SD-URA plates in order to check for

petite strains and to ensure that there was no plasmid. Yeast that had grown on the YP-Glycerol plates were used to make stock solutions that were stored in the -80°C freezer.

Firefly luciferase assay

Yeast strains of interest were struck out from the -80°C freezer onto YPD plates and incubated for 2 days at 30°C. Colonies were added into 4mL of YPD for an overnight growth step. The cultures were diluted to an OD₆₀₀ of 0.1 the next morning. Once the cultures reached mid-log phase, a standard yeast plasmid transformation protocol was followed. Two plasmids, either PDG 101 or PDG 102, were transformed into the strains containing a luciferase gene composed of rare codons or normal codons. Yeast cultures with the luciferase plasmids were made into glycerol stocks and stored in the -80°C.

Yeast strains containing a luciferase plasmid were struck out from the -80°C freezer onto SD-URA plates and grown for 2 days at 30°C. The colonies were transferred by a sterile stick into a 96 well plate with 150µL of SC-URA, and the side chambers were filled with water. The plate was incubated for 24 hours at 30°C. The next day, the yeast was mixed by pipetting up and down, and 10µL were transferred from each well to a new 96 well plate that had 140µL of fresh SC-URA media. The plate was placed in the 30°C incubator until the OD₆₀₀ had reached mid log-phase or an OD₆₀₀ of about 0.6. A new white 96-well plate (Greiner Bio-one) was obtained, and 40µL of 1x lysis buffer (Promega) was added in each well. After, 40µL of cells from the original 96-well plate was added into the lysis buffer. The plate was incubated at 25C and 300RPM for 30 minutes. While this was incubating 170ul of Stop and Glo substrate (Promega) was added to 8.5mL of the Stop and Glo solution in a 15mL conical tube. The conical tube was mixed by vortexing along with an additional conical tube with the LAR solution. The

Synergy H1 Microplate Reader (BioTek) with an injector module was primed with 2mL from the Stop and Glo and LAR solutions. Once the 96-well plate was done incubating, it was added to the Synergy H1 Microplate Reader and the luciferase reagents were added by the injector module and the luminescence was measured from each well.

Bridge

In chapter II, I compared pseudouridylation levels of Pus4 targets between [*BIG*⁺] cells and naïve cells using direct tRNA sequencing. I found that there were no differences in the levels of pseudouridylation. I became curious if I could detect other modifications in *S. cerevisiae* tRNAs using nanopore sequencing.

I explained in chapter I that tRNAs are the most densely modified RNA species. This makes detecting modifications more difficult than in other RNAs. In chapter III, I focused on optimizing our nanopore sequencing protocol to detect all the modifications in the T-loop of *S. cerevisiae* tRNAs- m⁵U₅₄, Ψ₅₅, and m¹A₅₈. I was also curious if these modifications were dynamic, so we grew cells to saturation to see if their modification levels would change under stress.

CHAPTER III

COMBINING NANOPORE DIRECT RNA SEQUENCING WITH GENETICS AND MASS SPECTROMETRY FOR ANALYSIS OF T-LOOP BASE MODIFICATIONS ACROSS 42 YEAST tRNA ISOACCEPTORS

This chapter contains work that is in review for publication. This work is co-authored by Ethan A. Shaw, Niki K. Thomas, Joshua D. Jones, Robin L. Abu-Shumays, Abigail L. Vaaler, Mark Akeson, Kristin S. Koutmou, Miten Jain, and David M. Garcia. My contributions included growing yeast, isolating tRNA, sequencing tRNAs, and aligning the sequencing data to our reference sequences.

Introduction

tRNA is the most densely modified RNA species in nature. Biochemical and biophysical methods have long been used to determine tRNA sequences and their modifications per isoacceptor (RajBhandary & Köhrer, 2006; Yoluç et al., 2021). Due to cost and time, however, these approaches are not scalable to the transcriptome. More recently, high-throughput sequencing methods that begin with reverse transcription of RNA, followed by PCR, have achieved tRNA sequencing at the transcriptome scale. With few exceptions (Behrens et al., 2021; Hernandez-Alias et al., 2023), these methods detect modifications individually in each sequenced tRNA. Nanopore direct-RNA sequencing (DRS) permits simultaneous detection of chemically modified nucleosides on individual, full-length, tRNA molecules (Begik et al., 2021b; Thomas et al., 2021).

Previously, we applied DRS to directly sequence full-length *E. coli* tRNA molecules, including all 43 isoacceptors (Thomas et al., 2021). Evidence for nucleotide modifications was observed in sequence miscalls when comparing molecules from wild-

type cells with synthetic tRNA controls containing identical canonical nucleotides. We and others have also demonstrated that base miscalls in DRS data can be associated with the presence of specific chemical modifications in mRNA, rRNA, and tRNA (Begik et al., 2021b; Lucas et al., 2023; Smith et al., 2019; Sun et al., 2023; Tavakoli et al., 2023; Thomas et al., 2021; White et al., 2023; Workman, Tang, Tang, Jain, Tyson, Razaghi, Zuzarte, Gilpatrick, Payne, Quick, Sadowski, et al., 2019). Given the importance of advancing Nanopore-based measurements for RNA (Alfonzo et al., 2021), particularly for eukaryotic tRNAs which are even more densely modified than tRNAs in prokaryotes (Boccaletto et al., 2022), cross-validation with appropriate biological controls is essential.

Among >50 distinct chemical modifications in eukaryotic tRNAs (Boccaletto et al., 2022; Jühling et al., 2009), 25 of them exist in the tRNAs of the budding yeast *Saccharomyces cerevisiae* (*S. cerevisiae*) (Boccaletto et al., 2022; Phizicky & Hopper, 2023). We examined closely-spaced, conserved modifications in the T-loop of 42 cytosolic tRNA isoacceptors in *S. cerevisiae* using Nanopore DRS. We focused on the T-loop (**Figure 1a**) for three reasons. (I) The T-loop in yeast tRNA isoacceptors contains three conserved chemical modifications: 5-methyluridine (m^5U , also referred to as “T” or “rT”, or ribo-thymidine), pseudouridine (Ψ), and 1-methyladenosine (m^1A). (II) These modifications occur in stereotyped positions on tRNAs across kingdoms (Machnicka et al., 2014). (III) T-loop modifications contribute to variations in thermostability for different isoacceptors (Roovers et al., 2021). In budding yeast tRNAs, m^5U and m^1A modifications have been documented only in the T-loop at stereotyped positions 54 and 58, respectively (Boccaletto et al., 2022). In contrast, Ψ has been documented both in the T-loop (position 55) and in other positions in many tRNA isoacceptors (Boccaletto et al.,

2022). Recently, Lucas et. al. (Lucas et al., 2023) published a method that improved throughput for Nanopore tRNA sequencing using yeast tRNA. Their work documented evidence of known T-loop modification circuits using a knockout strain that eliminated Ψ_{55} , across 30 isoacceptors. However, this study ascribed signals in their data to m^5U or m^1A without providing data from control yeast strains in which m^5U or m^1A were eliminated.

The work herein leverages more extensive use of yeast genetics along with sequence miscall-based machine learning classifiers to predict modifications in the T-loop across 42 yeast isoacceptors. We sequenced tRNA from yeast strains in which each one of the three enzymes responsible for modifying the T-loop was knocked out, as well as an *in vitro* transcribed (IVT) library of the same 42 isoacceptor sequences lacking all modifications. Using these data, we inferred the presence of Ψ_{55} and m^1A_{58} across all 42 cytosolic tRNA isoacceptors. Moreover, we observed that Ψ_{55} strongly influenced addition of m^1A_{58} on more isoacceptors, than has been previously documented for this modification “circuit” (Barraud et al., 2019; Lucas et al., 2023). A combination of total nucleoside LC-MS/MS analysis and tRNA sequencing by LC-MS/MS as orthogonal methods were used to validate or refute DRS-based inferences of modification status. We also devised an improved library preparation strategy to facilitate machine learning of modification-associated ionic current signatures. Synthesis of these approaches establishes a rigorous framework for analyzing multiple chemical modifications simultaneously in tRNA, advancing understanding of tRNA structure and function more broadly.

Results

Direct sequencing of yeast tRNAs

We sequenced the 42 tRNA isoacceptors—41 elongator tRNAs and 1 initiator tRNA—from the budding yeast cytosol using Nanopore DRS. By modifying the strategy we previously implemented for sequencing *E. coli* tRNA (Thomas et al., 2021) (see **Materials and Methods**), we isolated ~60-85 nt long RNA molecules from 100 µg of total RNA using PAGE. The total RNA pool was then ligated to oligonucleotide splint adaptors designed to anneal and ligate with mature tRNA NCCA-3' ends. This product was subsequently ligated to the Oxford Nanopore Technologies (ONT) RNA sequencing adapter (**Figure 3.1b**).

The adapted tRNA molecules were sequenced using ONT MinION R9.4.1 flow cells and Nanopore SQK-RNA002 kits. A representative tRNA ionic current trace is shown in **Figure 3.1c**. Segments corresponding to the adapters and the tRNA molecule were distinguishable because the ONT adapters, and part of the tRNA splint adaptors (both 3' and 5'), are composed of deoxyribonucleotides which have different amplitudes and translocation times than ribonucleotides. Conversion of ionic current patterns to nucleotide sequence base calls was performed using ONT Guppy software (version 3.0.3) (**Figure 3.1d,e**). This earlier Guppy version was chosen because it can infer sequence information from ionic current for short RNA molecules better than more recent versions (Thomas et al., 2021). Each tRNA DRS experiment yielded between 22,500 and 383,000 RNA reads per flow cell (**Supplementary Table 3.4**). The range in reads per flow cell was likely due to a combination of variation in tRNA adaptation, library preparation, and flow cell performance. We aligned reads to a curated set of yeast tRNA isoacceptor sequences (**Supplementary Table 3.5**) using the BWA-MEM aligner (H. Li, 2013).

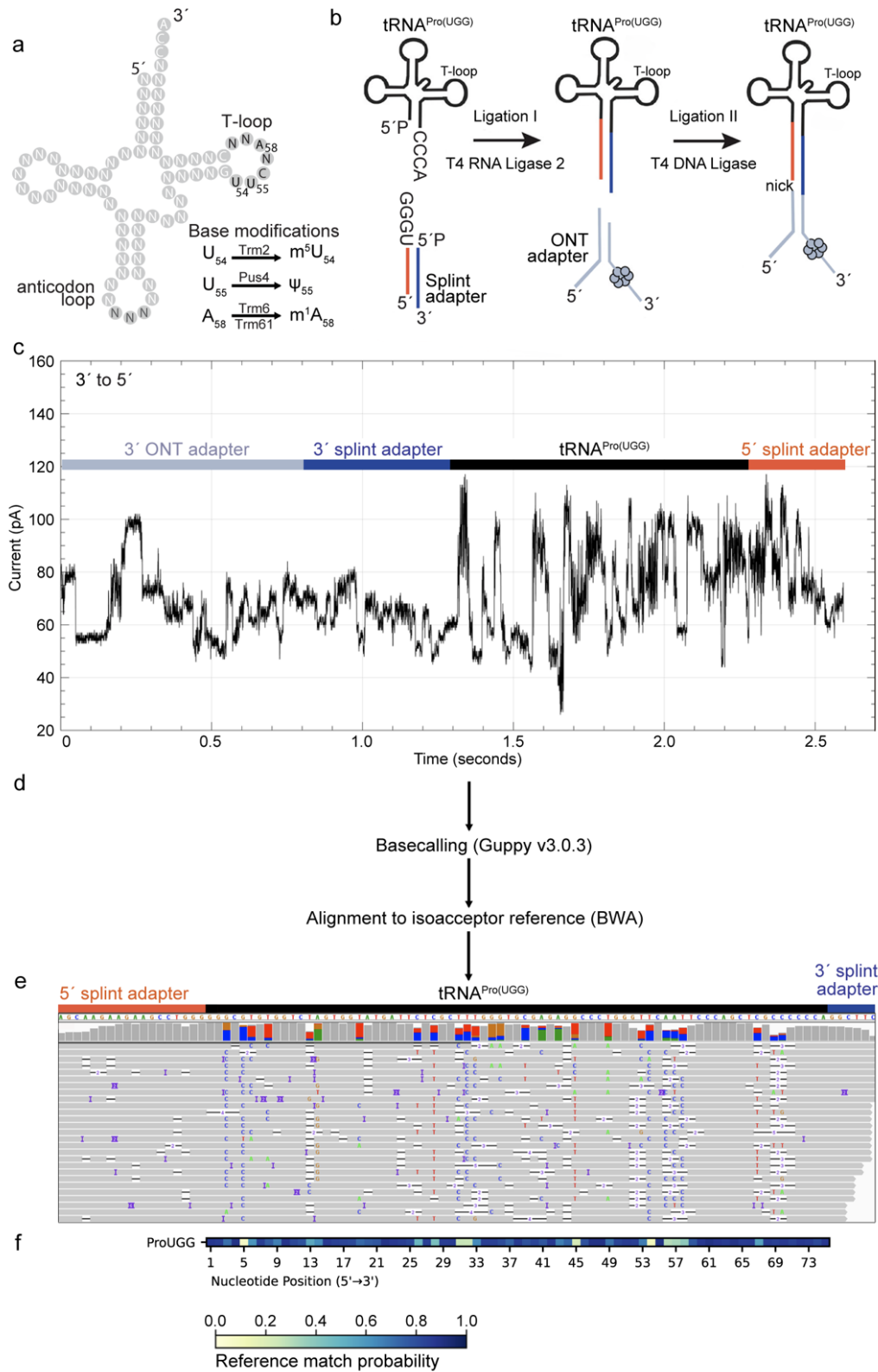


Figure 3.1. Overview of tRNA library preparation, sequencing, and alignment strategy. a) Illustration of a generic yeast tRNA, highlighting overall structural

segments, three chemical modifications that can occur in the T-loop and the names of the enzymes that catalyze them. **b)** tRNAs are ligated to a double-stranded splint adapter with RNA Ligase 2 by taking advantage of the tRNA's 3' NCCA overhang. A second ligation is performed using T4 DNA Ligase with the tRNA and ONT sequencing adapters. **c)** Ionic current trace measured in picoamperes for an adapted tRNA^{Pro(UGG)} molecule as it translocates from the 3' to 5' direction through a Nanopore. **d)** Ionic current is basecalled using Guppy v3.0.3. Fastq files are aligned to our *S. cerevisiae* reference sequences using BWA-MEM. **e)** Alignments are visualized in Integrative Genomics Viewer (29). The reference sequence for tRNA^{Pro(UGG)} is on the top. Read coverage is designated by the height of the gray bar at that position. In the panel containing gray or colored vertical bars, gray represents a match to the reference base for at least 80% of the reads, and colored represents the relative proportion of alternative nucleotide calls at that position. Colored bars (U/T=red; A=green; C=blue, G=gold) indicate positions where base call differs from the listed reference base. Rows below show alignments of individual reads with the reference, interrupted by: non-reference basecalls (colored letters); deletions (white spaces bisected with a black bar); and insertions (purple spaces bisected with a black bar). **f)** Reference match probabilities are calculated with marginCaller (27) and used to generate a heatmap, where the nucleotide position is shown from 5'–3' along the tRNA. Dark blue indicates that the base-called nucleotide matches the reference nucleotide more frequently given the alignment, and yellow indicates that the base-called nucleotide matches the reference nucleotide less frequently.

Each yeast strain derived tRNA DRS experiment yielded between 5,000 and 200,000 MAPQ1-aligned tRNA reads per flow cell (**Supplementary Table 3.4**). RNA reads that failed to align were likely due to: (i) inadequate training of the Nanopore base caller for short RNA molecules; (ii) the overall 86% median accuracy of the RNA base caller; and (iii) constraints in the alignment software when dealing with short, error-prone reads. The median alignment identity observed across all 42 tRNA isoacceptors was 83%, which is lower than the 90% median identity observed for biological poly(A) RNA (Jain et al., 2022). This was expected because tRNA have a much higher abundance and density of modifications compared to mRNA (Thomas et al., 2021). In contrast, the IVT total tRNA DRS experiment yielded ~500,000 MAPQ1-aligned reads, 91% of which aligned to full-length molecules, reflective of their complete lack of modifications (**Supplementary Table 3.4**). Importantly, most aligned tRNA reads from yeast cells (83–

93%) were full-length sequences (**Supplementary Table 3.4**). Among the four replicates of wild-type *S. cerevisiae* tRNA, the lowest number of aligned reads was between 3 and 106 for tRNA^{Ser(UGA)}, and the highest number ranged from 1,170 to 12,237 for tRNA^{Leu(CAA)} (**Supplementary Table 3.6, Supplementary Table 3.7**). A representative alignment of Nanopore reads for biological tRNA^{Pro(UGG)} is shown in **Figure 3.1e**. The "reference match probability" for each of the tRNA positions are shown in the heatmap compiled in **Figure 3.1f**. The values at each tRNA position in the heat map indicate the probability that a Nanopore base call matched the canonical unmodified reference nucleotide, measured using an error model based on mismatches, insertions, and deletions derived from IVT DRS data and other parameters (see **Materials and Methods**).

DRS detects conserved pseudouridine modifications in the T-loop of yeast tRNAs

To visualize base miscalls in the alignments of DRS data for yeast tRNA isoacceptors, we assembled composite heatmaps using reference match probabilities that were aligned at the tRNA 5'-end (nucleotide position 1, **Figure 3.2a**). The heatmap for wild-type yeast demonstrates that most of the tRNA sequences align as expected, yielding dark blue squares. However, a subset of positions across all tRNAs mismatch the reference nucleotide, yielding yellow-toned squares which indicate likely sites of modification. The heatmap for IVT tRNA sequences (**Supplementary Figure 3.1**), which accounts for mismatches that may result from certain canonical nucleotide sequence contexts, supports our claim that the majority of yellow and lighter-toned squares in the wild-type heat map result from sites of chemical modification. The most distinct of these miscall patterns was observed within the T-loop, outlined for each isoacceptor with white boxes in **Figure 3.2**.

Nucleotides at position 55 of the T-loop were the most consistently miscalled in 41 of the 42 isoacceptors. The one exception was tRNA^{iMet}, the only yeast tRNA known to lack a pseudouridine at that position (Simsek & RajBhandary, 1972). Therefore we reasoned that this miscall pattern was due to a highly conserved pseudouridine in tRNA (Ψ_{55}) (Takakura et al., 2019), as seen in our previously documented Nanopore DRS data for *E. coli* tRNA (Thomas et al., 2021). To test this, we sequenced tRNAs from a yeast strain (*pus4* Δ) that lacks the enzyme Pus4, that catalyzes conversion of U₅₅ to Ψ_{55} (**Figure 3.2b**). Miscalls at this position in this *pus4* Δ strain were significantly reduced. Other miscall patterns across the T-loop were also altered for some isoacceptors, suggesting that additional Pus4-dependent base miscalls occur at positions 57–59 (**Figure 3.2c**). Miscall patterns outside the T-loop were highly similar between the two strains, suggesting that Pus4 pseudouridylation did not influence other modifications elsewhere in any tRNAs.

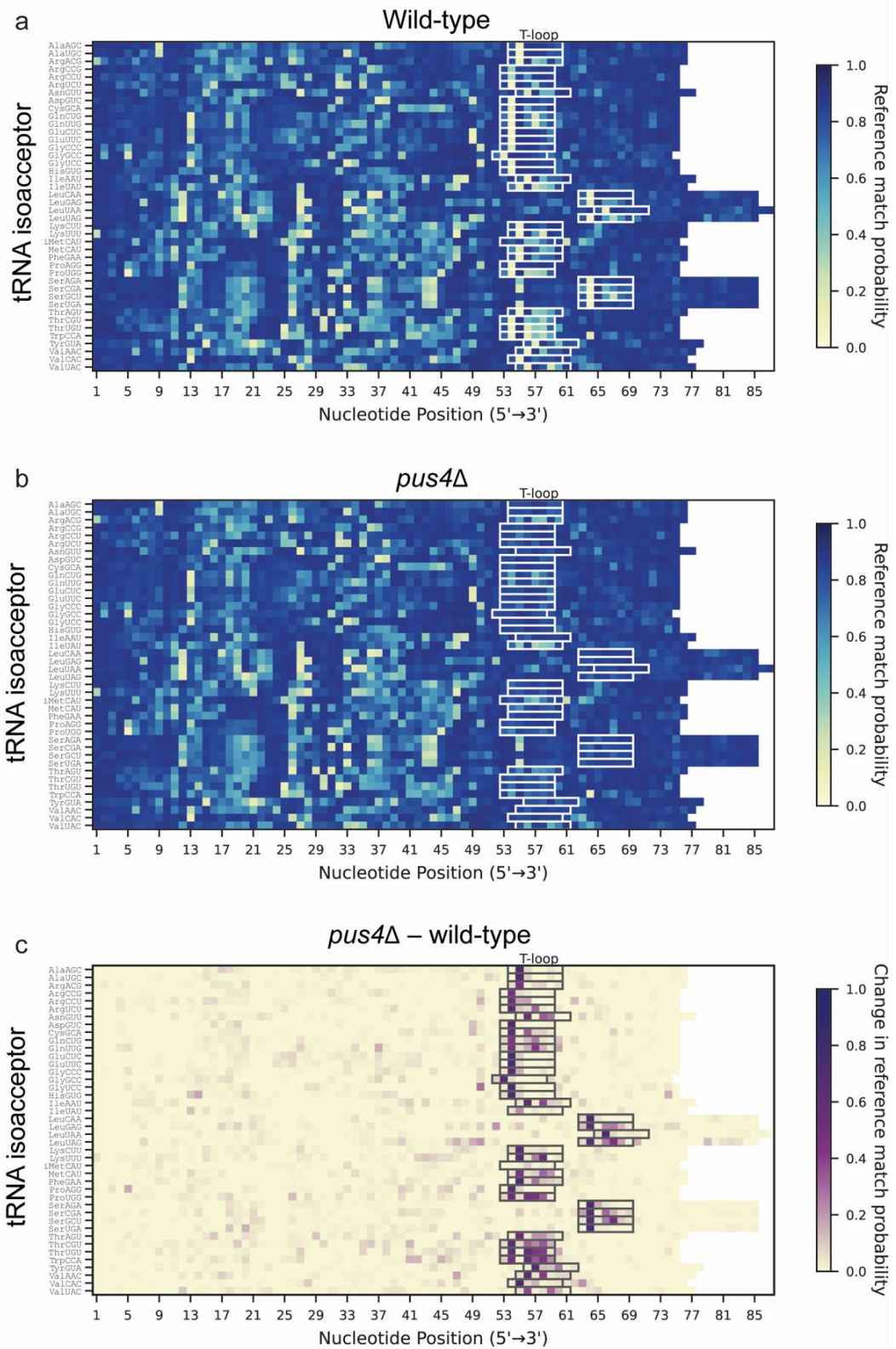


Figure 3.2. Heatmaps representing comprehensive alignments of 42 *S. cerevisiae* isoacceptors exhibit miscalls coincident with modified positions in the T-loop. a)

Wild-type (WT) aligned isoacceptors. A higher reference match probability (dark blue) corresponds to positions where the base-called nucleotide more frequently concurs with the reference nucleotide given the alignment, and a lower reference match probability (light yellow) corresponds to positions where the base-called nucleotide more frequently disagrees with the reference nucleotide. Note that tRNA^{His(GUG)} reads were aligned beginning with position (-1) due to non-templated addition at 5' end (33). The T-loop in each isoacceptor is outlined with a white box. While pseudouridine is present at the 55th nucleotide of many tRNAs, due to length differences 5' of this site, its actual position can vary from anywhere between the 54th nucleotide (e.g. tRNA^{Gly(GCC)} and many other isoacceptors) to the 66th nucleotide (e.g. tRNA^{Leu(UAA)}) of a given tRNA. **b)** *pus4*Δ aligned isoacceptors, otherwise as described above. **c)** The change in reference match probabilities between *pus4*Δ and wild-type aligned isoacceptors. As described above except that dark purple squares correspond to large differences in basecalls between tRNAs in the two strains and yellow squares show basecalls that are not different between the two strains, and for increased contrast the T-loops are outlined with gray boxes.

The T-loop is seven nucleotides in all yeast cytosolic tRNAs, with some positions being conserved and others variable (**Figure 3.3a,b** and **Supplementary Table 3.8**). To analyze systematic miscall patterns in T-loops, we anchored the wild-type and *pus4*Δ heatmaps to begin at the first nucleotide at the 5'-end of the T-loops of all isoacceptors (**Figure 3.3b**). This clarified the miscall pattern observed in **Figure 2** showing that *pus4*Δ lacks a miscall at position 55 and exhibits alteration in miscall patterns towards the 3'-end of the T-loop.

To verify that the catalytic activity of Pus4 was responsible for the loss of Ψ₅₅ and its associated miscall patterns, and not some other role of this enzyme, we generated a yeast strain that expresses a Pus4 protein containing an R286K mutation predicted to inactivate its catalytic activity. The mutation was based on homology to TruB, the bacterial homolog of Pus4 (Friedt et al., 2014) (**Supplementary Figure 3.2**). This *PUS4* R286K strain produced a miscall pattern nearly identical to cells missing the *PUS4* gene entirely (**Figure 3.3b**). Therefore, we concluded that the miscall patterns in the T-loop

were due to changes in tRNA modification status (U_{55}/Ψ_{55}), and not other activities of the enzyme itself.

DRS detects conserved 1-methyladenosine modifications in the T-loop of yeast tRNAs

While the miscall pattern observed at position 55 was wholly consistent with extensive prior literature documenting pseudouridine at that position in most tRNAs in nature (Becker et al., 1997; Boccaletto et al., 2022; Charette & Gray, 2000) (REF), we considered other possible explanations for the additional miscalls in positions 57-59. Nanopore sequencing errors arising from sequence context are unlikely to be responsible because wild-type, and *pus4* Δ and IVT tRNA isoacceptors have the same canonical sequences, and IVT sequences did not produce strong miscalls anywhere in the T-loops of all 42 isoacceptors (**Figure 3.3c**). We next examined if pseudouridine might lead to base miscalls at the level of nucleotide kmers and not individual nucleotides, as previously observed for m^7G in 16S rRNA in Nanopore data (Smith et al., 2019). However, the initiator methionine tRNA is not pseudouridylated at position 55 and miscalls proximal to the 3' side of the T-loop were still observed for this tRNA in both WT and *pus4* Δ data (**Figure 3.3b**). Furthermore, prior studies of Ψ using DRS in other types of RNAs have consistently observed single nucleotide miscalls matching known modified positions (Bailey et al., 2022; Begik et al., 2021b; Fleming et al., 2023; Smith et al., 2019; Tavakoli et al., 2023; White et al., 2023).

A biochemical explanation thus seemed most likely. Since the miscall pattern was consistently proximal to position ~58 (the 5th position of the T-loop), we reasoned that it might be due to the presence of a 1-methyl-adenosine modification at position 58 (m^1A_{58}) (Oerum et al., 2017). We grouped the tRNA isoacceptors in our T-loop heat map based

on prior evidence of m¹A₅₈ cataloged by Modomics, the widely used RNA modifications annotation database (*Modomics - A Database of RNA Modifications*, n.d.) (**Figure 3.3c**). In general, miscalls proximal to position 58 reported by Nanopore correlated well with Modomics annotations specifying the presence of m¹A modification (tRNAs in blue font) or its absence (tRNAs in red font). Yeast tRNA isoacceptors with unknown m¹A₅₈ status, according to Modomics, demonstrated a mixture of miscall patterns, with some predicting the presence of m¹A₅₈ and others predicting its absence (**Figure 3.3c**, wild-type, black font).

To determine the source of miscalls proximal to position 58, we compared basecalls from wild-type cells to basecalls from a yeast strain lacking the gene encoding the enzyme Trm6 (Anderson et al., 1998). Trm6 forms a methyltransferase complex with Trm61 to methylate the conserved A₅₈ (Anderson et al., 2000). The gene *TRM6* is essential due to the fact that tRNAs lacking m¹A₅₈ become destabilized and subsequently degraded by the Rapid tRNA Decay (RTD) pathway (Alexandrov et al., 2006), causing lethality. This defect can be suppressed via constitutive overexpression of one of four yeast iMet tRNA gene copies, whose encoded tRNAs are methylated by this complex that is important for their structural stability (Anderson et al., 1998). We sequenced this strain—*trm6*Δ, with high-copy plasmid *IMT4*, henceforth referred to as “*trm6*Δ”—in order to determine whether m¹A₅₈ was responsible for the pattern of miscalls at positions 57–59 in wild-type yeast. We observed that the *trm6*Δ strain produced nearly no miscalls at these positions in the T-loop of tRNAs that were previously reported to have m¹A₅₈ (**Figure 3.3c**). This strongly suggested that these miscalls observed in wild-type cells were due to m¹A catalyzed by the Trm6/Trm61 methyltransferase complex. Importantly,

the base miscall pattern observed at position 55 that results from pseudouridylation in wild-type yeast was maintained in *trm6Δ* cells. We also observed a similar pattern of base miscalls for a yeast strain lacking *TRM61*, that also inactivates the methyltransferase activity (Anderson et al., 1998) (**Supplementary Figure 3.3**). This suggests that pseudouridylation either precedes adenosine methylation, or that m¹A₅₈ modification does not appreciably influence Pus4 activity.

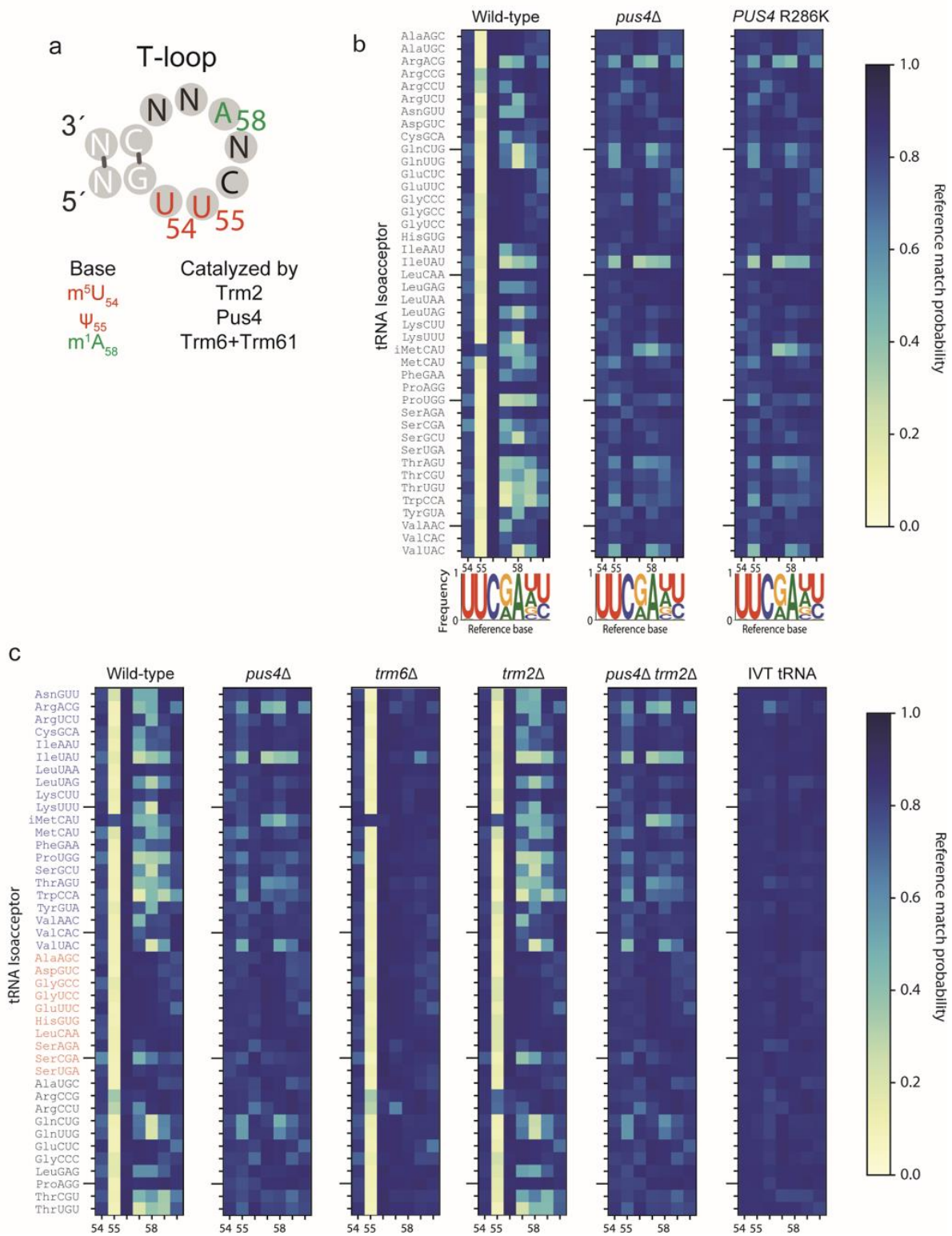


Figure 3.3. Reference match probabilities identify changes corresponding to modifications in the T-loop across 42 isoacceptor tRNAs. a) Illustration of a generic

yeast tRNA T-loop, including its three possible chemical modifications and the names of the enzymes that catalyze them. **b)** Reference match probability heat maps of aligned T-loop sequences across 42 isoacceptor tRNAs, in WT, *pus4* Δ and *PUS4* R286K strains. Conventional tRNA position numbers of modifications (m^5U_{54} ; Ψ_{55} ; m^1A_{58}) are shown below each plot. In the sequence logos below, the height of each unmodified nucleotide letter matches its frequency in shown tRNA sequences. (Note that for tRNA^{iMet}, in contrast to other 41 isoacceptors, positions 54 and 60 are adenosines, barely visible in the logo.) **c)** Reference match probability heat maps for tRNAs purified from WT, *pus4* Δ , *trm6* Δ , *trm2* Δ , *pus4* Δ *trm2* Δ strains, and *in vitro* transcribed (IVT) control sequences. tRNAs are ordered differently than in previous panels. tRNAs in blue letters are those annotated in Modomics (14) to contain m^1A in the T-loop; tRNAs in red letters are those annotated in Modomics to not contain m^1A in the T-loop; tRNAs in black letters are those not included in the current version of Modomics.

Agreement between m^1A_{58} annotations by DRS and other methods

We were able to detect m^1A_{58} in 24 of 42 cytosolic tRNAs via the changes in mismatch probabilities at positions 57–59 between wildtype and *trm6* Δ (**Supplementary Table 3.9, Supplementary Table 10**). We made these predictions using a ≥ 0.3 posterior probability cutoff, the default used by marginAlign. DRS corroborated 18 of the 21 tRNAs stated to contain m^1A_{58} by Modomics. Three tRNAs that did not match Modomics m^1A_{58} predictions were tRNA^{Leu(UAA)}, tRNA^{Lys(CUU)}, and tRNA^{Val(CAC)}. These tRNA were also not predicted to have m^1A_{58} by ARM-seq, a reverse transcriptase (RT)-based sequencing method (Cozen et al., 2015). Another RT-based method, mim-tRNAseq, previously revealed modest base misincorporation at position 58 for these three tRNAs during reverse transcription—corroborating Modomics status (Behrens et al., 2021). These differences could be due to sample or biological variation between experiments and differences in the limit of detection between different technologies. A recent Nanopore DRS-based study also associated base miscalls with T-loop modifications and observed overall agreement with Modomics annotations, however it did not perform

analysis to make specific assignments for which isoacceptors were predicted to have m¹A₅₈, nor did it provide a mutant lacking m¹A₅₈ for comparison (Lucas et al., 2023).

Modomics specifies that 10 tRNAs are *not* modified at position 58. Our DRS miscall-based predictions agreed for 9 of these 10 tRNA isoacceptors (**Supplementary Table 3.9**). The exception, tRNA^{Ser(CGA)}, was also reported to contain m¹A₅₈ by ARM-seq and mim-tRNAseq (Behrens et al., 2021; Cozen et al., 2015). Modomics does not report any chemical modifications for 11 additional tRNA isoacceptors—not only at position 58, but at any position—due to lack of prior experimental data. Using the ≥ 0.3 posterior probability cutoff from WT data (and excluding cases where this threshold was also exceeded in *trm6* Δ data), we predicted the presence of m¹A₅₈ on the Gln(CUG), Gln(UUG), Leu(GAG), Thr(CGU), and Thr(UGU) isoacceptor groups, and absence of m¹A₅₈ on Ala(UGC), Arg(CCG), Arg(CCU), Glu(CUC), Gly(CCC), and Pro(AGG). ARM-seq and mim-tRNAseq corroborate all 11 of these DRS-based predictions (**Supplementary Table 3.9**) (Behrens et al., 2021; Cozen et al., 2015).

5-methyluridine does not yield robust base miscalls in the T-loop

A recent study profiling tRNAs by DRS reported that 5-methyluridine (m⁵U) led to a significant amount of base miscalls in the first position of yeast tRNA T-loops (Lucas et al., 2023). We performed a m⁵U-specific mismatch analysis using our data, but accounted for three additional parameters that were not accounted for in that study. First, we used a genetic control in which the modification was eliminated (*trm2* Δ). Second, we addressed the potential miscall signal “bleed-through” from proximal modifications. Third, we accounted for DRS sequencing error by using IVT tRNA controls to establish a canonical RNA error model (see **Methods**) (Jain et al., 2015). We performed this analysis

using a randomly downsampled set of 120 reads per tRNA isoacceptor. At position 54, the median miscall probability was 0.16 in aligned reads from IVT data (**Supplementary Table 3.10**). For wild-type data, the median miscall probability at position 54 was 0.21 (**Supplementary Table 3.10**). For *trm2* Δ and *pus4* Δ strains, the median miscall probability at position 54 was 0.16 and 0.2, respectively (**Supplementary Table 3.10**). We argue that these base miscalls at position 54 cannot be confidently attributed to the m⁵U₅₄ modification because they fell within the bounds of DRS error, or a mismatch probability of less than 0.3. Software improvements for base calling and ionic current analysis will be required for a better identification of m⁵U₅₄ signatures in tRNA.

Even though m⁵U₅₄ did not result in a miscall pattern in Nanopore DRS, we reasoned that analysis of *trm2* Δ mutants lacking m⁵U could be used to investigate if this modification had an influence on catalysis of Ψ_{55} or m¹A₅₈. Loss of m⁵U₅₄ had little-to-no impact on the m¹A₅₈ base miscall signal (**Figure 3.3c**). There were no tRNA isoacceptors that had noticeably altered reference match probabilities proximal to position 58 in *trm2* Δ strains—i.e. the m¹A₅₈ status in *trm2* Δ strains appears unchanged for all isoacceptors. If biologically relevant changes in m¹A₅₈ did occur depending on m⁵U₅₄ status, they were under our threshold of detection comparing *trm2* Δ cells to wild-type using miscalls.

Loss of Trm2 alone did not appear to generally reduce the presence of Ψ_{55} across tRNA isoacceptors either (**Figure 3.3c**). Two possible exceptions, however, were tRNA^{Arg(CCG)} and tRNA^{Arg(CCU)} which have a reduced base mismatch probability at position 55 compared to wild-type cells. This suggests that they may have had lower levels of pseudouridylation when m⁵U₅₄ is absent.

Ψ_{55} promotes m¹A₅₈ installation in certain tRNAs

Several groups have reported evidence of coordination of RNA modifications in tRNAs, also referred to as modification “circuits” (Arimbasseri et al., 2016; Barraud et al., 2019; Barraud & Tisné, 2019; Benítez-Páez et al., 2010; Guy et al., 2012; Han et al., 2017; Han & Phizicky, 2018; Kimura et al., 2022; Lucas et al., 2023; Mörl et al., 1995; Müller et al., 2015; Rubio et al., 2006, 2017; Tuorto et al., 2018; Yamagami et al., 2016; Zhou et al., 2015). We reasoned that this phenomenon should be evident in our data because direct RNA sequencing can simultaneously profile multiple modifications on individual, full-length strands (e.g. Ψ_{55} and m^1A_{58}). Both m^5U_{54} and Ψ_{55} have been shown to influence addition of m^1A_{58} in yeast tRNA^{(Phe)GAA}, using purified enzymes and synthetic tRNAs (Barraud et al., 2019). To assess this possibility across the other 41 yeast tRNA isoacceptors, we analyzed mutants lacking each of the three T-loop modifying enzymes (Pus4, Trm2 and Trm6). Elimination of the Ψ_{55} lead to a strong reduction in the base miscalls attributed to Trm6 catalysis (**Figure 3.3c**). Ordering tRNAs by m^1A_{58} status helped identify at least four classes of tRNAs based on the role of Ψ_{55} in promoting m^1A_{58} modification (**Supplementary Table 3.11**). Class I contains a single example: the iMet tRNA, which does not have Ψ_{55} but does have m^1A_{58} . Therefore its m^1A_{58} is added independent of Ψ_{55} . Class II are tRNAs that have Ψ_{55} but lack m^1A_{58} . Therefore Ψ_{55} also has no influence on them being substrates for the Trm6/Trm61 methyltransferase complex. Class III are examples similar to tRNA^{Phe(GAA)} that have both Ψ_{55} and m^1A_{58} , and for which addition of Ψ_{55} appears to strongly promote m^1A_{58} catalysis. This was evident by the fact that when these tRNAs lose Ψ_{55} , they also have significantly diminished m^1A_{58} levels (**Figure 3.3c**, *pus4* Δ). Class IV are tRNAs with both Ψ_{55} and m^1A_{58} , but in which loss of Ψ_{55} does not appreciably reduce m^1A_{58} . These include

Arg(ACG), Ile(UAU), Thr(AGU), and Val(UAC) tRNAs. We note that these assignments are based on data in which cells are growing exponentially, and thus could vary under other conditions. Because previous reports indicated independent contributions of Ψ_{55} and m^5U_{54} on m^1A_{58} addition, we constructed *pus4 Δ trm2 Δ* . This double mutant lacks both Ψ_{55} and m^5U_{54} in the T-loop of all tRNA isoacceptors. The base miscall pattern proximal to position 58 generated by this mutant very closely resembled that of the *pus4 Δ* strain (**Figure 3.3c**).

Nanopore DRS reveals increased m^1A_{58} frequency on some tRNAs upon nutrient depletion

All data reported thus far were from yeast strains harvested during exponential growth in nutrient-rich media when the growth rate is maximal. To investigate if a different growth condition could affect T-loop modifications, we grew wild-type yeast cultures to saturation. Under these conditions, growth essentially stops as nutrients become limited. While base miscall patterns remained unchanged for most tRNAs in this sample (**Figure 3.4a**), some had noticeable differences. In particular, tRNA^{Lys(CUU)} showed a newly appearing pattern of base miscalls proximal to A_{58} that was absent from this tRNA in exponentially growing cells (**Figure 3.4a**). The miscall pattern was consistent with the miscalls present across other tRNAs that have m^1A_{58} . To test whether it was m^1A_{58} that caused this change, we grew *trm6 Δ* yeast to saturation and sequenced their tRNAs. In this strain the miscall cloud proximal to A_{58} disappeared, confirming that the change was due to an increase in m^1A_{58} catalyzed by Trm6 (**Figure 3.4b**). We also observed a similar pattern for the Arg (CCU), Leu (UAA) and Val (CAC) tRNAs. In summary, while these four tRNAs did not have observable base miscalls around position 58 in the cells grown

exponentially, we documented *TRM6*-dependent base miscalls after they reached saturation.

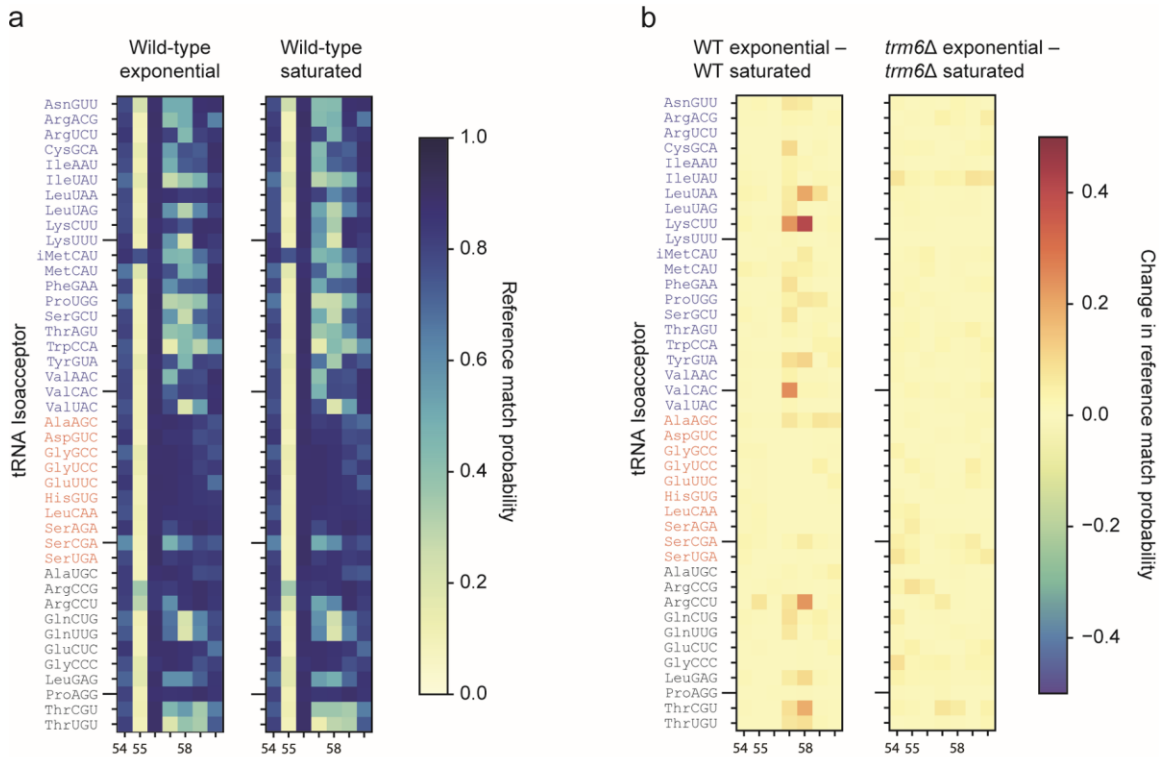


Figure 3.4. Nanopore reveals increased m¹A₅₈ frequency on some tRNAs upon nutrient depletion. a) Reference match probability heat maps of the T-loop in wild-type cells growing exponentially (reprinted from Figure 3c) or to saturation. Otherwise as displayed in Figure 3c. b) Bi-directional, differential reference match probability heat maps of the T-loop in wild-type or *trm6Δ* cells, comparing changes observed between exponentially growing and saturated cells. A positive change in reference match probability (red squares) indicates an increase in base miscalls during saturated phase. Comparison between heat maps indicates that several isoacceptors, most prominently tRNA^{Lys}(CCU), had increases in m¹A₅₈ during saturation that was catalyzed by Trm6.

We hypothesize that the proportion of these tRNAs that contain m¹A₅₈ varies under different growth conditions. This can range from being absent in exponentially growing cells to abundant in saturated cells. This may also explain variation in prior annotations for these specific isoacceptors. For example, depending on how cells are grown, the m¹A₅₈ signal may be more pronounced, while in other conditions the

magnitude of the miscall is under the minimum threshold. Previous studies report that m^1A_{58} plays a role in stabilizing tRNA structure (Droogmans et al., 2003; Horie et al., 1985; Oerum et al., 2017), and can prevent the degradation of the yeast iMet(CAU) tRNA (Anderson et al., 1998). Additionally, in mammalian cell lines it has been shown that m^1A_{58} levels respond to glucose availability (Liu et al., 2016). Thus, it is possible that in some tRNAs, the stress experienced by cells grown to saturation leads to an increase in m^1A_{58} .

Mass spectrometry measurements confirm and extend evidence of interrelated changes to tRNA modifications in mutant strains

To validate if the Nanopore sequencing miscalls in the T-loop were caused by the presence of Ψ_{55} and m^1A_{58} , we used LC-MS/MS as an orthogonal method to measure global modified ribonucleoside abundance. We purified total yeast tRNA from wild-type, *pus4* Δ , *trm6* Δ , *trm2* Δ , and *pus4* Δ *trm2* Δ yeast strains and then converted the complete tRNA molecules to mono-ribonucleosides using a two-step enzymatic digestion (Jones, Franco, et al., 2023). The resulting ribonucleosides were separated by reversed phase chromatography and quantified using multiple reaction monitoring on a triple quadrupole mass spectrometer. This method provides a broad quantitative picture of how the tRNA modification landscape is altered among different enzyme knockouts (**Supplementary Figure 3.4a**). It also allowed us to determine the relative purity of our tRNA samples by analysis of modifications known to be present in *S. cerevisiae* rRNA, but not tRNA (Boccaletto et al., 2022; Taoka et al., 2016). Two such modifications, m^3U and $m^1\Psi$, were found in 0.006% and 0% of nucleosides, respectively, in our wild-type samples, verifying that our tRNA samples had minimal contaminating rRNA fragments.

In wild-type total yeast tRNA, we documented that Ψ and dihydrouridine (D) were the most abundant ribonucleosides (**Figure 3.5a, Supplementary Figure 3.4b, Supplementary Table 3.12**), consistent with previous studies (Boccaletto et al., 2022; Brégeon et al., 2022; Xing et al., 2004). The amount of individual modified ribonucleosides matched expectations for each knockout: Ψ was considerably reduced in *pus4* Δ but not completely absent because other Pus enzymes can catalyze pseudouridine outside the T-loop in tRNA; m^1A was completely eliminated from *trm6* Δ cells, confirming that the A_{58} site in the T-loop was the only position modified by this enzyme; m^5U was completely eliminated from *trm2* Δ cells; and Ψ and m^5U were correspondingly reduced and eliminated, respectively, from *pus4* Δ *trm2* Δ cells (**Figure 3.5a**). The Nanopore sequencing results suggested that the global reduction in Ψ in *pus4* Δ by LC-MS/MS could be attributed to the loss of Ψ_{55} across all tRNAs. In summary, this provided direct physical and quantitative evidence that miscalls observed in DRS at position ~55 were due to Ψ_{55} and those at positions 57-59 in the T-loop were due to m^1A_{58} .

The total ribonucleoside LC-MS/MS data provided further evidence that knockout of RNA modifying enzymes broadly altered the tRNA modification landscape within the T-loop of total yeast tRNA. For example, in *pus4* Δ cells we detected a reduction in the abundance of m^1A by ~40% and m^5U by ~30% in addition to the reduction of total Ψ by ~30% (**Figures 3.5a,b**). For m^1A , this corroborated the DRS data, which showed a decrease in miscalls at positions 57-59 across many of the tRNA isoacceptors. For m^5U , this provided independent measurement of a modification that was not associated with a base miscall in DRS data, but did match previous observations of the influence of Ψ_{55} on

m^5U_{54} (Barraud et al., 2019). We also noted reciprocal and combinatorial effects for the other mutants— m^1A and Ψ were both modestly reduced in the *trm2* Δ cells, while the *pus4* Δ *trm2* Δ strain showed further decreases in the levels of Ψ and m^1A in comparison with either *pus4* Δ or *trm2* Δ alone (**Figure 3.5a**). We note that some changes in the mass spectrometry analysis of *trm6* Δ cells could be confounded by the dramatically altered relative abundances of tRNAs in this mutant (**Supplementary Table 3.7**). Together, these findings provide evidence for the importance of combining DRS analysis with an orthogonal physical measurement like LC-MS/MS of total ribonucleosides to provide a comprehensive and quantitative picture of the tRNA modification landscape.

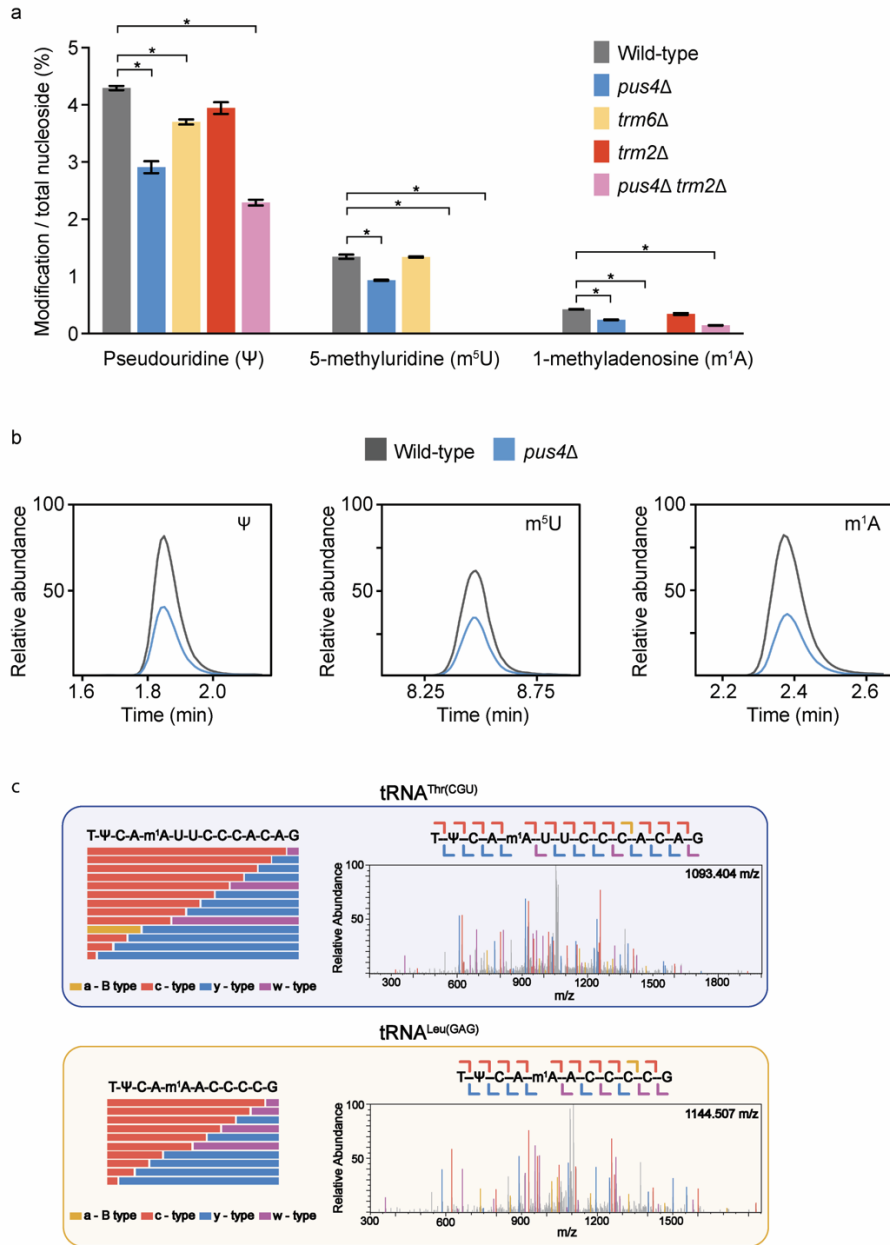


Figure 3.5. LC-MS/MS confirms DRS-based modification predictions. a) Modification abundance in wild-type (grey), *pus4Δ* (blue), *trm6Δ* (gold), *trm2Δ* (red) and *pus4Δtrm2Δ* (pink) total tRNA quantified using LC-MS/MS ribonucleoside modification profiling. Significant changes ($p < 0.01$) are noted with an asterisk. **b)** Extracted ion chromatograms of m¹A and m⁵U signals in wild-type (grey) and *pus4Δ* (blue) displaying a decrease in abundance in *pus4Δ* total tRNA. **c)** (left) Sequence coverage maps displaying sequence informative MS/MS fragmentation ions for m¹A containing oligonucleotide digestion products resulting from RNase T1 digestion of tRNA^{Thr}(CGU) and tRNA^{Leu}(GAG). (right) The respective MS/MS spectra for tRNA^{Thr}(CGU) and tRNA^{Leu}(GAG) are displayed where each detected sequence information fragmentation ion is displayed in gold (a-B type), red (c-type), blue (y-type), and purple (w-type).

Nanopore-based predictions of m¹A₅₈ sites are confirmed by LC-MS/MS-based direct tRNA sequencing

As described above, the base miscall profile associated with m¹A₅₈ was concordant with prior measurements for 27 out of 31 isoacceptors currently listed in the Modomics database. We did not predict m¹A₅₈ on tRNAs Leu(UAA), Lys(CUU) and Val(CAC), while Modomics does. Conversely, our DRS analyses did predict m¹A₅₈ on Ser(CGA) while Modomics did not.

For the 11 other isoacceptors not currently listed in Modomics, we used DRS miscalls to predict the status of m¹A₅₈, and then attempted to cross validate those using orthogonal methods. We first compared our data with mim-tRNAseq and ARM-seq and noted majority agreement among the predictions (**Supplementary Table 3.9**). We then confirmed the status of the m¹A₅₈ sites by analyzing data collected using “bottom-up” RNA sequencing methodology that performs direct sequencing of tRNA using LC-MS/MS (Jones, Simcox, et al., 2023). In short, wild-type yeast total tRNA was partially digested by RNase T1 to shorter oligonucleotide fragments that could be assigned to spectra with or without a unique set of modifications. Oligonucleotides were separated by hydrophilic interaction chromatography and sequenced using high-resolution MS/MS (**Supplementary Figure 3.4a**).

Direct sequencing of total yeast tRNA by LC-MS/MS confirmed the presence of m¹A₅₈ in 14 out of 21 tRNAs previously annotated to contain m¹A₅₈ in the Modomics database. Similarly, these assays failed to detect m¹A₅₈ on six of the ten tRNAs reported to lack m¹A₅₈ (**Supplementary Table 3.9**). For the 11 tRNAs lacking any prior annotations of modifications in the Modomics database, but for which our DRS data predicted five of them as having m¹A₅₈, this method was able to confirm two of those

five contained m¹A₅₈: tRNA^{Leu(GAG)} and tRNA^{Thr(CGU)} (**Figure 3.5c, Supplementary Table 3.9**). The nine remaining isoacceptors were either too low in abundance to be detected by this method or did not produce unique spectra.

Development of a model to predict T-loop modifications in tRNA

The heat map representation of reference match probabilities at positions along the tRNAs provided a qualitative analysis of cumulative miscalls and their association with modifications (**Figure 3.3**). To extend these qualitative results with statistics, we employed a support vector machine (SVM) to generate a classifier whose input is a T-loop miscall profile (see Methods). This could be used, for example, to generate a list of putative modification sites within the T-loop which could be verified with other methods. While tRNA modifications have been profiled extensively in yeast tRNAs, little is known about the modification landscape in nearly all other eukaryotic organisms.

The bounds for our analysis was a 9-mer window, composed of the seven nucleotide T-loop and one nucleotide upstream (guanosine) and one downstream (cytidine), as this base pair identity is conserved across all isoacceptors and its signal is likely to influence that in the terminal bases of the loop. Our training sets for the classifier consisted of: i) a “global” profile representing miscall data from all 42 wild-type isoacceptors; and ii) a series of 42 independent “local” profiles, representing miscall data from each individual isoacceptor (see **Methods**). These two classes of models were trained by assigning the status for a modification as being “present” or “absent”—a two-class classifier—based on existing Modomics annotations and our bottom-up LC-MS/MS data, but not the DRS data. We then used a reference match probability threshold of ≥ 0.3 on Nanopore data to make a prediction for whether a miscall could be associated with a

modification (see Methods). The labels in the testing set were assigned based on those predictions (**Supplementary Table 3.3**).

The classification accuracies of global models for predicting presence or absence of m^1A_{58} and m^5U_{54} on a tRNA isoacceptor ranged between 91-94% and between 51-57%, respectively (**Supplementary Figure 3.5a, Supplementary Table 3.3**). For reference, a 50% accuracy for a two-class classifier suggests that the model is unable to differentiate between them. Thus, due to the conclusions regarding the lack of miscall signal at U_{54} described above, the model did not predict the presence of this modification. The classification accuracies of isoacceptor-specific models for predicting presence or absence of m^1A_{58} and m^5U_{54} ranged between 51-92% (88% overall) and between 51-62% (56% overall), respectively (**Supplementary Table 3.3**). Accuracy values ~50% were observed for isoacceptors predicted to lack m^1A_{58} —this was expected as the signal profile in wild-type data closely matched that in *trm6* Δ , so the classifier chose each option equally. As observed for the global model, the local m^5U_{54} model accuracy remained poor because it could not distinguish between wild-type and the *trm2* Δ reads. We did not train a global model for Ψ_{55} because of the strongly correlated dependence of m^1A_{58} on Ψ_{55} , as observed in the in the *pus4* Δ strain described above. The isoacceptor-specific models to test the combined absence of Ψ_{55} and m^1A_{58} had a median accuracy of 70% (**Supplementary Figure 3.5b**). While most of the model accuracies are polarized at either 50% or near 100%, an intermediate accuracy of ~70% suggests that the modification at A_{58} may be intermittent in some tRNAs. Lastly, we trained models using miscalls over the entire T-loop, comparing between wild-type and IVT tRNA data. The

median accuracy for these models was 94% (global profiles) and 95% (isoacceptor-specific profiles)(**Supplementary Figure 3.5a,b**).

Extending adapter length for tRNA ionic current analysis

The analyses presented thus far allowed us to associate base miscalls with modifications in the T-loop. These associations were confirmed using genetic controls and LC-MS/MS. To make DRS analysis of tRNAs more quantitative, it would be desirable to use the raw nanopore ionic current signal for modification detection, as has been done for some rRNA and mRNA modifications. Presently, most DRS-based modification analysis tools use either Nanopolish (Workman, Tang, Tang, Jain, Tyson, Razaghi, Zuzarte, Gilpatrick, Payne, Quick, & Others, 2019) or Tombo algorithms (*Tombo: Tombo Is a Suite of Tools Primarily for the Identification of Modified Nucleotides from Raw Nanopore Sequencing Data*, n.d.) to convert the raw ionic current data into mean current amplitude (pA), standard deviation (pA), and dwell time (s) with 5-mers in individual aligned reads. This approach has been applied for detecting m6A (Leger et al., 2021)(Hendra et al., 2022; Pratanwanich et al., 2021), inosine (Chen et al., 2023; Nguyen et al., 2022), and pseudouridine (Huang et al., 2021), in longer RNA molecules. For tRNA, however, these approaches present challenges because the signal generated from the complete translocation of a tRNA through a flow cell pore is brief (typically <1s), relative to the Nanopore sequencing adapter that is composed of DNA bases that take longer to translocate through the pore (typically 2-4s). Since ionic current analysis tools like Nanopolish require RNA-based ionic current signal periods that exceed the length from the DNA-based adaptors (typically in excess of 4s), as a result,

the adapted tRNA molecules as presented above require further modifications in order for these programs to convert their raw ionic current signal into base calls.

To address this need, we extended the length of the splint adapters using RNA nucleotides to thereby increase the RNA-associated translocation time. This increased ionic current signal can sufficiently permit Nanopolish kmer-level alignments for yeast tRNA. For the 5'-tRNA splint adapter we increased the number of ribonucleotides from 18 to 120, and for the 3'-tRNA splint adapter we increased from 6 to 46 ribonucleotides (**Figure 3.6a**). We then sequenced wild-type yeast tRNA using these longer splint adapters. An example of the tRNA Pro^{UGG} isoacceptor with long adapters is shown in **Figure 3.6b**. When accounting for all 42 isoacceptors from this experiment, 10,901 single tRNA reads out of 47,612 total aligned reads, or 23%, could be analyzed by Nanopolish. In contrast, with the shorter adapters for wild-type tRNA samples, *zero* reads were amenable to Nanopolish analysis. In summary, use of these longer adapters on tRNAs demonstrate that it is possible to perform ionic current-based modification analysis for shorter RNA molecules. For future studies on tRNAs and other shorter RNA molecules, we therefore recommend using longer extended adapter sequences as we have here to enable ionic current analysis of tRNAs using existing software like Nanopolish. This will bring analysis of tRNA modifications into a truly “quantitative” realm.

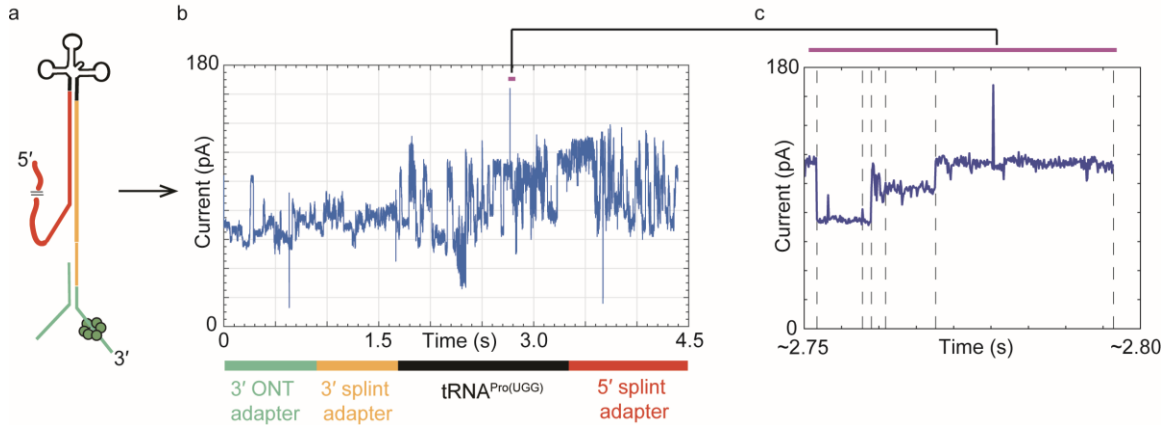


Figure 3.6. Longer adapters enable ionic current analysis using Nanopolish. a) An illustration of the adaptation method, derived from Figure 1 but using a longer RNA-based splint adapter. The 5' adapter is in red (120 nts), the 3' adapter in yellow (46 nts), and the standard ONT adapters in green. b) Ionic current trace from a single tRNA^{Pro}(UGG) molecule with long adapters. c) Nanopolish generated segmentation of the ionic current from panel b. The region between each pair of vertical dashed lines represents an ionic current segment associated with a 5-mer, assigned by Nanopolish.

Discussion

In this study, we leveraged Nanopore direct RNA-sequencing (DRS), LC-MS/MS, and yeast genetics to profile T-loop modifications across all 42 budding yeast cytosolic tRNA isoacceptors. Our results established the most comprehensive list of the Ψ 55–m1A58 T-loop modification circuit known from any species. Moreover, we discovered a novel nutrient-dependent increase in m1A58 on some isoacceptors. We also used bioinformatic analysis to build a T-loop modification classifier permitting prediction of modifications from DRS data, and we enhanced our protocol by extending adapter sequence lengths to enable direct ionic current analysis in the future.

Our study will draw obvious comparisons to a recent publication presenting “Nano-tRNAseq” (Lucas et al., 2023), due to similar methodology and results on yeast cytosolic tRNAs. The duplexed adaptor methodology presented in the current study was identical in design to our previous work on *E. coli* tRNAs (Thomas et al., 2021), whereas

the Nano-tRNAseq used a similar adaptor design but with an additional reverse transcriptase step to linearize the tRNA, which we did not perform. A major focus of the Lucas et al. paper was to improve throughput, which they achieved primarily by optimizing the data collection software settings. While both groups provided evidence for the ability of Nanopore sequencing to document previously identified T-loop modification circuits (Barraud et al., 2019), our study addresses this topic more thoroughly.

The study herein examined base calling errors in the T-loop in WT and in genetic knockouts for the three enzymes responsible for T-loop modifications. We also employed an error model based on IVT controls for all 42 isoacceptors, to generate posterior probabilities at each nucleotide position. In contrast, the Lucas et al. study used base calling rates in WT vs. *pus4* Δ to make its conclusions. They asserted that all the reported “crosstalks” (aka circuits), including Ψ 55 influencing addition of m5U54 and m1A58, were supported by their Nanopore data. In contrast, we show that only the Ψ 55 influencing m1A58 circuit is demonstrated in our Nanopore results. This is because the base calling error due to m5U54 is close to the background Nanopore error, which we show using data from a *trm2* Δ yeast strain. Moreover, our use of the *trm6* Δ strain, that removes m1A58, permitted clear delineation of the base calling error associated with this modification. This in turn provides evidence and prediction of the m1A58 modification in isoacceptors not yet documented in Modomics with regard to T-loop modifications. As both our and the Lucas et al. studies demonstrated, total nucleoside mass spectrometry measurements can improve interpretation of Nanopore sequencing results. Only our study, however, extended mass spectrometry analysis to a bottom-up RNA-sequencing

dataset, permitting direct validation of the position of modifications in specific isoacceptor T-loops that had been predicted by DRS.

Currently, *E. coli* and yeast are the only organisms for which the sequences, including many but not all modifications, of most of the tRNA isoacceptors are known, as referenced in the Modomics database. For other organisms, however, there remains a limited catalog of isoacceptor sequences and an even more limited catalog of their RNA modifications. Our study showcases the capability for DRS, particularly when supported with LC-MS/MS analysis and genetics, to measure the interdependence of multiple and closely spaced tRNA modifications at transcriptome scale.

Our multiclass model for predicting m1A in tRNA isoacceptors using base miscall information not only enabled our discovery that m1A58 is increased significantly on some isoacceptors in yeast cells undergoing nutrient starvation, but it promises utility beyond yeast. We note that human tRNA isoacceptors share significant identity in their T-loop sequences with those in yeast—approximately half of known human T-loop sequences share identical 7-mers to the yeast isoacceptors analyzed in this study. Therefore this type of classification model could permit analysis of T-loop modification dynamics or circuits in human tRNA. It is also possible that modification circuits that appear common in yeast T-loops may be conserved in other organisms. If so, it will be useful to have synthetic control tRNA molecules with different combinations of entailed modifications, for improved model training. And because it is possible that deletion of a modification catalyzing enzyme could enable other RNA modifying enzymes to ectopically modify the same position, or a neighboring position, LC-MS/MS will be essential for verification of modifications.

Forthcoming technological improvements will steadily address current limitations associated with tRNA analysis by Nanopore DRS. For example, tRNA sequence analyses are limited by baseline DRS base calling accuracy, and an ONT-sourced basecaller that is not specially trained on shorter RNA molecules, such as tRNAs. Median Nanopore DRS accuracy has improved from 86% in 2019 to 96% in 2023 (unpublished data, M. Jain, Northeastern University). In the current study we relied on comparison of reference match probabilities between different strains or conditions, but the numerical variation in probabilities at specific sites across different isoacceptors do not represent a quantitative measurement of the abundance of a modification. Ionic current analysis of tRNA molecules is essential for quantitative learning of signal differences between unmodified and modified nucleotides, and thus prediction of modification stoichiometry.

Measuring modifications in other segments of tRNAs by DRS, particularly the anticodon loop where they most directly influence protein synthesis, could yield additional insights into the coordination of tRNA chemical modifications across environments and organisms. The variety and combinatorial complexity of RNA modifications in these regions far surpass those in the T-loop. Therefore, at minimum, IVT controls, and biological controls that remove an RNA modification of interest are critical for interpreting how that modification influences the Nanopore signal. We propose that the combination of these controls, along with LC-MS/MS measurements, represent the “best practices” approach for analyzing RNA modifications using Nanopore DRS.

Materials and Methods

Yeast Strains

See **Supplementary Table 3.1** for the list of strains used in this study and their genotypes.

YDG973 was constructed from crossing haploids YDG221 and YDG963 (**Supplementary Table 3.1**). A colony from each haploid was patched onto either side of a YPD plate and mixed in the middle in an additional patch. The plate was incubated overnight at 30°C and replica-printed using sterile velvets to SD-Lys, SD-Met, and SD-Lys-Met dropout plates to select for diploids. A small globule of the cell mixture from the SD-Lys-Met plate was streaked to single colonies on a new SD-Lys-Met plate to obtain a clonal diploid.

The diploid was sporulated by inoculating single colonies into 3mL of YPD media and incubating on a roller drum wheel at 30°C for two days. The yeast was washed 2x with 1mL of SPO media before being resuspended in 3mL of SPO media. The diploid was incubated on a roller drum wheel at 25°C for 6 days. The tubes were collected and 500µL of sample was added to a microcentrifuge tube and spun down. The supernatant was removed and 200µL of digestion cocktail (10µL B-mercaptoethanol, 10µL zymolyase, 200µL KPO4 solution) was used to resuspend the pellet. The yeast was digested for 8 minutes at room temperature then placed on ice after adding an additional 200µL KPO4 to stop digestion. Yeast was spread onto a YPD plate and dissected with the Singer MSM System series 200. The spores were genotyped by PCR to obtain a haploid that was both *pus4*Δ and *trm2*Δ.

For making the Pus4 catalytic mutant and HA-tagged Pus4, CRISPR plasmids targeted to cut at the R286 codon of PUS4 and at the C-terminus of *PUS4* were made from pJH2972 (<http://www.addgene.org/100956>). CRISPR plasmid construction

followed the protocol as described in (Ranjith Anand, Gonen Memisoglu , James Haber, 2017). The oligos and gBlocks used for construction of the CRISPR plasmids and the repair templates were made by IDT. Sequences are shown in **Supplementary Table 3.2**.

To create a PUS4-R286K mutant in which the AGG arginine codon at the 286th amino acid position of PUS4 is replaced with a AAG lysine codon, PDG266 was transformed by lithium-acetate transformation into wild type BY4741 yeast (YDG1) along with an 83bp template containing the desired mutation with homology to the surrounding region. The transformation was plated on SD-Ura media. The plasmid was lost through growth on 5-FOA before proceeding with future experiments.

A 3xHA tag was inserted at the C-terminus of PUS4 using a similar procedure in which PDG342 was transformed into yeast along with a 170bp template containing the 90bp sequence of the 3xHA tag with 40bp of homology to the target site on either side. YDG1033 which contains both the R286K mutation and a C-terminal HA tag on PUS4 was created by using CRISPR to create the R286K mutation in the HA-tagged YDG989.

Yeast Growth Conditions

Yeast strains were struck out from the -80°C freezer onto YPD plates and grown for 2 days at 30°C. Three colonies were used to inoculate three culture tubes containing 3mL of YPD media. The tubes were grown overnight on a roller drum wheel at 30°C. The next morning the cultures were diluted in 5mL YPD media to an OD₆₀₀ of 0.1. The cultures were grown for ~6 hours at 30°C on a roller drum wheel to an OD₆₀₀ of ~0.8. The yeast was centrifuged in 15mL conical tubes at 3,000g and 4°C for 2 minutes. The supernatant was removed, and the yeast was resuspended in 1mL of cold PBS and transferred to microcentrifuge tubes. The tubes were then centrifuged at 9500RPM for 1

minute at 4°C. The supernatant was poured out, and the microcentrifuge tubes were immediately placed into liquid nitrogen to flash freeze. They were stored at -80°C. To grow yeast to saturation the same protocol was used, except strains were grown for ~72 hours.

tRNA Purification

The yeast pellets, generated from cultures described above, were removed from the -80°C freezer and thawed on ice. The pellets were resuspended with 400µL of TES buffer made with a final concentration of 10mM Tris pH 7.5, 10mM EDTA, and 0.5% SDS. To lyse open the yeast cells, 400µL of acidic phenol was added, and the tubes were incubated for an hour at 65°C with 10 seconds of vortexing every 15 minutes. The lysates were placed on ice for 5 minutes and centrifuged at 13,000RPM for 10 minutes at 4°C. The top aqueous layer was transferred to a fresh tube followed by the addition of 400µL of chloroform. The solution was vortexed for 10 seconds and centrifuged once again at 13,000RPM for 10 minutes at 4°C. These steps were repeated one more time- the aqueous layer was removed, chloroform was added, and the tubes were vortexed and centrifuged. The aqueous layer was removed one last time into a clean microcentrifuge tube and 1/10 volume of 3M NaAc pH5.5 and 2.5 volumes of cold 100% EtOH were added. The tubes were incubated at -80°C for an hour and centrifuged at 13,000RPM for 10 minutes at 4°C. The supernatant was removed and 500µL of cold 70% EtOH was added. The tubes were centrifuged again at 13,000RPM for 10 minutes at 4°C, and the pellet was resuspended in 25µL of water.

An 8% acrylamide gel was made using National Diagnostics SequaGel 19:1 Denaturing Gel System. The gel was pre-run at 45mA for 30 minutes. Total RNA was

diluted to 10 μ L at 10 μ g/ μ L, and 10 μ L of 2x RNA Loading Dye (NEB) was mixed with the RNA. The RNA was incubated at 70°C for 8 minutes and loaded into the gel. The gel was run at 60mA for one hour in 1X TBE pH 8.3. It was removed from the gel apparatus and stained with SYBR Gold (Invitrogen) for visualization on an Amersham Typhoon (Cytiva). tRNA was isolated by cutting the gel to select RNA from 60-85 nt in length. The gel fragments were placed into a microcentrifuge tube with 450 μ L of 0.3M NaCl and incubated on a tube inverter overnight at 4°C. The next day the liquid was transferred to a fresh microcentrifuge tube and 1.05mL of 100% EtOH was added. The tubes were incubated at -80°C for an hour and then centrifuged at 13000RPM for 30 minutes at 4°C. The supernatant was removed, and the pellet was allowed to air dry for 10 minutes. The pellet was resuspended in 20 μ L of water, and the tRNA was stored at -80°C.

Splint adapter preparation

The RNA and DNA oligonucleotides for the splint adapters were made by IDT. Their sequences are shown in **Supplementary Table 3.2**. Separate 10 μ M stock solutions of the five double stranded splint adapters were assembled in 1X TNE (10 mM Tris, 50 mM NaCl, 1 mM EDTA) by combining equimolar concentrations of the common adapter that abuts the 3' end of the tRNA, and one of five adapter strands complementary to the 3' tRNA overhang of ACCA, GCCA, UCCA, CCCA or CCA (see **Supplementary Table 3.2** for sequences). The splints were annealed by heating to 75°C for 1 min and then slow cooling to RT.

tRNA sequencing

250ng (~10pmol) of total tRNA was ligated to five different double-stranded splint adapters specific to ACCA (8pmol), GCCA (8pmol), UCCA (8pmol), CCCA

(4pmol) and CCA (4pmol) tRNA 3' overhangs (see **Supplementary Table 3.2** for oligonucleotide sequences). Prior to the ligation reaction, the tRNA was heated to 95°C for 2 min, placed at RT for 2 min, then placed on ice for 2 min. The first ligation was done in a total volume of 20µL and included, in addition to the tRNA and splint adapters, 1X RNA Ligase II buffer (NEB), 5% PEG 8000, 6.25 mM DTT, 6.25 mM MgCl₂, 2 mM ATP and 0.5 unit/µL T4 RNA Ligase 2 (NEB, stock concentration 10,000 U/mL, a total of 10 units per reaction). The ligation reaction was performed at RT for 45 min. The reaction was purified using magnetic beads (RNAXPClean, Beckman Coulter) using 1.8 X beads. The nucleic acid-bound beads were washed twice with 80% ethanol. The ligated tRNA was then eluted from the beads using 23µL of nuclease free (NF) H₂O. The second ligation to the RMX motor adapter was performed using the ligation 1 product, 8µL of 5X quick ligase buffer, 6µL of RMX and 3µL of T4 DNA ligase (2,000,000 units/mL) in a total volume of 40µL for 30 min at RT. The ligation 2 product was bead purified with 1.5X (60µL) RNAXP beads. The bead purification, elution of the library, flow cell priming and loading followed the SQK-RNA002 protocol. All sequencing was done on the minION platform.

Ligation with longer splints

With the goal of enabling current based analysis of tRNA, long splint adapters were employed. The long splints consisted of a 120 nt RNA 5' oligonucleotide which hybridized to the 3'NCCA end of tRNA and a common 60 nt strand composed of 46 RNA and 14 DNA nucleotides that abutted the 3' end of the tRNA. Ligation conditions were similar to the standard adapters with the following modifications. Following the first ligation the bead cleanup was performed with 1X RNAXP beads and washed with

70% Ethanol. Following the second ligation 0.8X rather than 1.5X bead concentration was used.

IVT tRNA construction and nanopore Sequencing

The DNA oligonucleotides for the IVT constructs were made by IDT. Their sequences are shown in **Supplementary Table 3.2**. Yeast IVT tRNAs were generated using the HiScribe T7 Quick High Yield RNA Synthesis Kit (NEB, E2050) similar to that done for *E. coli* tRNA^{Ala(UGC)} (1), but without gel purification. Two DNA oligonucleotides were used to make each IVT construct. A common 27 nt T7-promoter containing strand was used for all IVT tRNAs (**Supplementary Table 3.2**). For each of 42 tRNA isoacceptor types, a template strand was designed to hybridize with the common 27-nt adapter and to encode a transcript that included the 18 nt 5' RNA adapter sequences followed by the tRNA, followed by the 8 nt 3' RNA adapter sequences followed by a 3' 14 nt polyA tail (**Supplementary Table 3.2**). The sequence used for each isoacceptor was based on the sequences in GtRNAdb (gtRNAdb.ucsc.edu) (Chan & Lowe, 2016). For tRNAs with multiple isodecoders, we selected the sequence with greatest gene copy number as the representative isoacceptor. 200 pmol of the common 27mer and 50pmol of the template for each of the 42 tRNA IVT constructs were hybridized separately in 1X TNE (10 mM Tris, pH 8.0, 50 mM NaCl, 1 mM EDTA) by heating to 75C for 1min and slowly cooling to RT. One microliter of each of the 42 hybrids was pooled, and 7µL of this stock was used for the IVT reaction. The IVT reaction was run for 16hr at 37°C, DNase I treated for 30 min at 37°C, cleaned up with 1.3X RNAXP beads and eluted in 20µL nuclease free water. One microliter (934ng total, roughly 25ng for each IVT construct) of the reaction was sequenced following the SQK-

RNA002 protocol for mRNA sequencing. 1.3X and 1X magnetic bead volumes were used for cleanup following the RTA and RMX ligations, respectively.

Bioinformatic methods

Ionic current files were basecalled with Guppy v3.0.3 and aligned with BWA-MEM (parameters “-W 13 -k 6 -x ont2d”) to a custom BY4741 strain specific yeast isoacceptor reference generated using tRNAscan-SE (Chan et al., 2021; H. Li, 2013; Wick et al., 2019; Winston et al., 1995). Each isoacceptor reference also included the corresponding adaptor sequences (**Supplementary Table 3.2**). The FASTQ files were concatenated and processed to convert all “U” nucleotide calls to “T” (following analysis software will not work without this step). Alignments were then filtered to a mapping quality score of greater than one (Q1) using samtools (H. Li et al., 2009). Alignment and error hidden markov models for each experimental condition were produced with marginAlign and used to calculate posterior probabilities with the subprogram marginCaller (parameter “--threshold 0”) (Jain et al., 2015). The IVT alignment model was used for the “error model” in all experiments. This model incorporates mismatch, insertion and deletion information. The resulting posterior probabilities were visualized in heatmaps with matplotlib (Hunter, 2007). Other general alignment statistics were calculated with samtools and marginStats (**Supplementary Figure 3.1**).

The scikit-learn SVM package was used for machine learning of T-loop miscall error profiles under different genetic conditions (wild-type, *trm2* Δ , *pus4* Δ , *trm6* Δ , and IVT). Read IDs and basecalls from a 9-mer window, consisting of the T-loop (7-mer) and two adjacent up (G) and downstream (C) positions, were extracted from Q1 filtered alignment files. The T-loop basecall data were then split in a 60:20:20 ratio of training,

testing, and withheld sets, respectively. Two methods of classification were utilized on these sets; global and isoacceptor specific. Under global classification, training sets consisted of reads from all isoacceptors known to have the modification being assessed (Boccaletto et al., 2022). Under isoacceptor classification, training sets consisted of reads from only one isoacceptor at a time. For each condition, training reads were labeled as positive for the presence of a certain modification or negative for the presence of that modification depending on the literature, and testing reads were labeled based on qualitative heat map derived predictions. The prediction power of the models was assessed by calculating accuracy, ROI, and F1 score (**Supplementary Table 3.3**).

The marginCaller default posterior probability threshold to make an alternative nucleotide call is 0.3 (30%). However, marginCaller thresholds are only applied to a specific alternative nucleotide (Jain et al., 2015). Modifications do not always make consistent alternative nucleotide calls (e.g. the Ψ_{55} U to C miscall), so it is best to assess their miscall impact through the complementary probability to the reference (any alternative, also referred to as ‘mismatch probability’).

$$P(A') = 1 - P(A)$$

To determine this mismatch probability, we first extracted a random subset of 120 reads per tRNA isoacceptor from wild-type and IVT alignments. These subsets were run through marginCaller, and then posterior probabilities from positions affected by T-loop modifications were examined. In wild-type, if the mismatch probability was ≥ 0.3 , those tRNAs were considered to have statistically robust miscalls. IVT results served as a negative control, as none of the mismatch probabilities from canonical sequence met the cutoff requirements (**Supplementary Figures 3.2a,b**).

Global ribonucleoside modification profiling by LC-MS/MS

The RNA modification abundance of yeast total tRNA was quantified using a highly multiplexed targeted ribonucleoside LC-MS/MS assay as previously described (Jones, Franco, et al., 2023). Briefly, total tRNA (100 ng) was degraded to monoribonucleosides using a two-step enzymatic digestion. The RNA was first hydrolyzed to ribonucleotide monophosphates using 300 U/ μ g nuclease P1 (NEB, 100,000 U/mL) overnight at 37°C in 100 mM ammonium acetate (pH 5.5) and 100 μ M ZnSO₄. Following, the nucleotides were dephosphorylated using 50 U/ μ g bacterial alkaline phosphatase (Invitrogen, 150 U/ μ L) for 5 hrs at 37°C in 100 mM ammonium bicarbonate (pH 8.1) and 100 μ M ZnSO₄. Prior to use, the enzymes were buffer exchanged into their corresponding reaction buffers using a BioRad Micro Bio-Spin 6 size exclusion spin column to remove glycerol and other ion suppressing contaminants in the enzyme storage buffers. After the reactions, the samples were lyophilized and resuspended in 10 μ L of water containing 40 nM 15N₄-inosine internal standard.

The resulting ribonucleosides were separated by reversed phase chromatography and quantified using multiple reaction monitoring on a triple quadrupole mass spectrometer as previously described (Jones, Franco, et al., 2023).

LC-MS/MS bottom-up RNA-sequencing

This analysis was performed on wild-type commercial yeast total tRNA (900 μ g; Sigma Aldrich). The tRNA was digested to smaller oligonucleotide fragments using 100 U/ μ g RNase T1 (ThermoFisher, 1000 U/ μ L) in 220 mM ammonium acetate (unadjusted pH) at 37C for 1 hr in 600 μ L total reaction volume. The RNase T1 digestion was quenched by the addition of 600 μ L acid phenol:chloroform:isoamyl alcohol (125:24:1;

Supelco; 77619). The mixture was vortexed and centrifuged at 8,000 x g for 5 min. The aqueous phase was transferred to a clean microcentrifuge tube and washed with 600 μ L chloroform. The mixture was vortexed and centrifuged at 8,000 x g for 2 min. The aqueous phase was transferred to a clean tube. Quick calf intestinal phosphatase (NEB) was added to the resulting oligonucleotide digestion mixture to a final concentration of 0.13 U/ μ g. The mixture was incubated for 1 hr at 25°C. Following this, the dephosphorylation reaction was as described above for the RNase T1 digestions. The resulting oligonucleotides were precipitated with 2 μ L glycoblue, 65 μ L 3 M NaOAc pH 5.2, and 2 mL 100% ethanol.

Prior to LC-MS/MS analysis, the oligonucleotides were resuspended in 20 μ L 200 mM ammonium acetate (unadjusted pH), and 5 μ L of the mixtures was injected onto the column. The tRNA digestion mixture was separated by hydrophilic interaction chromatography (HILIC) on a Waters ACQUITY Premier BEH Amide VanGuard FIT column (1.7 μ m, 2.1 x 100 mm, 130A) on an Agilent Infinity II 1290 Bio liquid chromatograph equipped with an Agilent 1290 II DA detector. Mobile phase A was 25 mM LC-MS grade ammonium acetate (unadjusted pH) with 2.5 μ M medronic acid (Agilent InfinityLab Deactivator Additive) in 100% water, and mobile phase B was 25 mM LC-MS grade ammonium acetate (unadjusted pH) with 2.5 μ M medronic acid in 80:20 acetonitrile:water (unadjusted pH). The flowrate was 250 μ L/min and the column temperature was 55°C. The HILIC separation was interfaced to a ThermoFisher Orbitrap Fusion Lumos mass spectrometer. The electrospray ionization spray voltage was -2.8 kV, the sheath gas was 35, the aux gas was 10, the sweep gas was 0, and the RF lens was 50%. The ion transfer tube temperature was 350C and the vaporizer temperature was

350C. To sequencing oligonucleotides by MS/MS, data dependent acquisition (DDA) was performed using the Orbitrap for both precursor and product ion scans at 60 K and 30 K resolution, respectively. MS1 scans were collected over 300 - 2000 m/z with a maximum injection time of 100 ms and normalized automatic gain control (AGC) target of 120%. The MS2 scans were collected over 150 - 2000 m/z with a maximum injection time of 200 ms and normalized AGC target of 200%. Up to five precursor ions with charge state between 2-6 with a signal intensity above 25,000 counts were selected for a fragmentation scan. Precursor ions were isolated with a 2 m/z isolation window and were fragmented using collision induced dissociation with a collision energy of 35% and activation time of 10 ms. Following fragmentation, the ion was excluded for 3 seconds before being selected for fragmentation again.

LC-MS/MS data was analyzed using ThermoFisher BioPharma Finder 5.1. Oligonucleotide digestion product identifications were filtered to be within 10 ppm and greater than 90% to be confirmed a confident identification. The MS/MS spectrum of all identified oligonucleotides were manually inspected for proper monoisotopic mass deconvolution and high MS/MS quality.

Western blot

The Western blot showing expression of Pus4-R286K and wild type Pus4 from strains with a C-terminal HA tag on Pus4 was created by separating protein prepared using trichloroacetic acid lysis on a 4-15% gel in 1X SDS buffer. Protein was transferred to a nitrocellulose membrane, blocked in a 5% milk solution in 1X PBS-T and probed for Pus4 using a 1:500 dilution of Invitrogen rabbit polyclonal anti-HA antibody (SG77; 71-5500; Lot XH355482) as a primary antibody, and a 1:1000 dilution of Sigma goat anti-

rabbit HRP conjugated antibody (A6154; Lot SLCD6835) as the secondary antibody. The blot was probed for histone H3 as a loading control using a 1:2000 dilution of Abcam rabbit anti-H3 antibody (ab1791; Lot GR3297878-1) as the primary antibody and the same anti-rabbit secondary antibody. All antibodies were diluted in 5% milk solutions in 1X PBS-T and each incubation in antibody was followed by three washes in 1X PBS-T. The blot was imaged on an Amersham Typhoon using Bio-Rad Clarity Western ECL Substrate.

Bridge

I helped to optimize the use of direct RNA sequencing on *S. cerevisiae* tRNAs to study modification dynamics. Using yeast genetics, direct RNA sequencing, and mass spectrometry, Ψ_{55} and m^1A_{58} were both detected and the modification circuit between them was analyzed across every isoacceptor. Additionally, the amount of m^1A_{58} was shown to change on a few isoacceptors when yeast stopped growing under nutrient starvation. Furthermore, a new strategy was laid out to use longer adapters on tRNAs for future studies to allow ionic current analysis. In chapter IV, I summarize my findings from chapters II and III and write about the future directions for these studies.

CHAPTER IV

CONCLUDING SUMMARY

I originally hypothesized that there would be a change in Pus4-dependent pseudouridylation in [*BIG*⁺] cells that could explain their enhanced translation. I partially disproved this hypothesis by showing that there was no change in pseudouridylation between [*BIG*⁺] cells and naïve cells. There was no difference in pseudouridylation levels on the mRNA *TEF1* and across every cytoplasmic tRNA isoacceptor. However, changes to pseudouridylation levels on mitochondrial tRNAs and other Pus4 targets have not been ruled out.

Other mechanisms driving the amplified translation in [*BIG*⁺] cells now seem more likely. Pus4 could change its biophysical state when becoming [*BIG*⁺] causing associations with new proteins, or enhanced associations with a protein that Pus4 already interacts with. [*BIG*⁺] could have an altered interaction with a translation factor causing the translational program to be enhanced. If [*BIG*⁺] interacts with a protein affecting the ribosome quality control pathway it could cause proteins to be translated more quickly. The Garcia Lab has recently collected some evidence in support of this hypothesis showing that there is less ribosome stalling occurring on a GFP reporter in [*BIG*⁺] cells.

Alternatively, [*BIG*⁺] could be binding tRNAs differently. The bacterial Pus4, TruB, can act as a tRNA chaperone (Keffer-Wilkes et al., 2016). It's possible that Pus4 has a similar role in yeast. Pus4 may allow tRNAs to explore more conformations through its chaperone activity. After a change in conformation to [*BIG*⁺], this role could be enhanced or reduced. This would change the amount of tRNAs that are available to be

aminoacylated or brought to the ribosome, possibly causing widespread translational changes in the cell.

Learning more about the mechanism behind [*BIG*⁺] will further reveal a rare example of how protein synthesis can be epigenetically regulated. It will also move the field of prion biology forward, adding another example to the list of prions that can provide an adaptive advantage. Numerous prions have now been discovered in *S. cerevisiae* that can confer advantageous phenotypes raising the possibility that they have been selected through evolution as a general mechanism for adaptation to changing environmental conditions.

I also helped develop a method for detecting tRNA modifications in the T-loop of tRNAs. I used this method to investigate the important biology behind these tRNA modifications. I was able to check the validity of a known modification circuit where Ψ_{55} promoted the formation of m¹A₅₈ across every cytoplasmic isoacceptor in *S. cerevisiae*. I was also able to show that m¹A₅₈ was a dynamic modification in *S. cerevisiae*. When yeast were stressed from nutrient depletion, the amount of m¹A₅₈ increased on some tRNAs. Our study laid the important groundwork for identifying modifications through combining yeast genetics, mass spectrometry, and nanopore sequencing. This method of analysis was used exclusively on the T-loop of tRNAs. In the future, this analysis could be used to look at other parts of the tRNA.

Using this technique allows for the analysis of every modification that causes a change in the ionic current in the nanopore. Nanopore sequencing will eventually be used to look at many more modifications in other parts of the tRNA. Using this method to

detect tRNA modifications in *S. cerevisiae* will help us further understand their importance.

Eventually, we could also sequence tRNAs from other organisms. In humans there are 429 distinct tRNA genes, and there is evidence that around half of them can be transcribed (Chan & Lowe, 2016; Kutter et al., 2011). Each of these tRNAs needs to be extensively modified making the production of RNA modifying enzymes an important priority for a cell to function. Mitochondrial diseases, neurological disorders, cancers, and type 2 diabetes have all been linked with aberrant tRNA modifications (T. Suzuki, 2021). Quickly and effectively quantifying modification levels across tRNAs could help in the diagnosis of diseases.

The most promising method to quantify tRNA modifications across a pool of different isoacceptors is nanopore sequencing. It is relatively quick, and it requires a low input of tRNA. However, there is a long road ahead for researchers before this could be used as a diagnostic method in humans. So far, there have been 39 different tRNA modifications identified in human cytoplasmic tRNAs (de Crécy-Lagard et al., 2019; Jühling et al., 2009). The modifications range from a simple isomer of a base, like pseudouridine, to the addition of a long chain of over 10 new atoms, like wybutosine. Being able to identify them all through nanopore sequencing will be a challenge.

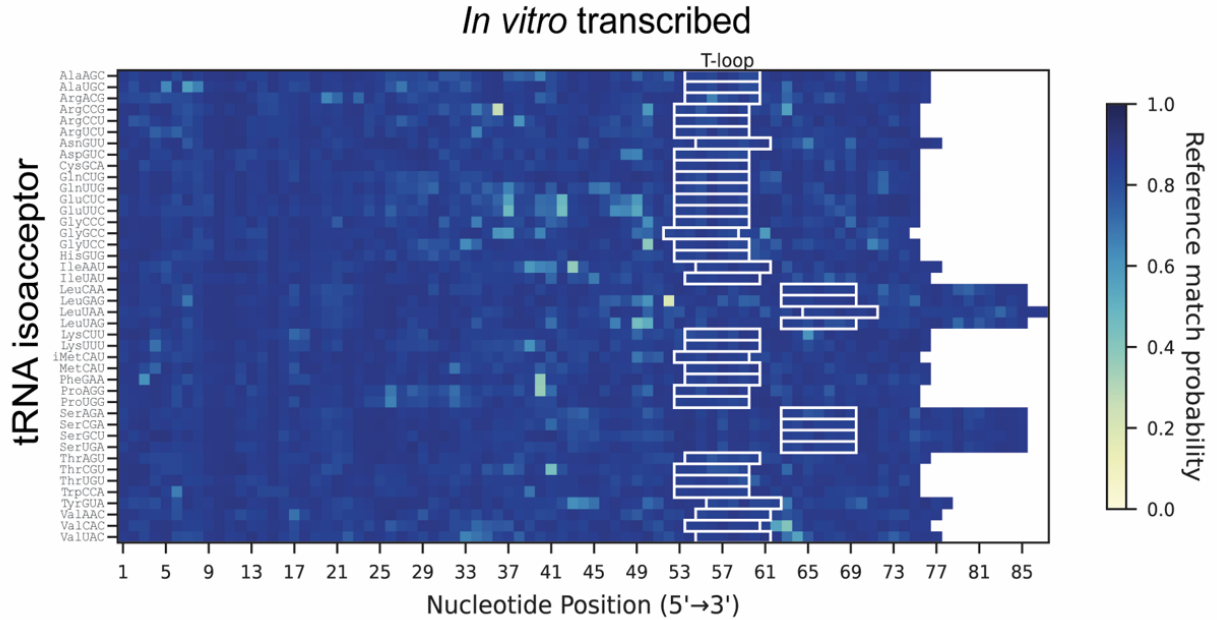
During nanopore sequencing the ionic current flowing through the nanopore is disrupted in a characteristic manner to allow the basecaller to distinguish the four different canonical RNA bases. Five nucleotides are flowing through the nanopore at any given time, so at any point the ionic current will depend upon the two nucleotides upstream and downstream of each nucleotide being basecalled. Some modifications can

influence the ionic current more than others affecting not only the basecall on itself but also for the surrounding nucleotides. Additionally, on tRNAs modifications are frequently close to each other which makes accurate basecalling even more difficult. It will be a massive undertaking to make a basecaller that could recognize each modification, but it is something that should be done. Detecting the position of each modification and quantifying how much is present will help us better understand the significance of epitranscriptomics in biology.

APPENDICES

APPENDIX A

SUPPLEMENTARY FIGURES FOR CHAPTER III

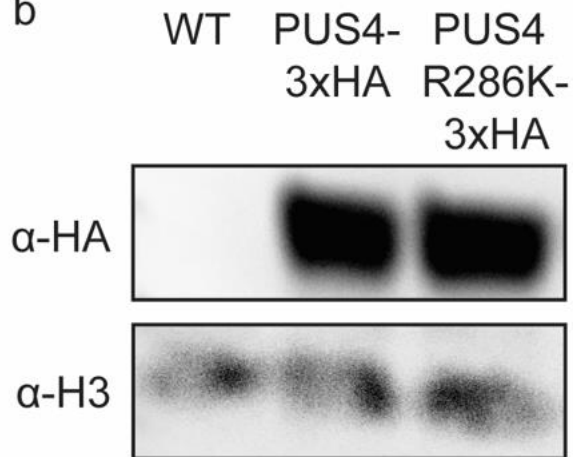


Supplementary Figure 3.1. Heatmap representing IVT tRNA sequences of 42 *S. cerevisiae* isoacceptors. A higher reference match probability (dark blue) corresponds to positions where the base-called nucleotide more frequently concurs with the reference nucleotide given the alignment, and a lower reference match probability (light yellow) corresponds to positions where the base-called nucleotide more frequently disagrees with the reference nucleotide. Note that tRNA^{His}(GUG) reads were aligned beginning with position (-1) due to non-templated addition at 5' end (7). The T-loop in each isoacceptor is outlined with a white box. While pseudouridine is present at the 55th nucleotide of many tRNAs, due to length differences 5' of this site, its actual position can vary from anywhere between the 54th nucleotide (e.g. tRNA^{Gly}(GCC) and many other isoacceptors) to the 66th nucleotide (e.g. tRNA^{Leu}(UAA)) of a given tRNA.

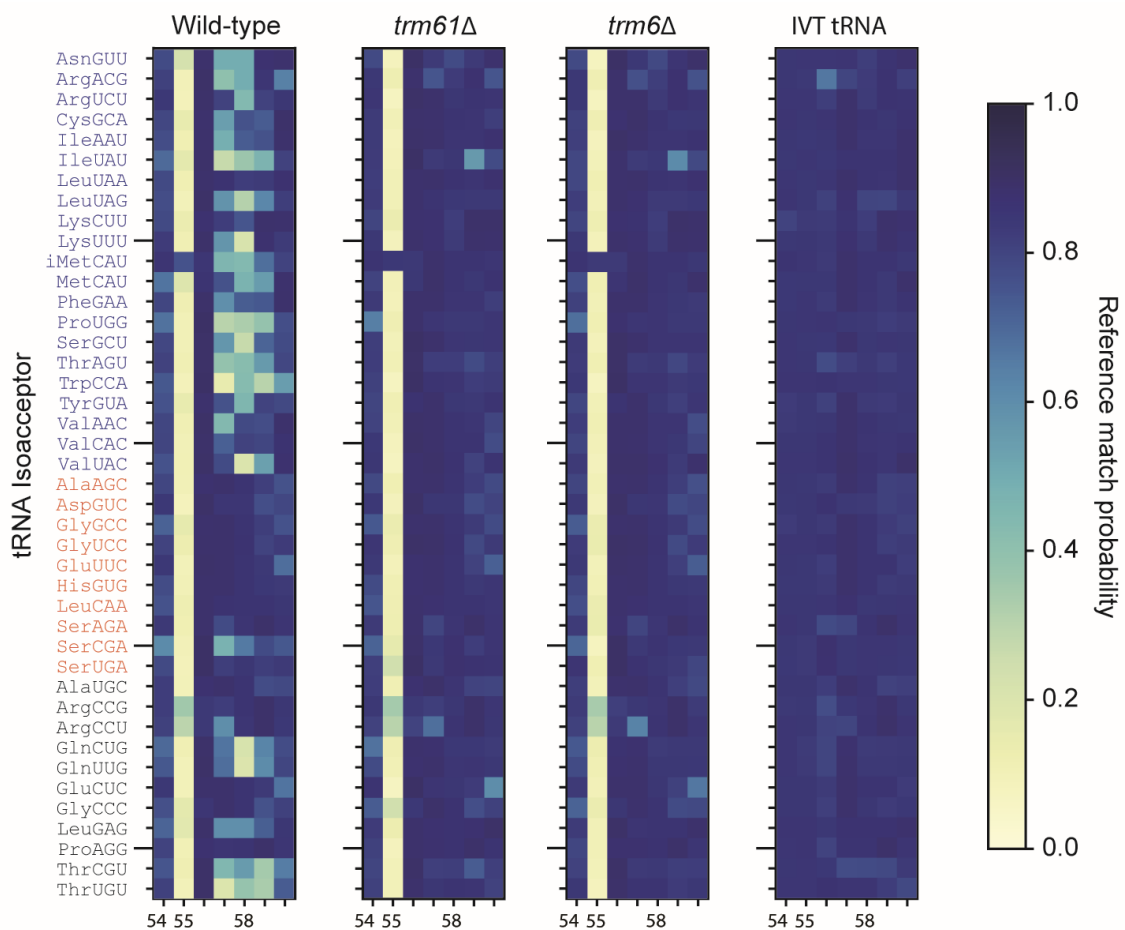
a

Ψ55-synthase catalytic residue			
<i>S. cerevisiae</i>	Pus4	SSGTYI R SLVSDIG	R286
<i>E. coli</i>	TruB	SKGTYI R TIIDDLG	R181
<i>H. sapiens</i>	TRUB1	GGGFYI R SLVSDIG	R256

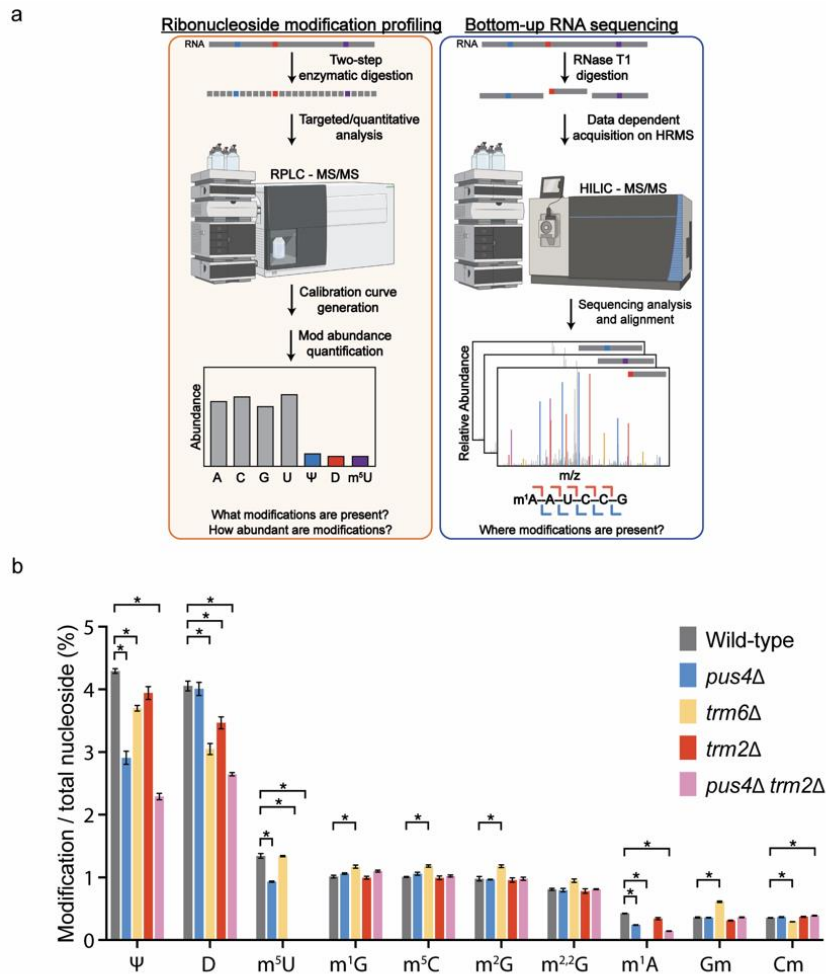
b



Supplementary Figure 3.2. Pus4 catalytic mutant. a) Protein sequence alignment of Pus4 and its *E. coli* and human homologs showing the conserved catalytic arginine that was mutated to a lysine in the Pus4-R286K catalytic mutant. b) Western blot showing expression of HA-tagged Pus4-R286K catalytic mutant is comparable to HA-tagged wild-type Pus4. Histone H3 protein is probed as a loading control.

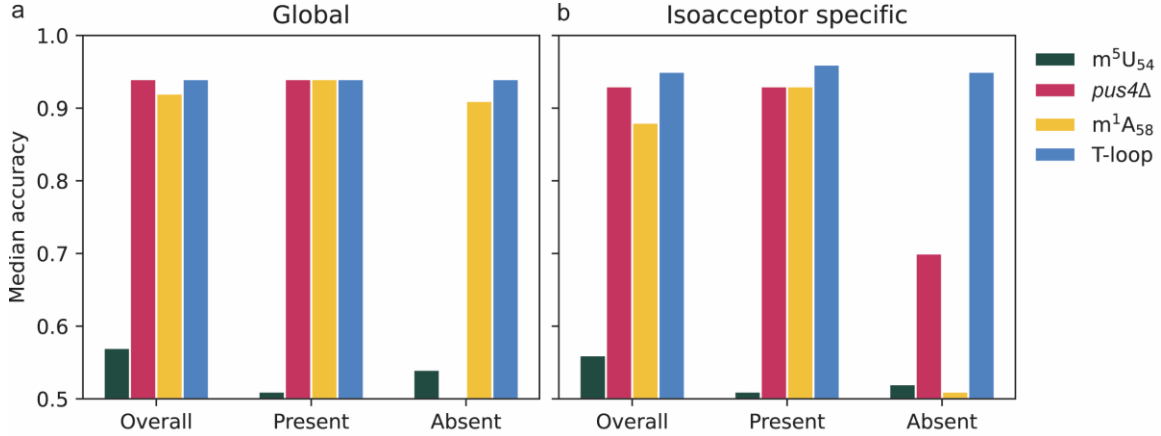


Supplementary Figure 3.3. Reference match probability maps for *trm61Δ* match results obtained for *trm6Δ*. Reference match probability heat maps of aligned T-loop sequences across 42 isoacceptor tRNAs, in WT, *trm61Δ*, *trm6Δ*, and in vitro transcribed (IVT). Note that wild-type, *trm6Δ* and IVT are reprinted from Figure 3c. Otherwise as described in Figure 3c



Supplementary Figure 3.4. Two different mass spectrometry techniques allow for the bulk quantification of each modification in a pool of total tRNA or the sequence specific location of RNA modifications. a) (left) Ribonucleoside modification profiling is performed from a two-step enzymatic digestion that degrades tRNA into monoribonucleosides. Reversed phase chromatography separates the ribonucleosides allowing for multiple reaction monitoring on a triple quadrupole mass spectrometer. This analysis allows for the quantification of individual RNA modifications from a pool of total tRNA. (right) Bottom-up RNA sequencing is performed by digestion of RNA using RNase T1. Individual tRNA sequences can then be mapped using hydrophilic interaction liquid chromatography coupled to tandem mass spectrometry. Sequence informative fragmentation ions are detected in MS/MS spectra allowing for the specific location of RNA modifications to be determined. **b)** Each bar depicts the average percentage of the top 10 modified nucleosides from a pool of three biological replicates. Total tRNA was taken from wild-type (grey), *pus4*Δ (blue), *trm6*Δ (yellow), *trm2*Δ (red), and *pus4*Δ,*trm2*Δ (pink). The error bars show the standard deviation, and significant changes ($p < 0.01$) are noted with an asterisk. In the *trm6*Δ strain, the relative abundance of tRNA tRNA^{Leu}(CAA) changed from 13% to 52%. This change can help explain the increases

observed in m1G, m5C, m2G, m2,2G, and Gm in the *trm6Δ* strain as tRNA^{Leu}(CAA) contains all of these modifications.



Supplementary Figure 3.5. *m*⁵U₅₄, *p*us4Δ, *m*¹A₅₈, and T-loop modification associated miscall profile classification accuracies. Median accuracies indicate how accurately single molecule isoacceptor reads were classified as being positive or negative for the presence of *m*⁵U₅₄, *m*¹A₅₈, Ψ55 and *m*¹A₅₈ (*p*us4Δ), or all possible modifications in the T-loop (*m*⁵U₅₄, Ψ55, and *m*¹A₅₈). **a)** Global profiles were generated with training data from isoacceptors that are known to have *m*⁵U₅₄, *m*¹A₅₈, Ψ55, or all T-loop modifications in wild-type from their corresponding knockout strains or canonical sample (*trm2*Δ, *trm6*Δ, and IVT). **b)** Isoacceptor-specific profiles are made similarly to global, but using isoacceptor specific subsets.

APPENDIX B

SUPPLEMENTARY TABLES FOR CHAPTER III

Supplementary Table 3.1 Yeast strains used in this study.

Strain	Phenotype	Genotype	Source
YDG1	Wild-type	MATa, <i>his3Δ1</i> , <i>leu2Δ0</i> , <i>met15Δ0</i> , <i>ura3Δ0</i>	This study
YDG127	Lacks Ψ_{55}	MATa, <i>PUS4::KanMX</i> , <i>his3Δ1</i> , <i>leu2Δ0</i> , <i>met15Δ0</i> , <i>ura3Δ0</i>	Yeast Knockout Library
YDG221	Lacks Ψ_{55}	MAT α , <i>PUS4::KanMX</i> , <i>his3Δ1</i> , <i>leu2Δ0</i> , <i>lys2Δ0</i> , <i>ura3Δ0</i>	Yeast Knockout Library
YDG630	Catalytically dead Pus4. Lacks Ψ_{55}	MATa, <i>PUS4-R286K</i> , <i>his3Δ1</i> , <i>leu2Δ0</i> , <i>met15Δ0</i> , <i>ura3Δ0</i>	This study
YDG963	Lacks m ⁵ U ₅₄	MATa, <i>TRM2::KanMX</i> , <i>his3Δ1</i> , <i>leu2Δ0</i> , <i>met15Δ0</i> , <i>ura3Δ0</i>	Yeast Knockout Library
YDG973	Lacks Ψ_{55} and m ⁵ U ₅₄	<i>PUS4::KanMX</i> , <i>TRM2::KanMX</i> , <i>his3Δ1</i> , <i>leu2Δ0</i> , <i>ura3Δ0</i>	This study

H2846 (YJA146)	Lacks m ¹ A ₅₈	MAT α , <i>TRM6::HisG</i> , <i>ura3-52</i> , <i>trp2</i> , <i>leu2</i> Δ , <i>his3</i> Δ , <i>PEP::HIS3</i> , <i>prb1</i> Δ , <i>can1</i> , GAL+ (plasmid h.c. IMT4, LEU2)	(Anderson et al. 1998)
H2847	Lacks m ¹ A ₅₈	<i>TRM61::URA3</i> , <i>ura3-52</i> , <i>leu2-3</i> , <i>leu2-112</i> , <i>trp1-289</i> , <i>his3-111</i> , <i>can1-100</i> , ADE+ (plasmid h.c. IMT4, LEU2)	(Anderson et al. 1998)
YDG 989	C-terminal 3xHA tag on Pus4	MAT α , <i>his3</i> Δ 1, <i>leu2</i> Δ 0, <i>met15</i> Δ 0, <i>ura3</i> Δ 0, <i>PUS4-3xHa</i>	This study
YDG 1033	C-terminal 3xHA tag on Pus4-R286K	MAT α , <i>his3</i> Δ 1, <i>leu2</i> Δ 0, <i>met15</i> Δ 0, <i>ura3</i> Δ 0, <i>PUS4-3xHA-R286K</i>	This study

Supplementary Table 3.2 The RNA and DNA oligonucleotides for the splint adapters and IVT constructs, and the oligos and gBlocks used for construction of the CRISPR plasmids and the repair templates.

See Table S2 on Supplemental_Tables_S2_S5_S7_S8_S10_S12.xlsx

Supplementary Table 3.3 Global and isoacceptor-specific profiles. This sheet provides information about how training and testing data were labeled, the depth of data used, and the accuracy of the models.

See Table S3 on Supplemental_Table_S3_Sequence_Level_Classification_Statistics.xlsx

Supplementary Table 3.4 Sequence and alignment statistics for tRNA purified from *S. cerevisiae* strains (wild-type, *pus4* Δ , *trm6* Δ , *trm61* Δ , *trm2* Δ , *pus4* Δ *trm2* Δ , and *PUS4* R286K) and for *in vitro* transcribed tRNA. For strains, “N” represents the number of biological replicates. Alignments were generated using a reference that contained the adapter sequences and were filtered at MAPQ>0.

Sample	Per flow cell			
	Total reads	Aligned tRNA reads	Full-length aligned tRNA reads	Full-length tRNA reads as a percent of aligned tRNA reads
Wild-type N = 4	67,200 - 95,451	27,882 - 37,800	24,261 - 32,938	87.23 - 91.45%
<i>pus4</i> Δ N = 3	99,165 - 113,095	51,635 - 59,884	28,485 - 48,205	89.41 - 91.45%
<i>trm6</i> Δ N = 3	23,452 - 138,054	6,194 - 42,767	5,354 - 36,588	85.75 - 86.44%
<i>trm61</i> Δ N = 1	124,939	42,607	35,157	82.51%
<i>trm2</i> Δ N = 3	22,580 - 45,849	10,834 - 17,960	9,520 - 36,175	87.87 - 89.09%
<i>pus4</i> Δ <i>trm2</i> Δ N = 3	25,908 - 383,570	13,374 - 200,097	11,643 - 176,647	87.06 - 88.62%
<i>PUS4</i> R286K N = 3	41,184 - 128,053	14,594 - 69,698	12,346 - 59,214	84.93 - 86.42%
IVT N = 1	603,915	515,091	466,251	90.52%

Supplementary Table 3.5 Custom BY4741 strain specific 42 yeast tRNA isoacceptor reference sequences.

See Table S5 on Supplemental_Tables_S2_S5_S7_S8_S10_S12.xlsx

Supplementary Table 3.6 Isoacceptor aligned reads ranges across four wild-type *S. cerevisiae* replicate strains.

Isoacceptor	Aligned reads (MAPQ>0)	Isoacceptor	Aligned reads (MAPQ>0)
Ala (AGC)	655-2803	Leu (UAA)	73-1150
Ala (UGC)	1060-1335	Leu (UAG)	129-726
Arg (ACG)	1319-1879	Lys (CUU)	957-4878
Arg (CCG)	182-532	Lys (UUU)	248-1517
Arg (CCU)	187-551	iMet (CAU)	13-580
Arg (UCU)	823-1714	Met (CAU)	324-444
Asn (GUU)	1034-1544	Phe (GAA)	725-1322
Asp (GUC)	3191-4403	Pro (AGG)	100-799
Cys (GCA)	333-1145	Pro (UGG)	177-320
Gln (CUG)	222-555	Ser (AGA)	2357-9565
Gln (UUG)	572-1583	Ser (CGA)	7-180
Glu (CUC)	194-229	Ser (GCU)	24-1028
Glu (UUC)	1272-1501	Ser (UGA)	3-106
Gly (CCC)	203-467	Thr (AGU)	1059-2413
Gly (GCC)	2195-10978	Thr (CGU)	78-171
Gly (UCC)	275-504	Thr (UGU)	63-198
His (GUG)	378-3887	Trp (CCA)	241-734
Ile (AAU)	978-1347	Tyr (GUA)	440-1717
Ile (UAU)	119-280	Val (AAC)	1390-1811
Leu (CAA)	1170-12237	Val (CAC)	263-452
Leu (GAG)	120-179	Val (UAC)	356-1072

Supplementary Table 3.7 Raw aligned reads for each replicate from wild-type, *pus4* Δ , *trm6* Δ , *trm2* Δ , and *pus4* Δ *trm2* Δ .

See Table S7 on Supplemental_Tables_S2_S5_S7_S8_S10_S12.xlsx

Supplementary Table 3.8 The T-loop sequences from 42 *S. cerevisiae* isoacceptors.

See Table S8 on Supplemental_Tables_S2_S5_S7_S8_S10_S12.xlsx

Supplementary Table 3.9 Predictions for the presence or absence of m¹A at position 58 across all cytoplasmic tRNA isoacceptors in wild-type yeast. Blue circles represent the predicted presence of m¹A₅₈. Magenta circles represent the predicted absence of m¹A₅₈. No circle represents an inconclusive prediction. Modomics annotations are taken from (1). DRS predictions were called if the posterior probabilities at positions 57, 58, or 59 matched or exceeded the threshold cutoff of 0.3. tRNA^{Arg(CCU)} also exceeded this threshold based on signal at position 57, however we excluded it from annotation as an m¹A₅₈-containing tRNA due to the fact that the same change is observed in the *trm6Δ* strain (**Figure 3c**, (i) vs. (iii)). Evidence for m¹A₅₈ through LC-MS/MS was taken from sequence informative fragmentation ions (2). mim-tRNAseq m¹A₅₈ predictions were considered positive for isoacceptors with misincorporation rates >10% and nucleotide coverage >2,000 reads at position 58 (3). ARM-seq m¹A₅₈ predictions were considered positive for isoacceptors with a two-fold or greater increase in the ratio of read counts from AlkB-treated versus untreated RNA and a p<0.01 (4).

tRNA	Modomics	DRS	LC-MS/MS	mim-seq	ARM-seq
AlaAGC	●	●	●	●	●
AlaUGC		●		●	●
ArgACG	●	●	●	●	●
ArgCCG		●		●	●
ArgCCU		●		●	●
ArgUCU	●	●	●	●	●
AsnGUU	●	●	●	●	●
AspGUC	●	●	●	●	●
CysGCA	●	●		●	●
GlnCUG		●		●	●
GlnUUG		●		●	●
GluCUC		●		●	●
GluUUC	●	●	●	●	●
GlyCCC		●		●	●
GlyGCC	●	●		●	●
GlyUCC	●	●		●	●
HisGUG	●	●	●	●	●
IleAAU	●	●	●	●	●
IleUAU	●	●	●	●	●
LeuCAA	●	●	●	●	●
LeuGAG		●	●	●	●
LeuUAA	●	●		●	●
LeuUAG	●	●	●	●	●
LysCUU	●	●		●	●
LysUUU	●	●		●	●
MetCAU	●	●		●	●
iMetCAU	●	●	●	●	●
PheGAA	●	●	●	●	●
ProAGG		●		●	●
ProUGG	●	●	●	●	●
SerAGA	●	●	●	●	●
SerCGA	●	●		●	●
SerGCU	●	●	●	●	●
SerUGA	●	●		●	●
ThrAGU	●	●	●	●	●
ThrCGU		●	●	●	●
ThrUGU		●		●	●
TrpCCA	●	●	●	●	●
TyrGUA	●	●		●	●
ValAAC	●	●	●	●	●
ValCAC	●	●	●	●	●
ValUAC	●	●		●	●

Supplementary Table 3.10 The posterior probabilities of an alternative nucleotide in the 3-mer window where the m¹A₅₈ signal occurs (positions 57–59), and at the single position 54 where m⁵U occurs. Each probability is derived from 120 aligned reads. If the probability was ≥ 0.3 , it passed the threshold that we considered to be a bonafide miscall. See Table S10 on Supplemental_Tables_S2_S5_S7_S8_S10_S12.xlsx

Supplementary Table 3.11 Classes of tRNAs as defined by the influence of Ψ_{55} on the catalysis of m¹A₅₈ in exponentially growing cells. Class I tRNAs do not have Ψ_{55} , but do have m¹A₅₈. Class II tRNAs have Ψ_{55} , but do not have m¹A₅₈. Class III tRNAs have both Ψ_{55} and m¹A₅₈, and the presence of Ψ_{55} promotes m¹A₅₈ catalysis. Class IV tRNAs have both Ψ_{55} and m¹A₅₈, but the loss of Ψ_{55} does not substantially reduce m¹A₅₈ modification.

	Class I	Class II	Class III	Class IV
tRNA isoacceptor	iMet (CAU)	Ala (AGC) Ala (UGC) Arg (CCG) Arg (CCU) Asp (GUC) Glu (CUC) Glu (UUC) Gly (CCC) Gly (GCC) Gly (UCC) His (GUG) Leu (CAA) Leu (UAA) Lys (CUU) Pro (AGG) Ser (AGA) Ser (UGA) Val (CAC)	Arg (UCU) Asn (GUU) Cys (GCA) Gln (CUG) Gln (UUG) Ile (AAU) Leu (GAG) Leu (UAG) Lys (UUU) Met (CAU) Phe (GAA) Pro (UGG) Ser (CGA) Ser (GCU) Thr (CGU) Thr (UGU) Trp (CCA) Tyr (GUA) Val (AAC)	Arg (ACG) Ile (UAU) Thr (AGU) Val (UAC)

Supplementary Table 3.12 Mass spectrometry ribonucleoside modification profiling abundances. Total tRNA was taken from wild-type, *pus4* Δ , *trm6* Δ , *trm2* Δ , and *pus4* Δ ,*trm2* Δ to perform the modification analysis. The average percentage of a modified nucleoside was taken from a pool of three biological replicates. Standard deviations were calculated for the abundance of every modification for each strain. P-values taken from a t-test are displayed showing the statistical significance of the difference between modification abundance in comparison to wild-type. The fold change represents the change in the level of a modification from wildtype to each strain. See Table S12 on Supplemental_Tables_S2_S5_S7_S8_S10_S12.xls

REFERENCES

- Alberti, S., Halfmann, R., King, O., Kapila, A., & Lindquist, S. (2009). A systematic survey identifies prions and illuminates sequence features of prionogenic proteins. *Cell*, *137*(1), 146–158.
- Alexandrov, A., Chernyakov, I., Gu, W., Hiley, S. L., Hughes, T. R., Grayhack, E. J., & Phizicky, E. M. (2006). Rapid tRNA decay can result from lack of nonessential modifications. *Molecular Cell*, *21*(1), 87–96.
- Alfonzo, J. D., Brown, J. A., Byers, P. H., Cheung, V. G., Maraia, R. J., & Ross, R. L. (2021). A call for direct sequencing of full-length RNAs to identify all modifications. *Nature Genetics*, *53*(8), 1113–1116.
- Anderson, J., Phan, L., Cuesta, R., Carlson, B. A., Pak, M., Asano, K., Björk, G. R., Tamame, M., & Hinnebusch, A. G. (1998). The essential Gcd10p-Gcd14p nuclear complex is required for 1-methyladenosine modification and maturation of initiator methionyl-tRNA. *Genes & Development*, *12*(23), 3650–3662.
- Anderson, J., Phan, L., Cuesta, R., Carlson, B. A., Pak, M., Asano, K., Björk, G. R., Tamame, M., and Hinnebusch, A. G. (1998) The essential Gcd10p-Gcd14p nuclear complex is required for 1-methyladenosine modification and maturation of initiator methionyl-tRNA. *Genes Dev.*, **12**, 3650–3662.
- Anderson, J., Phan, L., & Hinnebusch, A. G. (2000). The Gcd10p/Gcd14p complex is the essential two-subunit tRNA(1-methyladenosine) methyltransferase of *Saccharomyces cerevisiae*. *Proceedings of the National Academy of Sciences of the United States of America*, *97*(10), 5173–5178.
- Arimbasseri, A. G., Iben, J., Wei, F.-Y., Rijal, K., Tomizawa, K., Hafner, M., & Maraia, R. J. (2016). Evolving specificity of tRNA 3-methyl-cytidine-32 (m3C32) modification: a subset of tRNAs_{Ser} requires N6-isopentenylation of A37. *RNA*, *22*(9), 1400–1410.

Bailey, A. D., Talkish, J., Ding, H., Igel, H., Duran, A., Mantripragada, S., Paten, B., & Ares, M. (2022). Concerted modification of nucleotides at functional centers of the ribosome revealed by single-molecule RNA modification profiling. *eLife*, *11*.
<https://doi.org/10.7554/eLife.76562>

Barraud, P., Gato, A., Heiss, M., Catala, M., Kellner, S., & Tisné, C. (2019). Time-resolved NMR monitoring of tRNA maturation. *Nature Communications*, *10*(1), 3373.

Barraud, P., & Tisné, C. (2019). To be or not to be modified: Miscellaneous aspects influencing nucleotide modifications in tRNAs. *IUBMB Life*, *71*(8), 1126–1140.

Becker, H. F., Motorin, Y., Planta, R. J., & Grosjean, H. (1997). The yeast gene YNL292w encodes a pseudouridine synthase (Pus4) catalyzing the formation of Ψ 55 in both mitochondrial and cytoplasmic tRNAs. *Nucleic Acids Research*, *25*(22), 4493–4499.

Begik, O., Lucas, M. C., Prysycz, L. P., Ramirez, J. M., Medina, R., Milenkovic, I., Cruciani, S., Liu, H., Vieira, H. G. S., Sas-Chen, A., Mattick, J. S., Schwartz, S., & Novoa, E. M. (2021a). Quantitative profiling of pseudouridylation dynamics in native RNAs with nanopore sequencing. *Nature Biotechnology*, *39*(10), 1278–1291.

Begik, O., Lucas, M. C., Prysycz, L. P., Ramirez, J. M., Medina, R., Milenkovic, I., Cruciani, S., Liu, H., Vieira, H. G. S., Sas-Chen, A., Mattick, J. S., Schwartz, S., & Novoa, E. M. (2021b). Quantitative profiling of pseudouridylation dynamics in native RNAs with nanopore sequencing. *Nature Biotechnology*, *39*(10), 1278–1291.

Behrens, A., Rodschinka, G., & Nedialkova, D. D. (2021). High-resolution quantitative profiling of tRNA abundance and modification status in eukaryotes by mim-tRNAseq. *Molecular Cell*, *81*(8), 1802–1815.e7.

Benítez-Páez, A., Villarroya, M., Douthwaite, S., Gabaldón, T., & Armengod, M.-E. (2010). YibK is the 2'-O-methyltransferase TrmL that modifies the wobble nucleotide in *Escherichia coli* tRNA(Leu) isoacceptors. *RNA*, *16*(11), 2131–2143.

Boccaletto, P., Stefaniak, F., Ray, A., Cappannini, A., Mukherjee, S., Purta, E., Kurkowska,

M., Shirvanizadeh, N., Destefanis, E., Groza, P., Avşar, G., Romitelli, A., Pir, P., Dassi, E., Conticello, S. G., Aguilo, F., & Bujnicki, J. M. (2022). MODOMICS: a database of RNA modification pathways. 2021 update. *Nucleic Acids Research*, *50*(D1), D231–D235.

Botstein, D., Chervitz, S. A., & Cherry, J. M. (1997). Yeast as a model organism [Review of *Yeast as a model organism*]. *Science*, *277*(5330), 1259–1260.

Brégeon, D., Pecqueur, L., Toubdji, S., Sudol, C., Lombard, M., Fontecave, M., de Crécy-Lagard, V., Motorin, Y., Helm, M., & Hamdane, D. (2022). Dihydrouridine in the Transcriptome: New Life for This Ancient RNA Chemical Modification. *ACS Chemical Biology*, *17*(7), 1638–1657.

Brunel, C., Marquet, R., Romby, P., & Ehresmann, C. (2002). RNA loop-loop interactions as dynamic functional motifs. *Biochimie*, *84*(9), 925–944.

Cabello-Villegas, J., & Nikonowicz, E. P. (2005). Solution structure of psi32-modified anticodon stem-loop of Escherichia coli tRNAPhe. *Nucleic Acids Research*, *33*(22), 6961–6971.

Cappannini, A., Ray, A., Purta, E., Mukherjee, S., Boccaletto, P., Moafinejad, S. N., Lechner, A., Barchet, C., Klaholz, B. P., Stefaniak, F., & Bujnicki, J. M. (2024). MODOMICS: a database of RNA modifications and related information. 2023 update. *Nucleic Acids Research*, *52*(D1), D239–D244.

Carlile, T. M., Rojas-Duran, M. F., Zinshteyn, B., Shin, H., Bartoli, K. M., & Gilbert, W. V. (2014). Pseudouridine profiling reveals regulated mRNA pseudouridylation in yeast and human cells. *Nature*, *515*(7525), 143–146.

Caughey, B., & Chesebro, B. (2001). Transmissible spongiform encephalopathies and prion protein interconversions. *Advances in Virus Research*, *56*, 277–311.

Chakrabortee, S., Byers, J. S., Jones, S., Garcia, D. M., Bhullar, B., Chang, A., She, R., Lee, L., Fremin, B., Lindquist, S., & Jarosz, D. F. (2016). Intrinsically Disordered Proteins Drive Emergence and Inheritance of Biological Traits. *Cell*, *167*(2), 369–381.e12.

- Chakravarty, A. K., Smejkal, T., Itakura, A. K., Garcia, D. M., & Jarosz, D. F. (2020). A Non-amyloid Prion Particle that Activates a Heritable Gene Expression Program. *Molecular Cell*, *77*(2), 251–265.e9.
- Chan, P. P., Lin, B. Y., Mak, A. J., & Lowe, T. M. (2021). tRNAscan-SE 2.0: improved detection and functional classification of transfer RNA genes. *Nucleic Acids Research*, *49*(16), 9077–9096.
- Chan, P. P., & Lowe, T. M. (2016). GtRNAdb 2.0: an expanded database of transfer RNA genes identified in complete and draft genomes. *Nucleic Acids Research*, *44*(D1), D184–D189.
- Charette, M., & Gray, M. W. (2000). Pseudouridine in RNA: what, where, how, and why. *IUBMB Life*, *49*(5), 341–351.
- Chen, L., Ou, L., Jing, X., Kong, Y., Xie, B., Zhang, N., Shi, H., Qin, H., Li, X., & Hao, P. (2023). DeepEdit: single-molecule detection and phasing of A-to-I RNA editing events using nanopore direct RNA sequencing. *Genome Biology*, *24*(1), 75.
- Cohn, W. E., & Volkin, E. (1951). Nucleoside-5'-Phosphates from Ribonucleic Acid. *Nature*, *167*(4247), 483–484.
- Cozen, A. E., Quartley, E., Holmes, A. D., Hrabeta-Robinson, E., Phizicky, E. M., & Lowe, T. M. (2015). ARM-seq: AlkB-facilitated RNA methylation sequencing reveals a complex landscape of modified tRNA fragments. *Nature Methods*, *12*(9), 879–884.
- Davis, D. R. (1995). Stabilization of RNA stacking by pseudouridine. *Nucleic Acids Research*, *23*(24), 5020–5026.
- de Crécy-Lagard, V., Boccaletto, P., Mangleburg, C. G., Sharma, P., Lowe, T. M., Leidel, S. A., & Bujnicki, J. M. (2019). Matching tRNA modifications in humans to their known and predicted enzymes. *Nucleic Acids Research*, *47*(5), 2143–2159.
- Delaunay, S., Helm, M., & Frye, M. (2024). RNA modifications in physiology and disease: towards clinical applications. *Nature Reviews. Genetics*, *25*(2), 104–122.

- Denmon, A. P., Wang, J., & Nikonowicz, E. P. (2011). Conformation effects of base modification on the anticodon stem-loop of *Bacillus subtilis* tRNA(Tyr). *Journal of Molecular Biology*, *412*(2), 285–303.
- Dennis, E. M., & Garcia, D. M. (2022). Biochemical Principles in Prion-Based Inheritance. *Epigenomes*, *6*(1). <https://doi.org/10.3390/epigenomes6010004>
- Derkatch, I. L., Chernoff, Y. O., Kushnirov, V. V., Inge-Vechtsov, S. G., & Liebman, S. W. (1996). Genesis and variability of [PSI] prion factors in *Saccharomyces cerevisiae*. *Genetics*, *144*(4), 1375–1386.
- Droogmans, L., Roovers, M., Bujnicki, J. M., Tricot, C., Hartsch, T., Stalon, V., & Grosjean, H. (2003). Cloning and characterization of tRNA (m1A58) methyltransferase (TrmI) from *Thermus thermophilus* HB27, a protein required for cell growth at extreme temperatures. *Nucleic Acids Research*, *31*(8), 2148–2156.
- Duina, A. A., Miller, M. E., & Keeney, J. B. (2014). Budding yeast for budding geneticists: a primer on the *Saccharomyces cerevisiae* model system. *Genetics*, *197*(1), 33–48.
- Du, Z., Park, K.-W., Yu, H., Fan, Q., & Li, L. (2008). Newly identified prion linked to the chromatin-remodeling factor Swi1 in *Saccharomyces cerevisiae*. *Nature Genetics*, *40*(4), 460–465.
- Engel, S. R., Dietrich, F. S., Fisk, D. G., Binkley, G., Balakrishnan, R., Costanzo, M. C., Dwight, S. S., Hitz, B. C., Karra, K., Nash, R. S., Weng, S., Wong, E. D., Lloyd, P., Skrzypek, M. S., Miyasato, S. R., Simison, M., & Cherry, J. M. (2014). The reference genome sequence of *Saccharomyces cerevisiae*: then and now. *G3*, *4*(3), 389–398.
- Eyler, D. E., Franco, M. K., Batool, Z., Wu, M. Z., Dubuke, M. L., Dobosz-Bartoszek, M., Jones, J. D., Polikanov, Y. S., Roy, B., & Koutmou, K. S. (2019). Pseudouridylation of mRNA coding sequences alters translation. *Proceedings of the National Academy of Sciences of the United States of America*, *116*(46), 23068–23074.
- Fleming, A. M., Bommisetti, P., Xiao, S., Bandarian, V., & Burrows, C. J. (2023). Direct

Nanopore Sequencing for the 17 RNA Modification Types in 36 Locations in the Ribosome Enables Monitoring of Stress-Dependent Changes. *ACS Chemical Biology*.

<https://doi.org/10.1021/acscchembio.3c00166>

Friedt, J., Leavens, F. M. V., Mercier, E., Wieden, H.-J., & Kothe, U. (2014). An arginine-aspartate network in the active site of bacterial TruB is critical for catalyzing pseudouridine formation. *Nucleic Acids Research*, *42*(6), 3857–3870.

Garcia, D. M., Campbell, E. A., Jakobson, C. M., Tsuchiya, M., Shaw, E. A., DiNardo, A. L., Kaeberlein, M., & Jarosz, D. F. (2021). A prion accelerates proliferation at the expense of lifespan. *eLife*, *10*. <https://doi.org/10.7554/eLife.60917>

Giaever, G., Chu, A. M., Ni, L., Connelly, C., Riles, L., Véronneau, S., Dow, S., Lucau-Danila, A., Anderson, K., André, B., Arkin, A. P., Astromoff, A., El-Bakkoury, M., Bangham, R., Benito, R., Brachat, S., Campanaro, S., Curtiss, M., Davis, K., ... Johnston, M. (2002). Functional profiling of the *Saccharomyces cerevisiae* genome. *Nature*, *418*(6896), 387–391.

Glover, J. R., & Lindquist, S. (1998). Hsp104, Hsp70, and Hsp40: a novel chaperone system that rescues previously aggregated proteins. *Cell*, *94*(1), 73–82.

Goodenbour, J. M., & Pan, T. (2006). Diversity of tRNA genes in eukaryotes. *Nucleic Acids Research*, *34*(21), 6137–6146.

Griffey, R. H., Davis, D., Yamaizumi, Z., Nishimura, S., Bax, A., Hawkins, B., & Poulter, C. D. (1985). ¹⁵N-labeled *Escherichia coli* tRNA^{fMet}, tRNA^{Glu}, tRNA^{Tyr}, and tRNA^{Phe}. Double resonance and two-dimensional NMR of N1-labeled pseudouridine. *The Journal of Biological Chemistry*, *260*(17), 9734–9741.

Guy, M. P., Podyma, B. M., Preston, M. A., Shaheen, H. H., Krivos, K. L., Limbach, P. A., Hopper, A. K., & Phizicky, E. M. (2012). Yeast Trm7 interacts with distinct proteins for critical modifications of the tRNA^{Phe} anticodon loop. *RNA*, *18*(10), 1921–1933.

Han, L., Marcus, E., D’Silva, S., & Phizicky, E. M. (2017). *S. cerevisiae* Trm140 has two

recognition modes for 3-methylcytidine modification of the anticodon loop of tRNA substrates. *RNA*, 23(3), 406–419.

Han, L., & Phizicky, E. M. (2018). A rationale for tRNA modification circuits in the anticodon loop. *RNA*, 24(10), 1277–1284.

Hanson, G., & Collier, J. (2018). Codon optimality, bias and usage in translation and mRNA decay. *Nature Reviews. Molecular Cell Biology*, 19(1), 20–30.

Helm, M. (2006). Post-transcriptional nucleotide modification and alternative folding of RNA. *Nucleic Acids Research*, 34(2), 721–733.

Hendra, C., Pratanwanich, P. N., Wan, Y. K., Goh, W. S. S., Thiery, A., & Göke, J. (2022). Detection of m6A from direct RNA sequencing using a multiple instance learning framework. *Nature Methods*, 19(12), 1590–1598.

Hernandez-Alias, X., Katanski, C. D., Zhang, W., Assari, M., Watkins, C. P., Schaefer, M. H., Serrano, L., & Pan, T. (2023). Single-read tRNA-seq analysis reveals coordination of tRNA modification and aminoacylation and fragmentation. *Nucleic Acids Research*, 51(3), e17.

Horie, N., Hara-Yokoyama, M., Yokoyama, S., Watanabe, K., Kuchino, Y., Nishimura, S., & Miyazawa, T. (1985). Two tRNA^{Ile1} species from an extreme thermophile, *Thermus thermophilus* HB8: effect of 2-thiolation of ribothymidine on the thermostability of tRNA. *Biochemistry*, 24(21), 5711–5715.

Huang, S., Zhang, W., Katanski, C. D., Dersh, D., Dai, Q., Lolans, K., Yewdell, J., Eren, A. M., & Pan, T. (2021). Interferon inducible pseudouridine modification in human mRNA by quantitative nanopore profiling. *Genome Biology*, 22(1), 330.

Hunter, J. D. (2007). Matplotlib: A 2D Graphics Environment. *Computing in Science & Engineering*, 9(3), 90–95.

Jain, M., Abu-Shumays, R., Olsen, H. E., & Akeson, M. (2022). Advances in nanopore direct RNA sequencing. *Nature Methods*, 19(10), 1160–1164.

Jain, M., Fiddes, I. T., Miga, K. H., Olsen, H. E., Paten, B., & Akeson, M. (2015). Improved data analysis for the MinION nanopore sequencer. *Nature Methods*, *12*(4), 351–356.

Jarosz, D. F., Lancaster, A. K., Brown, J. C. S., & Lindquist, S. (2014). An evolutionarily conserved prion-like element converts wild fungi from metabolic specialists to generalists. *Cell*, *158*(5), 1072–1082.

Jones, J. D., Franco, M. K., Smith, T. J., Snyder, L. R., Anders, A. G., Ruotolo, B. T., Kennedy, R. T., & Koutmou, K. S. (2023). Methylated guanosine and uridine modifications in mRNAs modulate translation elongation. *RSC Chemical Biology*, *4*(5), 363–378.

Jones, J. D., Simcox, K. M., Kennedy, R. T., & Koutmou, K. S. (2023). Direct sequencing of total tRNAs by LC-MS/MS. *RNA*, *29*(8), 1201–1214.

Jühling, F., Mörl, M., Hartmann, R. K., Sprinzl, M., Stadler, P. F., & Pütz, J. (2009). tRNADB 2009: compilation of tRNA sequences and tRNA genes. *Nucleic Acids Research*, *37*(Database issue), D159–D162.

Kaeberlein, M. (2010). Lessons on longevity from budding yeast. *Nature*, *464*(7288), 513–519.

Karijolich, J., & Yu, Y.-T. (2011). Converting nonsense codons into sense codons by targeted pseudouridylation. *Nature*, *474*(7351), 395–398.

Karikó, K., Muramatsu, H., Welsh, F. A., Ludwig, J., Kato, H., Akira, S., & Weissman, D. (2008). Incorporation of pseudouridine into mRNA yields superior nonimmunogenic vector with increased translational capacity and biological stability. *Molecular Therapy: The Journal of the American Society of Gene Therapy*, *16*(11), 1833–1840.

Keffer-Wilkes, L. C., Veerareddygar, G. R., & Kothe, U. (2016). RNA modification enzyme TruB is a tRNA chaperone. *Proceedings of the National Academy of Sciences of the United States of America*, *113*(50), 14306–14311.

Kimura, S., Srisuknimit, V., McCarty, K. L., Dedon, P. C., Kranzusch, P. J., & Waldor, M. K. (2022). Sequential action of a tRNA base editor in conversion of cytidine to

pseudouridine. *Nature Communications*, 13(1), 5994.

Kushnirov, V. V., & Ter-Avanesyan, M. D. (1998). Structure and replication of yeast prions. *Cell*, 94(1), 13–16.

Kutter, C., Brown, G. D., Gonçalves, A., Wilson, M. D., Watt, S., Brazma, A., White, R. J., & Odom, D. T. (2011). Pol III binding in six mammals shows conservation among amino acid isotypes despite divergence among tRNA genes. *Nature Genetics*, 43(10), 948–955.

Leger, A., Amaral, P. P., Pandolfini, L., Capitanchik, C., Capraro, F., Miano, V., Migliori, V., Toolan-Kerr, P., Sideri, T., Enright, A. J., Tzelepis, K., van Werven, F. J., Luscombe, N. M., Barbieri, I., Ule, J., Fitzgerald, T., Birney, E., Leonardi, T., & Kouzarides, T. (2021). RNA modifications detection by comparative Nanopore direct RNA sequencing. *Nature Communications*, 12(1), 7198.

Li, C., Qian, W., Maclean, C. J., & Zhang, J. (2016). The fitness landscape of a tRNA gene. *Science*, 352(6287), 837–840.

Liebman, S. W., & Chernoff, Y. O. (2012). Prions in Yeast. *Genetics*, 191(4), 1041–1072.

Li, H. (2013). Aligning sequence reads, clone sequences and assembly contigs with BWA-MEM. In *arXiv [q-bio.GN]*. arXiv. <http://arxiv.org/abs/1303.3997>

Li, H., Handsaker, B., Wysoker, A., Fennell, T., Ruan, J., Homer, N., Marth, G., Abecasis, G., Durbin, R., & 1000 Genome Project Data Processing Subgroup. (2009). The Sequence Alignment/Map format and SAMtools. *Bioinformatics*, 25(16), 2078–2079.

Liu, F., Clark, W., Luo, G., Wang, X., Fu, Y., Wei, J., Wang, X., Hao, Z., Dai, Q., Zheng, G., Ma, H., Han, D., Evans, M., Klungland, A., Pan, T., & He, C. (2016). ALKBH1-Mediated tRNA Demethylation Regulates Translation. *Cell*, 167(3), 816–828.e16.

Li, X., Ma, S., & Yi, C. (2016). Pseudouridine: the fifth RNA nucleotide with renewed interests. *Current Opinion in Chemical Biology*, 33, 108–116.

Lovejoy, A. F., Riordan, D. P., & Brown, P. O. (2014). Transcriptome-wide mapping of pseudouridines: pseudouridine synthases modify specific mRNAs in *S. cerevisiae*. *PLoS One*,

9(10), e110799.

Lucas, M. C., Prysycz, L. P., Medina, R., Milenkovic, I., Camacho, N., Marchand, V., Motorin, Y., Ribas de Pouplana, L., & Novoa, E. M. (2023). Quantitative analysis of tRNA abundance and modifications by nanopore RNA sequencing. *Nature Biotechnology*.

<https://doi.org/10.1038/s41587-023-01743-6>

Machnicka, M. A., Olchowik, A., Grosjean, H., & Bujnicki, J. M. (2014). Distribution and frequencies of post-transcriptional modifications in tRNAs. *RNA Biology*, 11(12), 1619–1629.

Masison, D. C., & Wickner, R. B. (1995). Prion-inducing domain of yeast Ure2p and protease resistance of Ure2p in prion-containing cells. *Science*, 270(5233), 93–95.

Meier, U. T. (2005). The many facets of H/ACA ribonucleoproteins. *Chromosoma*, 114(1), 1–14.

Modomics - A Database of RNA Modifications. (n.d.). Retrieved April 13, 2017, from <http://modomics.genesilico.pl>

Mörl, M., Dörner, M., & Pääbo, S. (1995). C to U editing and modifications during the maturation of the mitochondrial tRNA(Asp) in marsupials. *Nucleic Acids Research*, 23(17), 3380–3384.

Müller, M., Hartmann, M., Schuster, I., Bender, S., Thüring, K. L., Helm, M., Katze, J. R., Nellen, W., Lyko, F., & Ehrenhofer-Murray, A. E. (2015). Dynamic modulation of Dnmt2-dependent tRNA methylation by the micronutrient queuine. *Nucleic Acids Research*, 43(22), 10952–10962.

Nguyen, T. A., Heng, J. W. J., Kaewsapsak, P., Kok, E. P. L., Stanojević, D., Liu, H., Cardilla, A., Praditya, A., Yi, Z., Lin, M., Aw, J. G. A., Ho, Y. Y., Peh, K. L. E., Wang, Y., Zhong, Q., Heraud-Farlow, J., Xue, S., Reversade, B., Walkley, C., ... Tan, M. H. (2022). Direct identification of A-to-I editing sites with nanopore native RNA sequencing. *Nature Methods*, 19(7), 833–844.

- Nobles, K. N., Yarian, C. S., Liu, G., Guenther, R. H., & Agris, P. F. (2002). Highly conserved modified nucleosides influence Mg²⁺-dependent tRNA folding. *Nucleic Acids Research*, *30*(21), 4751–4760.
- Oerum, S., Dégut, C., Barraud, P., & Tisné, C. (2017). m1A Post-Transcriptional Modification in tRNAs. *Biomolecules*, *7*(1). <https://doi.org/10.3390/biom7010020>
- Penzo, M., Guerrieri, A. N., Zacchini, F., Treré, D., & Montanaro, L. (2017). RNA Pseudouridylation in Physiology and Medicine: For Better and for Worse. *Genes*, *8*(11). <https://doi.org/10.3390/genes8110301>
- Phizicky, E. M., & Alfonzo, J. D. (2010). Do all modifications benefit all tRNAs? *FEBS Letters*, *584*(2), 265–271.
- Phizicky, E. M., & Hopper, A. K. (2010). tRNA biology charges to the front. *Genes & Development*, *24*(17), 1832–1860.
- Phizicky, E. M., & Hopper, A. K. (2023). The life and times of a tRNA. *RNA*, *29*(7), 898–957.
- Pratanwanich, P. N., Yao, F., Chen, Y., Koh, C. W. Q., Wan, Y. K., Hendra, C., Poon, P., Goh, Y. T., Yap, P. M. L., Chooi, J. Y., Chng, W. J., Ng, S. B., Thiery, A., Goh, W. S. S., & Göke, J. (2021). Identification of differential RNA modifications from nanopore direct RNA sequencing with xPore. *Nature Biotechnology*, *39*(11), 1394–1402.
- Prusiner, S. B. (1982). Novel proteinaceous infectious particles cause scrapie. *Science*, *216*(4542), 136–144.
- RajBhandary, U. L., & Köhrer, C. (2006). Early days of tRNA research: discovery, function, purification and sequence analysis. *Journal of Biosciences*, *31*(4), 439–451.
- Ranjith Anand, Gonen Memisoglu, James Haber. (2017). *Cas9-mediated gene editing in Saccharomyces cerevisiae*. <https://protocolexchange.researchsquare.com/article/nprot-5791/v1>
- Rintala-Dempsey, A. C., & Kothe, U. (2017). Eukaryotic stand-alone pseudouridine

synthases - RNA modifying enzymes and emerging regulators of gene expression? *RNA Biology*, *14*(9), 1185–1196.

Roovers, M., Droogmans, L., & Grosjean, H. (2021). Post-Transcriptional Modifications of Conserved Nucleotides in the T-Loop of tRNA: A Tale of Functional Convergent Evolution. *Genes*, *12*(2). <https://doi.org/10.3390/genes12020140>

Rubio, M. A. T., Gaston, K. W., McKenney, K. M., Fleming, I. M. C., Paris, Z., Limbach, P. A., & Alfonzo, J. D. (2017). Editing and methylation at a single site by functionally interdependent activities. *Nature*, *542*(7642), 494–497.

Rubio, M. A. T., Ragone, F. L., Gaston, K. W., Iba, M., & Alfonzo, J. D. (2006). C to U editing stimulates A to I editing in the anticodon loop of a cytoplasmic threonyl tRNA in *Trypanosoma brucei*. *The Journal of Biological Chemistry*, *281*(1), 115–120.

Sharp, S. J., Schaack, J., Cooley, L., Burke, D. J., & Söll, D. (1985). Structure and transcription of eukaryotic tRNA genes. *CRC Critical Reviews in Biochemistry*, *19*(2), 107–144.

Simsek, M., & RajBhandary, U. L. (1972). The primary structure of yeast initiator transfer ribonucleic acid. *Biochemical and Biophysical Research Communications*, *49*(2), 508–515.

Smith, A. M., Jain, M., Mulrone, L., Garalde, D. R., & Akeson, M. (2019). Reading canonical and modified nucleobases in 16S ribosomal RNA using nanopore native RNA sequencing. *PLoS One*, *14*(5), e0216709.

Sprinzl, M., & Vassilenko, K. S. (2005). Compilation of tRNA sequences and sequences of tRNA genes. *Nucleic Acids Research*, *33*(suppl_1), D139–D140.

Sun, Y., Piechotta, M., Naarmann-de Vries, I., Dieterich, C., & Ehrenhofer-Murray, A. E. (2023). Detection of queuosine and queuosine precursors in tRNAs by direct RNA sequencing. *Nucleic Acids Research*. <https://doi.org/10.1093/nar/gkad826>

Suzuki, G., Shimazu, N., & Tanaka, M. (2012). A yeast prion, Mod5, promotes acquired drug resistance and cell survival under environmental stress. *Science*, *336*(6079), 355–359.

- Suzuki, T. (2021). The expanding world of tRNA modifications and their disease relevance. *Nature Reviews. Molecular Cell Biology*, 22(6), 375–392.
- Takakura, M., Ishiguro, K., Akichika, S., Miyauchi, K., & Suzuki, T. (2019). Biogenesis and functions of aminocarboxypropyluridine in tRNA. *Nature Communications*, 10(1), 5542.
- Tanenbaum, M. E., Stern-Ginossar, N., Weissman, J. S., & Vale, R. D. (2015). *Regulation of mRNA translation during mitosis*. <https://doi.org/10.7554/eLife.07957>
- Taoka, M., Nobe, Y., Yamaki, Y., Yamauchi, Y., Ishikawa, H., Takahashi, N., Nakayama, H., & Isobe, T. (2016). The complete chemical structure of *Saccharomyces cerevisiae* rRNA: partial pseudouridylation of U2345 in 25S rRNA by snoRNA snR9. *Nucleic Acids Research*, 44(18), 8951–8961.
- Tavakoli, S., Nabizadeh, M., Makhamreh, A., Gamper, H., McCormick, C. A., Rezapour, N. K., Hou, Y.-M., Wanunu, M., & Rouhanifard, S. H. (2023). Semi-quantitative detection of pseudouridine modifications and type I/II hypermodifications in human mRNAs using direct long-read sequencing. *Nature Communications*, 14(1), 334.
- The Regulation of Cell Size. (2013). *Cell*, 154(6), 1194–1205.
- Thomas, N. K., Poodari, V. C., Jain, M., Olsen, H. E., Akeson, M., & Abu-Shumays, R. L. (2021). Direct Nanopore Sequencing of Individual Full Length tRNA Strands. *ACS Nano*, 15(10), 16642–16653.
- tombo: Tombo is a suite of tools primarily for the identification of modified nucleotides from raw nanopore sequencing data.* (n.d.). Github. Retrieved October 8, 2023, from <https://github.com/nanoporetech/tombo>
- Tomita, K., Ueda, T., & Watanabe, K. (1999). The presence of pseudouridine in the anticodon alters the genetic code: a possible mechanism for assignment of the AAA lysine codon as asparagine in echinoderm mitochondria. *Nucleic Acids Research*, 27(7), 1683–1689.
- True, H. L., & Lindquist, S. L. (2000). A yeast prion provides a mechanism for genetic

variation and phenotypic diversity. *Nature*, 407(6803), 477–483.

Tuorto, F., Legrand, C., Cirzi, C., Federico, G., Liebers, R., Müller, M., Ehrenhofer-Murray, A. E., Dittmar, G., Gröne, H.-J., & Lyko, F. (2018). Queuosine-modified tRNAs confer nutritional control of protein translation. *The EMBO Journal*, 37(18).
<https://doi.org/10.15252/embj.201899777>

Vendeix, F. A. P., Murphy, F. V., 4th, Cantara, W. A., Leszczyńska, G., Gustilo, E. M., Sproat, B., Malkiewicz, A., & Agris, P. F. (2012). Human tRNA(Lys3)(UUU) is pre-structured by natural modifications for cognate and wobble codon binding through keto-enol tautomerism. *Journal of Molecular Biology*, 416(4), 467–485.

White, L. K., Strugar, S. M., MacFadden, A., & Hesselberth, J. R. (2023). Nanopore sequencing of internal 2'-PO modifications installed by RNA repair. *RNA*, 29(6), 847–861.

Wickner, R. B. (1994). [URE3] as an altered URE2 protein: evidence for a prion analog in *Saccharomyces cerevisiae* [Review of *[URE3] as an altered URE2 protein: evidence for a prion analog in Saccharomyces cerevisiae*]. *Science*, 264(5158), 566–569.

Wickner, R. B. (2016). Yeast and Fungal Prions. *Cold Spring Harbor Perspectives in Biology*, 8(9). <https://doi.org/10.1101/cshperspect.a023531>

Wick, R. R., Judd, L. M., & Holt, K. E. (2019). Performance of neural network basecalling tools for Oxford Nanopore sequencing. *Genome Biology*, 20(1), 129.

Winston, F., Dollard, C., & Ricupero-Hovasse, S. L. (1995). Construction of a set of convenient *Saccharomyces cerevisiae* strains that are isogenic to S288C. *Yeast*, 11(1), 53–55.

Workman, R. E., Tang, A. D., Tang, P. S., Jain, M., Tyson, J. R., Razaghi, R., Zuzarte, P. C., Gilpatrick, T., Payne, A., Quick, J., & Others. (2019). Nanopore native RNA sequencing of a human poly (A) transcriptome. *Nature Methods*, 16(12), 1297–1305.

Workman, R. E., Tang, A. D., Tang, P. S., Jain, M., Tyson, J. R., Razaghi, R., Zuzarte, P. C., Gilpatrick, T., Payne, A., Quick, J., Sadowski, N., Holmes, N., de Jesus, J. G., Jones, K. L.,

- Soulette, C. M., Snutch, T. P., Loman, N., Paten, B., Loose, M., ... Timp, W. (2019). Nanopore native RNA sequencing of a human poly(A) transcriptome. *Nature Methods*, *16*(12), 1297–1305.
- Xing, F., Hiley, S. L., Hughes, T. R., & Phizicky, E. M. (2004). The specificities of four yeast dihydrouridine synthases for cytoplasmic tRNAs. *The Journal of Biological Chemistry*, *279*(17), 17850–17860.
- Yamagami, R., Tomikawa, C., Shigi, N., Kazayama, A., Asai, S.-I., Takuma, H., Hirata, A., Fourmy, D., Asahara, H., Watanabe, K., Yoshizawa, S., & Hori, H. (2016). Folate-/FAD-dependent tRNA methyltransferase from *Thermus thermophilus* regulates other modifications in tRNA at low temperatures. *Genes to Cells: Devoted to Molecular & Cellular Mechanisms*, *21*(7), 740–754.
- Yoluç, Y., Ammann, G., Barraud, P., Jora, M., Limbach, P. A., Motorin, Y., Marchand, V., Tisné, C., Borland, K., & Kellner, S. (2021). Instrumental analysis of RNA modifications. *Critical Reviews in Biochemistry and Molecular Biology*, *56*(2), 178–204.
- Zhang, W., Eckwahl, M. J., Zhou, K. I., & Pan, T. (2019). Sensitive and quantitative probing of pseudouridine modification in mRNA and long noncoding RNA. *RNA*, *25*(9), 1218–1225.
- Zhou, M., Long, T., Fang, Z.-P., Zhou, X.-L., Liu, R.-J., & Wang, E.-D. (2015). Identification of determinants for tRNA substrate recognition by *Escherichia coli* C/U34 2'-O-methyltransferase. *RNA Biology*, *12*(8), 900–911.